Diana Legutko-Bijoch

Matrix Metalloproteinase 9 in dendritic spine plasticity

PhD thesis
Completed in the Laboratory of Neurobiology
of the Nencki Institute of Experimental Biology
Polish Academy of Sciences

SUPERVISORS
Prof. Leszek Kaczmarek , Ph.D., D.Sc.
Dr. Ryohei Yasuda, Ph.D., D.Sc.

Warsaw, 2024

ACKNOWLEDGEMENTS

ABSTRACT

Neuronal plasticity, a process fundamental to memory formation manifests as changes in synaptic strength during encoding new information. Synapses undergo both structural and functional modifications, with dendritic spines—postsynaptic protrusions harbouring excitatory synapses—serving as primary sites for such remodelling. Long-term potentiation (LTP), a key form of plasticity, requires precise molecular coordination, consisting of well-characterized intracellular signalling cascades and less-understood extracellular events, particularly proteolysis.

This study investigates the role of matrix metalloproteinase 9 (MMP-9) in structural LTP (sLTP) using hippocampal organotypic slices from wild-type and genetically modified mice. MMP-9 activity was modulated through chemical inhibitors and gene knockouts, while its interplay with neurotrophic factor signalling was assessed by measuring activation of tropomyosin receptor kinase B (TrkB, the receptor for Brain-Derived Neurotrophic Factor, BDNF) and Insulin-like Growth Factor 1 Receptor (IGF1R). Molecular biology techniques and bioinformatics approaches were employed to identify MMP-9 target proteins.

My results demonstrate that MMP-9 is rapidly released upon stimulation and plays a pivotal role in spine growth and receptor activation. Inhibition or genetic knockout of MMP-9 significantly reduced sLTP-induced spine enlargement and impaired TrkB activation, indicating that MMP-9-mediated extracellular cleavage of proBDNF to mature BDNF is critical for sustained TrkB signalling. Furthermore, MMP-9 activity was shown to be essential for IGF1R activation, mediated through the cleavage of insulin-like growth factor-binding proteins (IGFBPs), with IGFBP2 identified as a likely target. Immunolabelling confirmed the localization of IGFBP2 in dendritic spines, implicating its involvement in this mechanism.

In conclusion, this study identifies MMP-9 as a key regulator of synaptic plasticity, coordinating structural spine remodelling and functional signalling pathways through extracellular proteolysis. By facilitating BDNF/TrkB and IGF1/IGF1R signalling, MMP-9 bridges extracellular and intracellular mechanisms, shedding new light on the extracellular proteolysis modulating synaptic plasticity.

STRESZCZENIE

Plastyczność neuronalna odgrywa kluczową rolę w procesie tworzenia pamięci, przejawiając się zmianami w sile synaptycznej podczas kodowania nowych informacji. Zarówno strukturalne, jak i funkcjonalne modyfikacje synaps są podstawą tego procesu, a kolce dendrytyczne, które są nośnikami synaps pobudzających, stanowią główne centra reorganizacji. Długotrwałe wzmocnienie synaptyczne (LTP), będące jedną z klasycznych form plastyczności, wymaga precyzyjnej koordynacji procesów molekularnych, obejmujących dobrze poznane wewnątrzkomórkowe kaskady sygnalizacyjne oraz mniej zbadane procesy zewnątrzkomórkowe, w tym proteolizę.

W niniejszej pracy zbadano rolę metaloproteazy macierzowej 9 (MMP-9) w strukturalnym LTP (sLTP) z wykorzystaniem organotypowych hodowli hipokampalnych pochodzących od myszy typu dzikiego oraz genetycznie zmodyfikowanych. Aktywność MMP-9 była modulowana za pomocą inhibitorów chemicznych oraz nokautów genowych, a jej wpływ na sygnalizację czynników neurotroficznych został zbadany poprzez pomiar aktywacji receptorów: kinazy tropomiozynowej B (TrkB, receptora dla BDNF, czynnika neurotroficznego pochodzenia mózgowego) oraz receptora insulinopodobnego czynnika wzrostu 1 (IGF1R). W celu identyfikacji substratów MMP-9 zastosowano zaawansowane techniki biologii molekularnej oraz narzędzia bioinformatyczne.

Uzyskane wyniki wykazały, że MMP-9 w odpowiedzi na stymulację jest natychmiastowo uwalniana do przestrzeni zewnątrzkomórkowej, odgrywając kluczową rolę we wzroście kolców dendrytycznych oraz aktywacji receptorów. Zarówno blokowanie, jak i brak MMP-9 na poziomie białkowym znacząco osłabiały wzrost kolców dendrytycznych w odpowiedzi na stymulację sLTP oraz zmniejszyły aktywację TrkB. Wyniki sugerują, że zewnątrzkomórkowe cięcie proBDNF do dojrzałego BDNF przez MMP-9 jest niezbędne dla uzyskania trwałej aktywacji TrkB. Dodatkowo, aktywność MMP-9 okazała się kluczowa dla aktywacji IGF1R. W tym efekcie pośredniczą białka wiążące IGF (IGFBPs), najprawdopodobniej IGFBP2, który służy jako substrat dla MMP-9 umożliwiając uwolnienie IGF1. Immunolokalizacja potwierdziła obecność IGFBP2 w kolcach dendrytycznych, co sugeruje jego potencjalną rolę w tym mechanizmie.

Podsumowując, ta praca identyfikuje MMP-9 jako kluczowego regulatora plastyczności synaptycznej. MMP-9 koordynuje strukturalne zmiany kolców dendrytycznych, które zachodzą poprzez zwiększanie dostępności czynników neurotroficznych. Zwiększając sygnalizację poprzez BDNF/TrkB i IGF1/IGF1R, MMP-9 łączy mechanizmy zewnątrz- i wewnątrzkomórkowe, rzucając nowe światło na funkcję zewnątrzkomórkowej proteolizy w plastyczności synaptycznej.

TABLE OF CONTENTS

LIST OF FREQUENTLY USED ABBREVIATIONS

2P – Two-photon

2pFLIM - two-photon fluorescence lifetime imaging

AMPA - α-amino-3-hydroxy-5-methyl-4-isoxazolepropionic acid

APMA - 4-aminophenylmercuric acetate

AMPAR – AMPA receptor

BDNF – Brain-derived neurotrophic factor

CaMKII - $Ca2+$/calmodulin-dependent protein kinase II

cAMP - Cyclic adenosine monophosphate

CREB - cAMP response element-binding protein

ECM - extracellular matrix

E-LTP – Early long-term potentiation

ER - endoplasmic reticulum

ES - extracellular solution

FLIM - Fluorescence Lifetime Imaging

fLTP – Functional Long-Term Potentiation

FRET - Fluorescence Resonance Energy Transfer

GFP - Green fluorescent prote

IGF-1 - insulin-like growth factor 1

IGF1R - insulin-like growth factor 1 receptor

IGFBPs - Insulin-like Growth Factor Binding Proteins

L-LTP – Late long-term potentiation

LTD - long-term depression

LTP - long-term potentiation

MMP-9 - matrix metalloproteinase 9

MNI-glutamate - 4-methoxy-7-nitroindolinyl-glutamate

NMDA - N-methyl-D-aspartate

NMDAR – NMDA receptor

PSD - postsynaptic density

RFP - red fluorescent protein

SEP - superecliptic pHluorin

sLTP - Structural Long-Term Potentiation

TIRF - total internal reflection fluorescence

TrkB - tropomyosin receptor kinase B

INTRODUCTION

One of the most remarkable features of the human brain is its ability to create and store memories. This capability has evolved from the brain's primary function: to process sensory information and respond adaptively to an ever-changing environment. The brain's immense information-processing power arises from the complexity of its neuronal network. Individual neurons communicate with thousands of other neurons through specialized connections called synapses. Each neuron receives inputs through synapses on its dendrites and cell body, and transmits signals via synapses at its axon.

The brain capacity for learning is fundamentally rooted in the rearrangement and modification of these synaptic connections. However, some changes in brain connectivity are driven by pathological processes, which can lead to a number of psychiatric disorders, like depression or schizophrenia. This thesis focuses on exploring specific molecular mechanisms involved in synaptic reorganization to better understand these processes.

Synapses

The first concept of synapses was introduced by Santiago Ramón y Cajal, who observed and described small, spike-like structures on the dendritic branches of neurons, now known as dendritic spines (Ramón y Cajal, 1894). He proposed that neurons communicate through specialized connections called synapses, located at these dendritic spines (Berlucchi & Buchtel, 2009; Mestres, 2019). His work laid the foundation for understanding the brain as a network of interconnected, yet distinct units.

The most common type of synapse in the brain is the chemical synapse, where signal transmission between neurons occurs via neurotransmitters (Figure 1). Glutamate is the predominant neurotransmitter at excitatory synapses in the brain. When a presynaptic neuron generates an action potential, it triggers the release of vesicles containing glutamate from the presynaptic terminal. The glutamate then diffuses across the synaptic cleft and binds predominantly to α-amino-3-hydroxy-5-methyl-4-isoxazolepropionic acid (AMPA) and N-methyl-D-aspartate (NMDA) receptors located on the dendritic spine of the postsynaptic neuron. This binding facilitates ion flow into the postsynaptic neuron, causing membrane depolarization which propagates along dendrites. Efficiency of the synapse, in simplified terms, depends on the probability of vesicle release from

a presynaptic site, and the number of AMPA receptors located at the postsynaptic membrane. Both of those features can be altered in response to synapse activity in a process called synaptic plasticity.
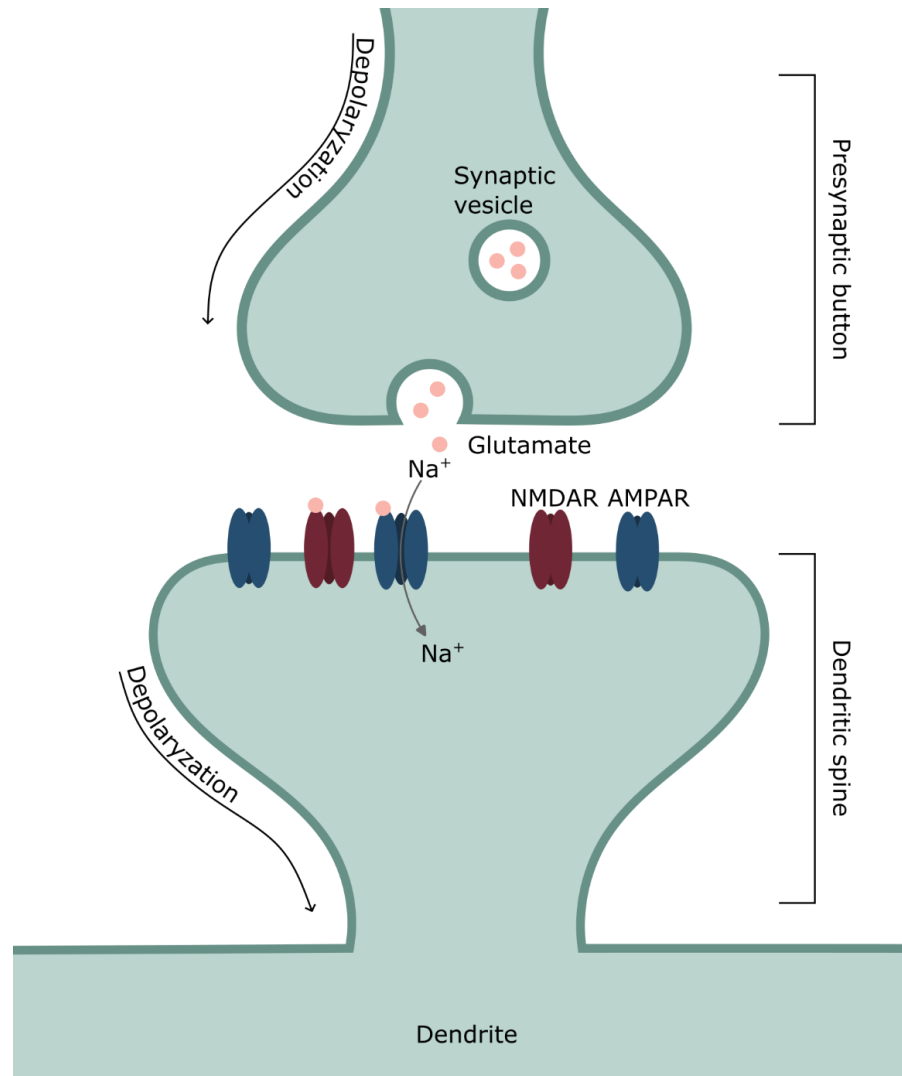
Figure 1. Schematic Representation of an Excitatory Synapse

The depolarization wave of an action potential reaches the presynaptic terminal, triggering synaptic vesicle fusion with the membrane and glutamate release into the synaptic cleft. Glutamate binds to AMPAR and NMDAR on the postsynaptic membrane of dendritic spines, leading to an influx of sodium ions (Na⁺) into the post synapse through AMPAR. At resting state potentials NMDAR does not contribute to ion influx due to Mg^{2+} block. The sodium influx generates a depolarization wave in the dendrite. The dendrite integrates depolarization signals from multiple active synapses and propagates the cumulative signal towards the soma (cell body), potentially triggering an action potential.

Synaptic Plasticity

Synaptic plasticity describes the brain's ability to modify synaptic strength in response to activity. Jerzy Konorski and Donald Hebb played a crucial role in introducing the principles of synaptic plasticity (Hebb, 1950; Konorski, 1948), suggesting that coordinated activity between presynaptic and postsynaptic neurons strengthens their connection. Experimental confirmation and mechanistic insights were later provided by Eric Kandel and colleagues, who demonstrated that short-lasting changes in synaptic plasticity require the activity of cyclic AMP (cAMP) (Hawkins et al., 1983). They further revealed that long-lasting changes of synaptic strength depended on the activation of cAMP response element-binding protein (CREB), which drives protein synthesis to stabilize and maintain plastic changes in Aplysia californica (Dash et al., 1990).

Subsequent research revealed that synaptic plasticity is bidirectional, meaning that synaptic strength can either increase or decrease depending on activity patterns. It is well illustrated in models of synaptic plasticity such as long-term potentiation (LTP) and long-term depression (LTD). LTP is typically triggered by high-frequency stimulation, and leads to a persistent strengthening of synaptic connections. In contrast, LTD, often induced by low-frequency stimulation, results in a sustained weakening of synaptic strength (Bliss & Lømo, 1973; Malenka & Bear, 2004). These complementary processes allow neural circuits to adapt dynamically, refining connections and optimizing their functionality.

The bidirectional nature of synaptic plasticity is tightly linked to molecular mechanisms, such as those identified by Kandel and colleagues. During LTP, high-frequency stimulation leads to calcium ions influx usually through NMDA receptors (NMDAR), triggering the activation of kinases like CaMKII (Ca^{2+}/calmodulin-dependent protein kinase II) and PKA (Protein Kinase A), initiating signalling cascade resulting in strengthening of synaptic connections. For LTD, low-frequency stimulation activates distinctive signalling molecules including activation of phosphatases such as PP1 (Protein phosphatase 1) and calcineurin, resulting in synaptic weakening (Malenka & Bear, 2004). These molecular cascades converge on shared pathways, including CREB activation for long-term changes, highlighting how activity-dependent molecular processes fine-tune neural circuits. Together, LTP and LTD ensure that neural networks remain flexible,

enabling the brain to adapt to environmental demands while maintaining the stability necessary for memory and cognition.

Long-Term Potentiation

LTP was discovered in the hippocampus by Bliss and Lømo in 1973, and since then, it has become a cornerstone for understanding synaptic modification and the cellular basis of learning and memory (Bliss & Lømo, 1973). Among the various forms of LTP, the classical NMDAR-dependent LTP, which is the focus of this thesis, has been extensively studied and will be discussed below. However, it is important to note the existence of other types of LTP, such as NMDAR-independent LTP (Citri & Malenka, 2008).

For instance, presynaptic LTP, driven by presynaptic cAMP signalling, enhances synaptic efficiency by increasing neurotransmitter release. Additionally, several types of metabotropic receptors—including mGluRs (metabotropic glutamate receptors), endocannabinoid receptors, and opioid receptors—have been identified as mediators of LTP through their distinct signalling pathways. Furthermore, voltage-gated calcium channels (VGCCs) expressed in certain brain regions also contribute to Ca^{2+} influx, similar to NMDA receptors, thereby initiating LTP (Lisman, 2017).

NMDAR-dependent LTP

The hippocampus, a region crucial for memory formation and spatial navigation, among others, serves as a key model for understanding synaptic plasticity. Within this region, the Schaffer collateral-CA1 synapse has been extensively studied, providing valuable insights into the molecular and structural processes driving LTP. A defining feature of LTP at these synapses is its dependence on NMDAR activation. These receptors act as molecular coincidence detectors, integrating presynaptic neurotransmitters release with postsynaptic depolarization to initiate the cascade of events that lead to synaptic strengthening (Malenka & Bear, 2004).

NMDARs coincidence properties come from the fact, that even when agonists are bound, the channel remains blocked by a magnesium ion (Mg^{2+}) at resting membrane potentials. Depolarization of the postsynaptic membrane, often achieved through AMPAR activation during synaptic activity, releases this Mg^{2+} block, allowing Ca^{2+} to flow into the cell. The influx of Ca^{2+} is particularly critical, as it is a secondary messenger that triggers a series

of intracellular signalling cascades, driving both functional and structural changes at the synapse (Wong et al., 1999) (Figure 2).

Upon influx, Ca^{2+} binds to calmodulin, a regulatory protein, forming a calcium-calmodulin complex that activates Ca^{2+}/calmodulin-dependent protein kinase II (CaMKII). CaMKII plays a central role in the early stages of LTP by binding to NMDAR and phosphorylating AMPAR, driving receptor clustering at the synapse and enhancing their conductance (Murakoshi et al., 2017; Tullis et al., 2023). Additionally, CaMKII facilitates the insertion of AMPAR-containing vesicles into the postsynaptic membrane, increasing the number of active receptors available for synaptic transmission (Choquet & Hosy, 2020; J. Yang et al., 2024). One of the critical CaMKII functions is activation of Rho GTPases particularly RhoA and Cdc42 driving actin skeleton remodelling. Those actions are essential for establishing LTP, though CaMKII role diminishes at the later phases, as the maintenance of LTP relies on other processes, such as structural changes and gene expression (Chang et al., 2017; Murakoshi et al., 2017).

Ca^{2+} influx also activates adenylyl cyclase, leading to the production of cAMP, in NMDAR-dependent LTP this process is critical for the maintenance of LTP (Wong et al., 1999). cAMP activates PKA (Tang & Yasuda, 2017). PKA phosphorylates a variety of targets, including extracellular signal-regulated kinases (ERK) that upon translocation to the nucleus activate CREB and serum-response factor (SRF). Those factors drive transcription of immediate early genes encoding e.g., c-Fos (Dragunow et al., 1989; Ghosh et al., 1994; Kaczmarek et al., 1988) – transcription regulator that further facilitates expression of the genes encoding synaptic receptors, scaffolding proteins and cytoskeletal regulators, which are essential for the consolidation of LTP. These transcriptional changes ensure that the molecular modifications induced during the early phases of LTP are stabilized and preserved over longer periods.

As previously mentioned, the binding of Ca^{2+}/calmodulin to CaMKII facilitates the trafficking of AMPARs into the synaptic membrane. This calcium-triggered exocytosis is a critical process in LTP, as it not only delivers AMPARs to the membrane to enhance synaptic strength but also supplies additional membrane material to support dendritic spine expansion (M. Park et al., 2006). Furthermore, the vesicles involved in this process carry additional cargo that initiates paracrine and autocrine signalling within the stimulated dendritic spine, further enhancing localized synaptic plasticity.

The SNARE (Soluble N-ethylmaleimide-Sensitive Factor Attachment Protein Receptor) complex forms the core molecular machinery essential for mediating vesicle fusion with target membranes, a critical process underpinning exocytosis in synaptic plasticity (Jurado et al., 2013). This complex operates through a tightly regulated system consisting of SNARE proteins, including syntaxins, SNAP proteins, and vesicle-associated v-SNAREs, which collectively drive vesicle docking and membrane fusion. For LTP induction and maintenance, this exocytosis is finely tuned by calcium-sensing regulatory proteins such as synaptotagmins, complexins, and CAPS (Calcium-Dependent Activator Protein for Secretion).

Among these regulatory proteins, synaptotagmins—specifically Syt1, Syt5, and Syt7—play pivotal roles in LTP by controlling AMPA receptor exocytosis (Helm et al., 2021; Wu et al., 2004). Their ability to sense Ca^{2+} influx allows them to trigger precise and timely vesicle fusion events at the synapse, a prerequisite for effective synaptic strengthening.

Complementing the role of synaptotagmins, complexins provide an additional layer of regulation by interacting with SNARE proteins such as Syntaxin-3 and SNAP-47. Like synaptotagmins, complexins have been implicated in AMPAR vesicle exocytosis during LTP, ensuring that vesicle fusion occurs in a controlled manner (Ahmad et al., 2012; Jurado et al., 2013). This interaction underscores the intricate orchestration of proteins required to support synaptic plasticity.

Further specialization within this regulatory network is provided by CAPS proteins. Of the two CAPS isoforms, CAPS1 has been confirmed to localize specifically in dendritic spines. CAPS1 interacts with SNARE proteins such as syntaxin1a, SNAP-25, and VAMP2, and is particularly notable for its role in the release of dense-core vesicles. These vesicles carry neurotrophic factors, including brain-derived neurotrophic factor (BDNF), nerve growth factor (NGF), and neurotrophin-3 (NT-3) (Helm et al., 2021; Ishii et al., 2021; Wu et al., 2004). Once released, these neurotrophic factors bind to their receptors Receptor Tyrosine Kinases (RTKs), specifically tropomyosin receptor kinases (Trks), receptors promoting LTP through activation of Ras/Raf/MAPK, PLC, Rac1, Cdc42 and PI3K signalling pathways that reinforce synaptic plasticity (Nakahata & Yasuda, 2018).

This coordinated mechanism establishes a robust positive feedback loop. By promoting the sustained delivery of AMPARs and neurotrophic factors, the process amplifies LTP and drives long-term structural and functional modifications within the synapse.
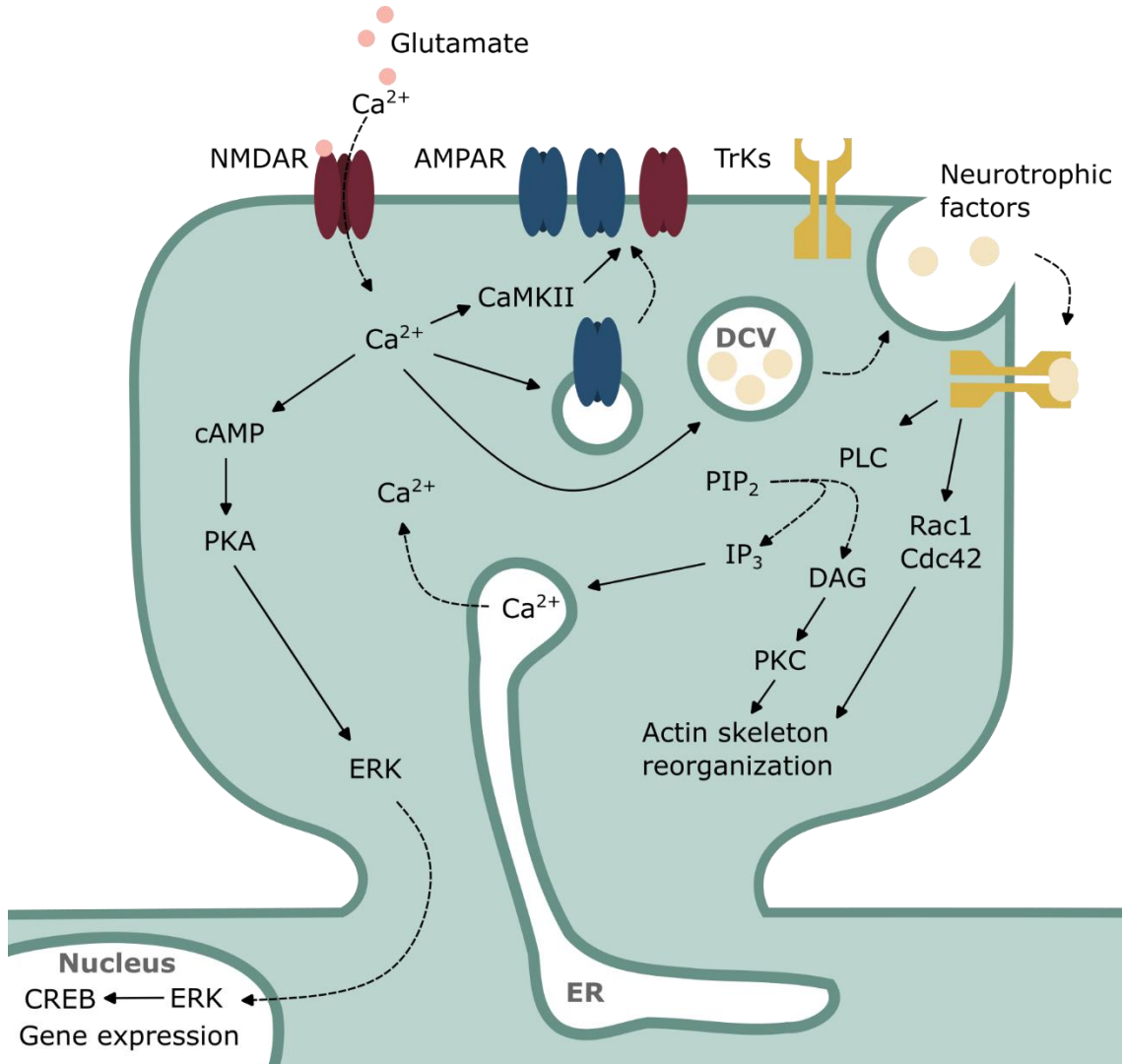
Figure 2. Mechanisms of NMDAR-Dependent Long-Term Potentiation
The figure illustrates the intracellular signalling cascades triggered by calcium influx through NMDA receptors during LTP. Calcium entry initiates multiple parallel pathways:

- *cAMP Pathway: Calcium activates the cAMP signalling pathway, which promotes protein synthesis through downstream effectors such as PKA and ERK, contributing to synaptic strengthening and gene expression in the nucleus via CREB and SRF.*

- *CaMKII Activation: Calcium-dependent activation of CaMKII facilitates AMPA receptor trafficking and immobilization at the synaptic membrane, enhancing synaptic strength. CaMKII also supports vesicle exocytosis, which delivers additional receptors and membrane material to the synapse.*

- *Dense-Core Vesicle (DCV) Release: Calcium influx drives the release of neurotrophic factors (NTFs) from DCVs. These factors bind to tropomyosin receptor kinase (TrKs) on the postsynaptic membrane, triggering autocrine and paracrine signalling. TrKs upon autophosphorylation lead to activation of*

downstream effectors like PLC, Rac1 and Cdc42. PLC hydrolyses PIP2 into IP3 (triggering Ca²⁺

release from ER) and DAG activating PKC. PKC, Rac1 and Cdc42 play a role in actin cytoskeleton

reorganization, facilitating structural changes in dendritic spines critical for LTP maintenance.

This positive feedback loop enhances synaptic efficacy and induces long-term structural and functional changes at the synapse.

Dendritic Spines: Key Sites of Synaptic Plasticity

Dendritic spines are small, actin-rich protrusions extending from neuronal dendrites, serving as compartmentalized sites of synaptic input. Their narrow necks restrict molecule diffusion, creating isolated environments for localized signalling. Spine morphology varies from thin, immature filopodia to mature, stable mushroom-shaped spines, with larger spine heads generally correlating with stronger synaptic transmission (Figure 3). These mature spines house greater densities of AMPA and NMDA receptors (Hruska et al., 2022; Matsuzaki et al., 2001). In contrast, some thin spines contain only NMDA receptors and are referred to as silent synapses, as they do not contribute to synaptic transmission at resting membrane potential. Spine morphology is positively correlated with synaptic strength, with larger spines and postsynaptic densities (PSDs) being associated with greater synaptic strength (Matsuzaki et al., 2001; Meyer et al., 2014). Notably, dendritic spines possess the remarkable ability to undergo bidirectional structural changes.
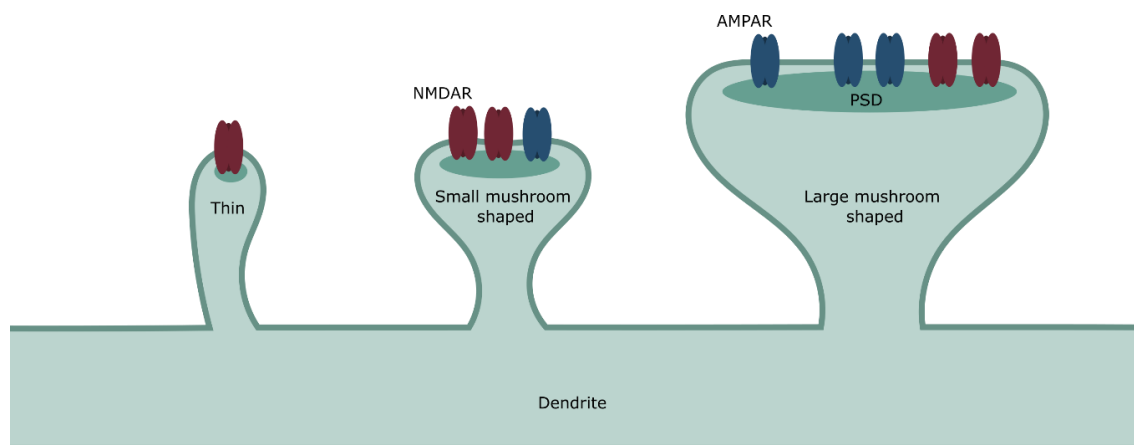
Figure 3. Schematic Representation of Dendritic Spine Types

The figure illustrates various types of dendritic spines and their characteristics. Immature thin spines, which primarily contain NMDARs, do not participate in synaptic activity unless the membrane is depolarized. These spines have the potential to undergo plastic changes, increasing in volume and transitioning into mature mushroom-shaped spines that acquire AMPARs. Larger spines are associated

with a bigger PSD, allowing them to anchor more AMPARs and NMDARs. Consequently, the size of a dendritic spine directly correlates with its synaptic transmission strength.

The dynamic nature of dendritic spines is central to structural plasticity, as they continuously form, grow, shrink, or disappear in response to neural activity. For instance, learning new motor skills or encountering novel sensory stimuli increases spine density and stability in relevant neural circuits, whereas spine elimination facilitates synaptic pruning to remove inefficient or redundant connections (Stein & Zito, 2019; Zuo et al., 2005). This adaptability underscores the importance of dendritic spine remodelling in shaping neural circuits during learning and memory (Holtmaat & Svoboda, 2009; Trachtenberg et al., 2002; Zuo et al., 2005).

Structural Long-Term Potentiation (sLTP)

sLTP represents the morphological hallmark of LTP, characterized by activity-dependent remodelling of dendritic spine architecture. This remodelling involves dynamic reorganization of the actin cytoskeleton, vesicle trafficking, and postsynaptic density (PSD) expansion (Figure 4).

This process is initiated by strong stimulation and Ca^{2+} influx leading to rapid CaMKII activation and the recruitment of PKC to the membrane, setting the stage for downstream signalling events (Colgan et al., 2018; Nakahata & Yasuda, 2018). Next the spine transformations can be divided into three distinct phases:

1. **Transient Phase:** During the transient phase, calcium-dependent vesicle trafficking and the membrane recruitment of PKC and p140Cap facilitate the initiation of extensive actin polymerization (Jaworski et al., 2009; Lledo et al., 1998; Patterson et al., 2010; Y. Yang et al., 2021). Concurrently, CaMKII activates the small GTPases Cdc42 and RhoA (Harvey et al., 2008; Murakoshi et al., 2011), while TrkB activation drives downstream signalling through PKC, Cdc42, and Rac1 (Colgan et al., 2018; Harward et al., 2016; Hedrick et al., 2016). These active GTPases regulate key effectors such as cofilin and Arp2/3, resulting in the intensive reorganization of the actin cytoskeleton. Additionally, the insulin-like growth factor 1 receptor (IGF1R) is rapidly activated during this phase. Its activity, likely mediated by the PLC/PKC pathway, is essential for spine

enlargement (Tu et al., 2023). This phase is critical for transitioning from initial actin polymerization to more stable structural changes. Approximately 1–2 minutes post-stimulation, dendritic spines reach their peak volume, followed by a slight decrease as dynamic actin remodelling processes take place.

2. **Sustained Phase:** The sustained phase focuses on stabilizing actin filaments through signalling mediated by Cdc42 and Rac1. Around 7 minutes post-stimulation, dendritic spines shrink slightly to their final volume, which remains larger than their initial pre-stimulation size. This phase is associated with increased postsynaptic sensitivity to glutamate and provides the structural stability necessary for maintaining long-term synaptic plasticity (Harward et al., 2016; Matsuzaki et al., 2004; Murakoshi et al., 2011).

3. **Consolidation Phase**: The consolidation phase involves an increase in scaffolding molecules, leading to PSD expansion. This phase is dependent on *de novo* protein synthesis, which is essential for solidifying the structural and functional changes required for sLTP (Borczyk et al., 2019; Bosch et al., 2014; Ghosh et al., 1994; Meyer et al., 2014; Y. Sun et al., 2021).

These three phases outline the tightly regulated processes underlying sLTP, highlighting the intricate interplay of molecular and structural mechanisms essential for synaptic remodelling and long-term synaptic stability.
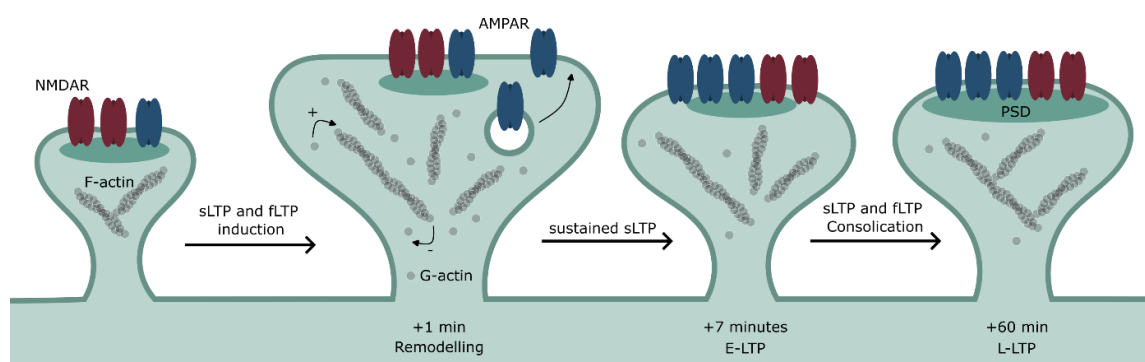
Figure 4. Representation of Dendritic Spine Phases During sLTP
The figure depicts the distinct phases of dendritic spine remodelling during structural long-term potentiation (sLTP). Upon stimulation, the spine undergoes rapid remodelling, characterized by actin cytoskeleton reorganization and vesicle trafficking, referred to as the Transient Phase. This is followed by the Sustained Phase, during which actin filaments are stabilized, and the spine incorporates a larger number of receptors. However, during this phase, the postsynaptic density (PSD) remains dynamic and

undergoes rearrangement, a process that requires newly synthesized proteins. Approximately one hour post-stimulation, the PSD becomes fully formed, anchoring receptors and integrating structural LTP (sLTP) with functional LTP (fLTP).

Techniques for studying sLTP

Two-photon (2P) glutamate uncaging

The study of structural plasticity in dendritic spines undergoing LTP has historically been challenging due to the limitations of traditional stimulation techniques. Previous approaches often relied on broad stimulation methods, such as electrical stimulation of axon bundles, leading to simultaneous activation of multiple synapses. As dendritic spines structure was indicating some level of isolation from dendritic shaft, lack of spatial precision made it difficult to resolve the specific signalling cascades occurring at individual dendritic spines. It was necessary to develop single spine stimulation technique to identify what kind of signals spread between the spines and what kind of signalling is exclusive for stimulated synapses.

The breakthrough in studying single-spine plasticity came with the development of caged neurotransmitters and two-photon (2P) laser scanning microscopy (Denk, 1994; Denk & Svoboda, 1997; Wieboldt et al., 1994). 2P microscopy allows for localized fluorescence excitation by simultaneous absorption of two photons of longer wavelengths (infrared range). This method significantly reduces photobleaching and photodamage, allowing imaging of thick, light-scattering tissues such as the cortex of living animals or hippocampal organotypic slices. Unlike primary neuronal cultures, these preparations preserve the three-dimensional structure and neuronal circuitry, providing a closer approximation of physiological conditions or allowing for studying actual physiological conditions like dendritic spine plasticity occurring during animal learning (Lendvai et al., 2000).

Caged compounds, including caged neurotransmitters, are key tools for achieving spatiotemporal control of single synapse modifications. These molecules are inactive due to a presence of photo-protecting group, which for example prevents the molecule from binding to its receptor. Upon targeted photolysis with light, the active molecule is released, enabling its binding to a protein and thus a precise manipulation of biological processes. The first caged neurotransmitters were developed in the 1990s (Wieboldt et

al., 1994), and since then, various caged glutamate compounds have been synthesized using different caging strategies and chromophores. Among these, 4-methoxy-7-nitroindolinyl-glutamate (MNI-glutamate) has become the gold standard for 2P uncaging due to its unique properties: highly stable and soluble under physiological conditions; efficient photolysis by near-UV light. 300 - 380 nm excitation and compatibility with two-photon excitation, enabling localized release of glutamate without phototoxicity (Ellis-Davies, 2019; Matsuzaki et al., 2001).

The integration of MNI-glutamate and 2P excitation allows for the precise release of glutamate in a highly controlled manner, both spatially and temporally (Figure 5). By focusing a 2P laser on a small volume, uncaging occurs only within the laser focal point, where the density of the photons is the highest, enabling stimulation of individual dendritic spines. This technique has been instrumental in demonstrating rapid and selective enlargement of stimulated spines, a hallmark of LTP-induced plasticity (Matsuzaki et al., 2004).

The combination of 2P imaging with glutamate uncaging has revolutionized the study of sLTP, leading to significant discoveries. Early studies demonstrated the dynamic changes in spine morphology during sLTP (Matsuzaki et al., 2004) and revealed that some signalling events are shared between neighbouring spines (Harvey et al., 2008). Since then, numerous molecules involved in sLTP, including GTPases, kinases, and transmembrane receptors, have been studied extensively. These studies have detailed the translocation of molecules to the stimulated spine and their diffusion from it, as well as the timing and dynamics of molecular activation during sLTP (Bosch et al., 2014; Chang et al., 2017; Colgan et al., 2018; Harvey et al., 2008; Harward et al., 2016; Hedrick et al., 2016; Murakoshi et al., 2011; Tang & Yasuda, 2017).
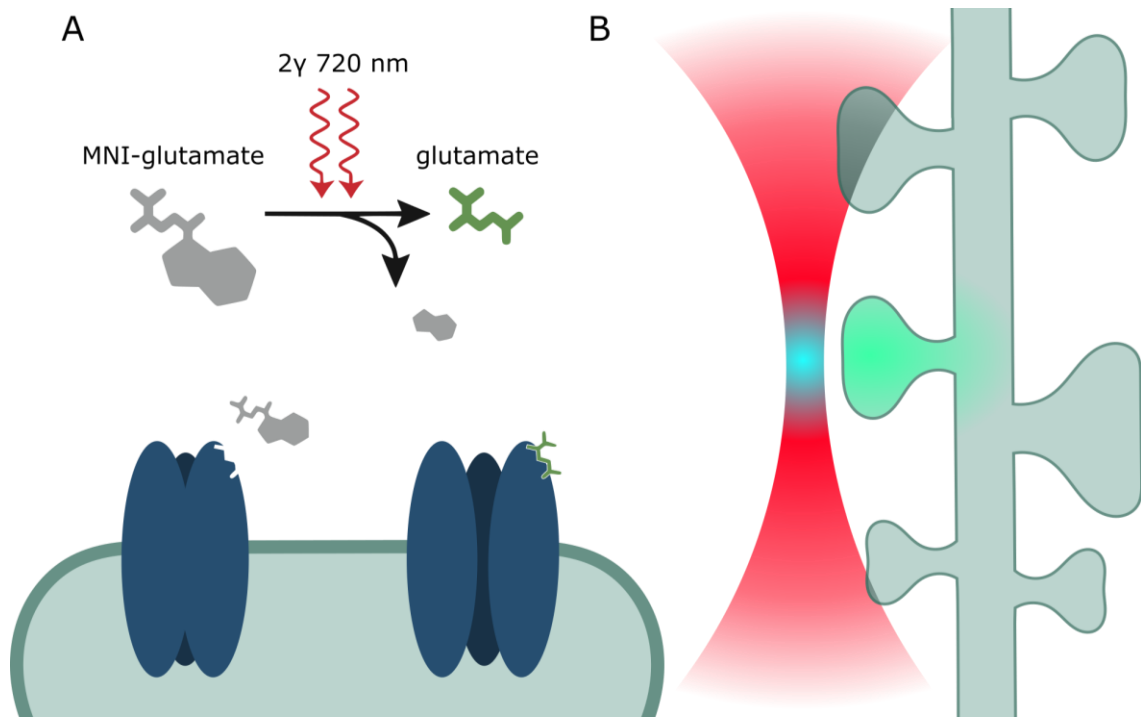
Figure 5. Single Spine Stimulation using 2p Uncaging of MNI-Glutamate

A. MNI-glutamate photoconversion into bioactive glutamate by simultaneous absorbtion of two 720nm photons.

B. Highest photon density occurs at the the focal point. It allows for localised glutamate release and activation of singular dendritic spine.

Adapted from Judkewitz et al., (2006).

Fluorescence Resonance Energy Transfer (FRET)

Central to these advances has been the application of Fluorescence Resonance Energy Transfer (FRET) sensors, which have become indispensable tools for studying the spatiotemporal dynamics of intracellular signalling (Miyawaki, 2003). FRET is a physicochemical process that relies on the non-radiative transfer of energy from an excited donor fluorophore to an acceptor fluorophore. It depends on two critical factors (Figure 6):

- The spectral overlap between the donor's emission and the acceptor's excitation spectra.
- The proximity between the donor and acceptor (typically below 10 nanometre range).

Because many biological processes rely on protein-protein interaction, thus the need of proximity between donor and acceptor is especially useful feature of FRET that can be used in designing biochemical sensors. In order to design biochemical sensors that can be introduced to a living cell, both donor and acceptor utilize fluorescent proteins which are attached to the protein(s) of interest. Green fluorescent protein (GFP) is widely used as a FRET donor in biosensors, often paired with red fluorescent protein (RFP) as the acceptor. By fusing these fluorophores with proteins of interest, researchers can measure protein interactions and signalling dynamics in living cells.
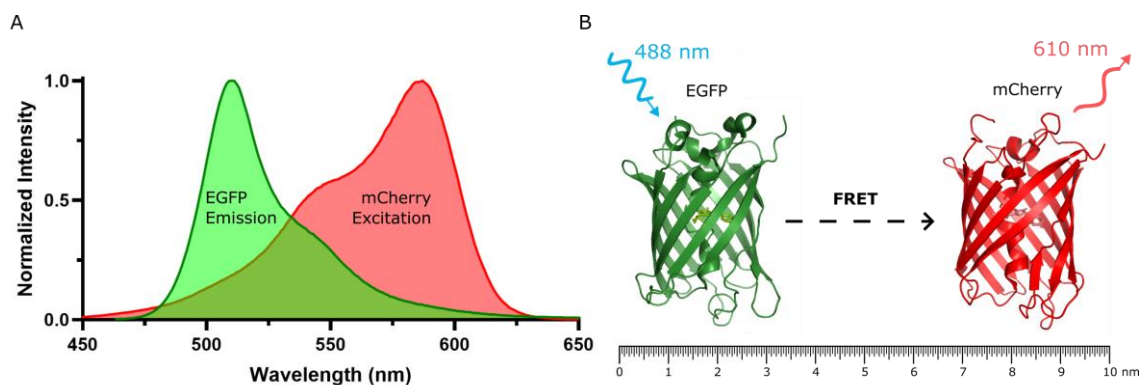
Figure 6. Fluorescence Resonance Energy Transfer (FRET)

A. FRET occurs when the emission spectrum of the donor molecule (e.g., GFP) overlaps with the excitation spectrum of the acceptor molecule (e.g., mCherry). Spectral data were obtained from FPbase.

B. For FRET to take place, the donor and acceptor molecules must be within a proximity of less than 10 nm. Upon excitation of GFP at 488 nm, energy is transferred to mCherry, leading to the emission of lower-energy photons. Protein structural data were sourced from the RCSB Protein Data Bank.

Fluorescence Lifetime Imaging (FLIM)

Even though FRET-based sensors are a great tool, their use present many practical challenges. One of them is a measurable change in the intensity of donor or acceptor fluorescence. Due to small differences between fluorescence intensity ratios and susceptibility to concentration changes, it is difficult to directly measure FRET in living systems. Fluorescence Lifetime Imaging (FLIM) has emerged as one of the most reliable methods for quantifying FRET efficiency. FLIM measures changes in the fluorescence lifetime of the donor—defined as the time a fluorophore spends in the excited state (after absorption of a photon) before returning to the ground state (emitting a photon). When FRET occurs, the donor's fluorescence lifetime shortens, providing a precise readout of

FRET efficiency (Figure 7). This method is independent of the relative concentrations of donor and acceptor fluorophores, making it highly accurate.

Recent developments in FLIM technology have integrated time-correlated single-photon counting (TCSPC) with two-photon laser-scanning microscopy (2pLSM), resulting in two-photon fluorescence lifetime imaging (2pFLIM). TCSPC measures the time between the detection of a single photon and the reference laser pulse, reconstructing the fluorescence decay profile with high temporal resolution (Becker, 2012).

The advent of 2pFLIM has enabled researchers to visualize signalling events in small neuronal compartments, such as dendritic spines, with unparalleled spatiotemporal precision (Yasuda, 2012). One of the use of FRET biosensors is monitoring proteolysis, for example during LTP (Stawarski et al., 2014). Proteolysis, like the kinase-driven processes discussed earlier, is essential for synaptic plasticity. Yet, despite its critical role, proteolytic activity remains relatively understudied in the context of sLTP.
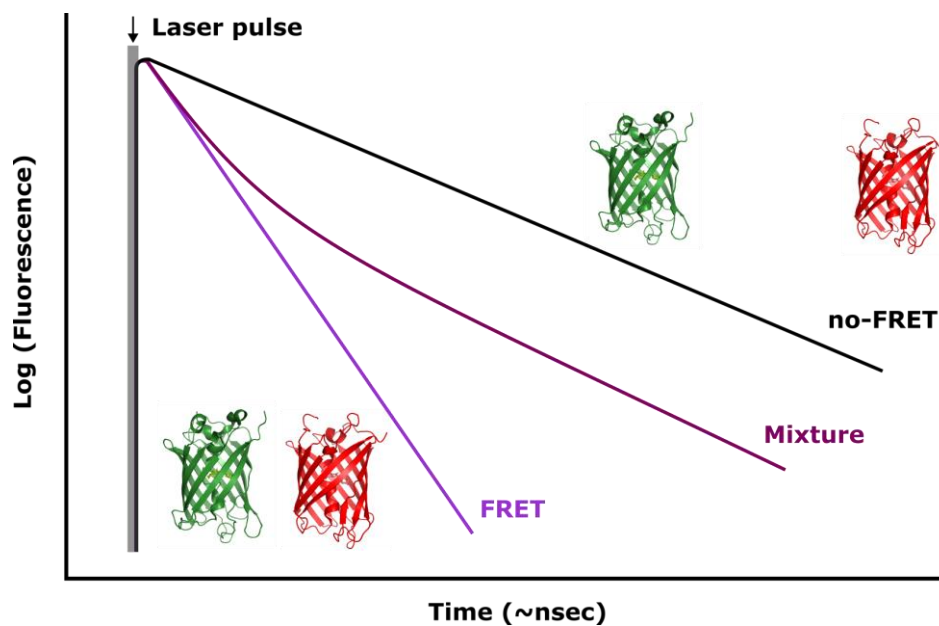
Figure 7. Fluorescence Lifetime Imaging (FLIM)

The fluorescence decay time of the donor molecule is measured relative to the reference laser pulse. When no FRET occurs, the decay follows a monoexponential function, with a slower decay as photons are emitted later on average. In the presence of FRET, the decay becomes faster because part of the energy is transferred to the acceptor, resulting in quicker photon emission by the donor.

If the imaged population contains a mixture of molecules undergoing FRET and those not undergoing FRET, the observed decay can be described by a double-exponential function. By fitting this function, the relative fractions of each population can be quantified. Adapted from Yasuda (2012).

Extracellular proteases

Structural plasticity does not occur in a vacuum. Cells, including neurons are surrounded by extracellular matrix (ECM) proteins which interacts with most of cell-surface proteins, therefore changes in dendritic spine shape must influence ECM and at the same time, ECM is expected to influence spine's shape. How extensive is a remodelling of ECM during structural plasticity, is still not well described, but in many tissues proteolysis of ECM is required for cell's shape changes or its movement. Also in LTP, extracellular proteolysis of proteins (including ECM proteins, cell adhesion molecules and cell surface receptors) is a fundamental mechanism that supports the signalling pathways engaged in the process of regulation of gene expression and cytoskeleton reorganization. There is increasing number of studies showing that synaptic plasticity is intricately linked to the restructuring of the extracellular space through the proteolytic cleavage of ECM components and cell adhesion molecules (CAMs) (Sonderegger & Matsumoto-Miyai, 2014).

A critical role of proteolysis in LTP is the processing of extracellular proBDNF into its mature form, mBDNF, a conversion essential for early-phase LTP (E-LTP) (Pang & Lu, 2004). This transformation enables mBDNF to activate tropomyosin receptor kinase B (TrkB), triggering downstream signalling pathways that promote synaptic strengthening.

Several extracellular proteases contribute to LTP, including tissue plasminogen activator (tPA), plasmin, Matrix Metalloproteinase 9 (MMP-9), neuropsin, and neurotrypsin. For instance, neuropsin plays a role in CAMs cleavage, while neurotrypsin is involved in the cleavage of agrin, a process essential for synapse maturation and plasticity (Conant et al., 2015; Tomimatsu et al., 2002; Tsilibary et al., 2014).

The tPA/plasmin system is a particularly well-documented proteolytic pathway in LTP. This system converts plasminogen into active plasmin, which participates in critical signalling events at the synapse (Tomimatsu et al., 2002). Plasmin may also activate MMP-9, integrating this system with additional downstream signalling processes required for synaptic remodelling (Chakraborti et al., 2003; Davis et al., 2001; Zhi Liu et al., 2005).

MMP-9 has been considered as a key downstream effector within tPA/plasmin system, contributing to several overlapping effects for those proteases. These include the cleavage of proBDNF into mBDNF, the processing of adhesion molecules like β-dystroglycan, and the activation of integrins. Collectively, these actions modulate the function of critical synaptic receptors, including NMDA and AMPA receptors, which are essential for LTP (Huntley, 2012; Michaluk et al., 2007; Nagy et al., 2006).

Among the proteases that regulate synaptic functions, MMP-9 has emerged as a pivotal regulator of spine morphogenesis and synaptic plasticity (Gorkiewicz et al., 2015; Magnowska et al., 2016; Sonderegger & Matsumoto-Miyai, 2014; Wang et al., 2008). By reshaping the extracellular environment and modulating receptor functions, MMP-9 plays a central role in orchestrating the molecular and structural changes required for LTP. Despite their established importance, the precise regulatory mechanisms of these proteolytic processes remain an area of active investigation.

Matrix Metalloproteinase 9

MMP-9 is a 92 kDa zinc- and calcium-dependent endopeptidase, belonging to the gelatinase subfamily. It is synthesized as an inactive precursor, pre-proMMP-9, which includes an N-terminal signal peptide that directs the enzyme to secretory pathway. Within the endoplasmic reticulum, the signal peptide is cleaved, producing proMMP-9, which is subsequently packaged into secretory vesicles and released into the extracellular space.

ProMMP-9 contains a propeptide domain that acts as a pseudo-substrate, preventing premature activation of the enzyme. Activation of MMP-9 requires proteolytic cleavage of the propeptide by other enzymes, such as MMP-3 or plasmin. This cleavage exposes the active catalytic site, converting proMMP-9 into its enzymatically active form, which is essential for its biological functions (Van den Steen et al., 2002).

Central to MMP-9 enzymatic activity is its catalytic domain, which houses a zinc ion binding site and three fibronectin type II inserts. These inserts are critical for enhancing substrate binding, particularly to gelatin (Dayer & Stamenkovic, 2015). The catalytic domain zinc ion resides at the active site and is coordinated by three histidine residues and a catalytic glutamic acid residue (E402), essential for its enzymatic function (Rowsell

et al., 2002). Additionally, five calcium ions contribute to the structural stability of the enzyme, ensuring its proper configuration during catalytic activity.

A proline-rich, heavily O-glycosylated linker connects the catalytic domain to the C-terminal hemopexin-like domain. This linker provides flexibility to the enzyme and influences the conformation of its domains, affecting substrate specificity (Rosenblum et al., 2007). The hemopexin-like domain, located at the C-terminus, plays a critical role in anchoring MMP-9 within the ECM. It optimizes the orientation of the catalytic domain, enhancing proteolytic activity and substrate specificity. Moreover, the hemopexin-like domain facilitates interactions with other proteins, further broadening the functional scope of MMP-9 (Dayer & Stamenkovic, 2015; Dufour et al., 2010)

MMP-9 is expressed in various cell types, including, e.g., neurons, glia, neutrophils, and monocytes. While its activity is predominantly extracellular, MMP-9 has also been identified in specific intracellular locations. In the nucleus of neurons, muscle cells, and glia, MMP-9 may influence nuclear processes (Hill et al., 2012; Yeghiazaryan et al., 2012).

MMP-9 has a wide range of molecular targets, therefore its activity must be tightly regulated to prevent unintended proteolysis (Cauwe et al., 2007; Egeblad & Werb, 2002). One of the critical mechanisms ensuring this regulation is described above removal of its propeptide. An additional layer of control is provided through local translation and activity-dependent synthesis. MMP-9 mRNA undergoes activity-dependent translation in response to strong neuronal stimulation (Dziembowska et al., 2012; Gkogkas et al., 2014; Janusz et al., 2013). Once locally translated and released, MMP-9 activity is further regulated through membrane binding and internalization. The enzyme interacts with cell adhesion molecules such as CD44, integrins, and receptors like LRP-1 and LRP-2, which facilitate its sequestration and regulate its activity at the cell membrane (Bauvois, 2012; Bourguignon et al., 1998; Van Den Steen et al., 2006). The final layer of MMP-9 activity regulation is provided by tissue inhibitors of metalloproteinases (TIMPs), particularly TIMP-1, which has the ability to inhibit MMP-9 activity (Brew & Nagase, 2010). These regulatory mechanisms collectively ensure that MMP-9's activity is spatially and temporally controlled, supporting its roles in cellular signalling and structural remodelling while protecting tissue integrity.

MMP-9 is engaged in both physiological and pathological processes. It serves as a critical mediator of ECM remodelling and signalling regulation, influencing tissue remodelling, cellular differentiation, and migration (Bauvois, 2012; Van den Steen et al., 2002). MMP-9 also regulates growth factor activity, including the release of insulin-like growth factor 1 (IGF-1), amplifying IGF1R-mediated signalling pathways (Chattopadhyay & Shubayev, 2009; Furuta et al., 2023; Rorive et al., 2008).

First link of MMP-9 and neuronal plasticity processes came from studies on kainate-induced epileptic seizures. These seizures, known to induce significant plasticity in the dentate gyrus, were accompanied by the upregulation of TIMP1 mRNA in this brain region (Nedivi et al., 1993; Zagulska-Szymczak et al., 2001). Follow-up research demonstrated that kainate injections also increase MMP-9 mRNA, protein, and activity levels in the dentate gyrus, implicating MMP-9 in the processes underlying neural plasticity (Szklarczyk et al., 2002).

MMP-9 has also been linked to spatial learning. Learning tasks that enhance spatial memory have been shown to elevate MMP-9 mRNA and protein levels (S. Meighan et al., 2006). Conversely, the inhibition of MMP-9, either through antisense oligonucleotides or pharmacological inhibitors, disrupts LTP and impairs learning (P. Meighan et al., 2007; Nagy et al., 2006).

Environmental enrichment, a condition that provides enhanced sensory and cognitive stimulation, also promotes brain plasticity via MMP-9. Studies have shown that enriched environments upregulate MMP-9 activity, contributing to adaptive structural and functional changes in the brain (W. Cao et al., 2014; Foscarin et al., 2011).

MMP-9 protein localizes at the synaptic cleft and within dendritic spines, with a notable preference for smaller-sized spines (Michaluk et al., 2007; Szepesi et al., 2014; Wilczynski et al., 2008). Moreover, MMP-9 synthesis occurs locally at activated synapses in response to strong neuronal stimulation. This activity-dependent, postsynaptic translation ensures rapid production of MMP-9 precisely at the sites of synaptic remodelling. Such spatially and temporally regulated synthesis allows MMP-9 to selectively mediate synaptic plasticity, dynamically supporting structural remodelling processes at synapses undergoing potentiation (Dziembowska et al., 2012; Gkogkas et al., 2014; Janusz et al., 2013).

The influence of MMP-9 on dendritic spine morphology is bidirectional. Under conditions of excessive MMP-9 activity, spines elongate and take on filopodia-like shapes, which are less effective at synaptic transmission. Conversely, when MMP-9 activity is physiologically balanced, by its endogenous inhibitor TIMP-1, spines adopt a mature, mushroom-shaped morphology associated with stronger synaptic transmission (Magnowska et al., 2016; Michaluk et al., 2011). MMP-9 is also essential for the stable expansion of dendritic spines during plasticity (Wang et al., 2008).

During LTP, MMP-9 is required for the conversion of small spines into larger, mushroom-shaped spines. This process is accompanied by the clustering, immobilization, and accumulation of AMPAR at the postsynaptic membrane, which are crucial for strengthening synaptic responses. By facilitating these changes, MMP-9 ensures that the structural modifications of dendritic spines are robust and support long-term synaptic plasticity (Szepesi et al., 2014).

MMP-9 is capable to drive spine remodelling by targeting a wide range of molecules that influence synaptic structure and function. Some of those target proteins that are present at the synapses and are directly related to sLTP (Sonderegger & Matsumoto-Miyai, 2014). Important MMP-9 substrates directly connected to spine remodelling are: Neurologin 1 (Ngl1), ICAM5 and proBDNF.

Neuroligin-1 cleavage by MMP-9 was demonstrated to occur within seconds upon glutamate uncaging. This process is critical for pre-postsynaptic rearrangements (Peixoto et al., 2012)

ICAM5 was demonstrated to be cleaved by MMP-9 within minutes from the NMDAR stimulation. This process leads to AMPAR subunits phosphorylation and increase of their presence at the synapse (Conant et al., 2010, 2015; Lonskaya et al., 2013)

proBDNF was demonstrated to be a substrate for MMP-9 in astrocytic cultures where MMP-9 dependent conversion of proBDNF to mBDNF was resulting in TrkB activation (Hwang et al., 2005). Similar dependency was observed in pentyneletetrazole (PTZ) induced kindling, that leads to mBDNF levels increase but not in MMP-9 $^{-/-}$ animals (Mizoguchi et al., 2011). However, we are still lacking direct evidence for the relevance

of MMP-9 dependent BDNF maturation in physiological plasticity context and if it occurs at the synaptic spine.

Moreover, considering importance of IGF/IGFIR signalling for sLTP and literature evidence for MMP-9 ability to amplify IGF1R signalling that has been demonstrated in several models, this interaction also should be investigated in the context of dendritic spine plasticity (Chattopadhyay & Shubayev, 2009; Furuta et al., 2023; Rorive et al., 2008).

Neurotrophic factors in LTP

Neurotrophic factors are a group of proteins that play a critical role in the growth, survival and maintenance of neurons. This group contain classical neurotrophins: Nerve Growth Factor (NGF), Brain Derived Neurotrophic Factor (BDNF), Neurotrophin-3 (NT3) and Neurotrophin- 4/5 (NT4/5), as well as non-standard neurotrophic factors such as: insulin-like growth factors (IGFs), fibroblast growth factors (FGFs) and vascular endothelial growth factors (VEGFs), protein families that all regulate neuronal plasticity (Dyer et al., 2016; H. Park & Poo, 2012). As discussed above, for NMDAR dependent sLTP two of these factors, BDNF and IGF1, were identified to directly contribute to spine enlargement (Harward et al., 2016; Tu et al., 2023).

Brain Derived Neurotrophic Factor (BDNF)

BDNF is extensively studied neurotrophin in the context of synaptic plasticity. Numerous studies have demonstrated its critical role in memory formation and cellular plasticity, highlighting its importance in learning processes (Lu et al., 2008; H. Park & Poo, 2012; Poo, 2001). BDNF was the second identified neurotrophin after nerve growth factor (NGF) and was initially recognized as a factor supporting neuronal survival (Barde et al., 1982).

BDNF is initially synthesized as pre-proBDNF, containing an N-terminal signal peptide that directs it to the secretory pathway. Within the endoplasmic reticulum (ER), the signal peptide is removed, producing proBDNF, a 30 kDa precursor protein. ProBDNF can then be processed through proteolytic cleavage into mature BDNF (mBDNF, 13 kDa) and a 15 kDa pro-domain.

There is ongoing debate about whether proBDNF cleavage occurs intracellularly or extracellularly, as endogenous proBDNF levels in the brain are relatively low, making these processes challenging to study. The general ratio of mBDNF to proBDNF in brain lysates is approximately 90% mBDNF and 10% proBDNF (Dieni et al., 2012; Matsumoto et al., 2008). However, electron microscopy of perisynaptic BDNF does not reflect this significant difference, suggesting that BDNF processing may vary depending on its origin—either from the soma or from local translation at dendritic spines (An et al., 2008; Tongiorgi et al., 2004).

Intracellular processing of proBDNF is mediated by furin within the Golgi apparatus, ensuring the availability of mBDNF for sustained plasticity. This mechanism has been shown to be essential for the maintenance of L-LTP (Pang et al., 2016). In contrast, extracellular processing was demonstrated to be particularly important during the induction and early phases of LTP. Proteases such as tissue plasminogen activator (tPA)/plasmin and MMP-9 contribute to proBDNF cleavage, facilitating E-LTP induction (Gray & Ellis, 2008; Mizoguchi et al., 2011; Pang & Lu, 2004).

The exact mechanisms of proBDNF processing at the synaptic terminal remains unclear. In contrast to that, the mechanism and timing of BDNF release had been well established.

In hippocampus BDNF is released from both pre- and postsynaptic compartments at CA3-CA1 synapses. Those processes are driven by neuronal activity and are associated with LTP. Postsynaptic release, in particular, plays a critical role in sLTP, supporting both the induction and maintenance of synaptic plasticity (Brigadski et al., 2005; Harward et al., 2016; Kuczewski et al., 2008; Lin et al., 2018).

The two forms of BDNF—mBDNF and proBDNF—have opposing effects on synaptic plasticity and neuronal excitability. While mBDNF promotes plasticity, increases excitability (Gibon et al., 2015; Pang et al., 2016) and drives local translation at synaptic sites, further supporting its role in strengthening synaptic connections (Kang & Schuman, 1996; Schratt et al., 2004), proBDNF leads to LTD induction and reduced excitability (Gibon et al., 2015; Woo et al., 2005). These effects are mediated by distinct receptors: mBDNF acts through TrkB, while proBDNF binds to p75^{NTR} (Sakuragi et al., 2013).

Upon binding to TrkB, mBDNF induces receptor autophosphorylation, triggering multiple downstream signalling pathways:

- **MAPK Pathway:** Activation of Ras GTPases initiates a cascade culminating in ERK translocation to the nucleus, driving transcription of plasticity-related genes.
- **PI3K/Akt Pathway:** Regulates translation and survival signalling.
- **Actin Remodelling:** Activation of Rac1 and Cdc42 promotes actin cytoskeleton reorganization.
- **PLC-γ Pathway:** Hydrolyses PIP_2 into DAG and IP_3, facilitating PKC activation for cytoskeletal reorganization and releasing calcium from intracellular stores to amplify calcium-dependent signalling (Poo, 2001).

proBDNF binds to $p75^{NTR}$ with high affinity. While its exact molecular role in LTP remains unclear, $p75^{NTR}$ is known to modulate synaptic plasticity by influencing spine density, receptor subunit expression, and synaptic signalling (Woo et al., 2005). Additionally, $p75^{NTR}$ is engaged in astrocytic recycling of proBDNF and facilitating its conversion to mBDNF. Through $p75^{NTR}$, proBDNF can be taken up and reprocessed for release as mBDNF, supporting neurotrophic signalling and synaptic strengthening (Bergami et al., 2008; Vignoli & Canossa, 2017).

Insulin-like growth factor 1

IGF-1 is a member of the insulin superfamily and a non-classical neurotrophic factor with a pivotal role in the development of the central nervous system (CNS). IGF-1 levels are highest prenatally, supporting critical developmental processes, but remain detectable in the brain throughout life. IGF-1 can be synthesized locally by most cell types and also enters the brain from circulation, with the liver serving as the primary source of systemic IGF-1. This growth factor is closely associated with cognitive functions, particularly learning and memory formation (Zhihui Liu et al., 2017; Nishijima et al., 2010; Stern et al., 2014; Trejo et al., 2007). Moreover, IGF-1 has been shown to directly contribute to sLTP (Tu et al., 2023).

IGF-1, like other secretory proteins, is initially synthesized as pre-proIGF-1. Following entry into the ER, the N-terminal signal sequence is cleaved, resulting in proIGF-1. The propeptide, also known as the E-peptide, is located at the C-terminus. ProIGF-1 can either undergo intracellular proteolysis before secretion or be secreted in its proIGF-1 form. Unlike BDNF, whose TrkB binding requires propeptide removal, proIGF-1 retains full

potency to activate its receptor, IGF1R, making maturation non-essential for receptor-mediated effects (Durzynska et al., 2013).

IGF-1 is released by neurons in an activity-dependent manner, triggered by Ca^{2+} influx (P. Cao et al., 2011). Upon release, IGF-1 binds to IGF1R, a receptor tyrosine kinase highly expressed in the hippocampus (S. Liu et al., 2024; Ogundele et al., 2018; Tu et al., 2023). IGF1R activation leads to receptor autophosphorylation, creating docking sites for adaptor proteins like insulin receptor substrate (IRS). IRS serves as a scaffold protein linking IGF1R signalling to the PI3K/Akt and Ras/MAPK pathways, both of which are also activated by BDNF/TrkB signalling (Chiu & Cline, 2010; Dyer et al., 2016). Notably, IGF-1 and BDNF exhibit a synergistic relationship, with both factors enhancing neuroprotective responses when co-applied, further emphasizing their complementary roles in central nervous system health and plasticity (McCusker et al., 2006).

IGF-1 signalling through IGF1R is intricately regulated by Insulin-like Growth Factor Binding Proteins (IGFBPs), which modulate the bioavailability and activity of IGF-1. IGF-1 exhibits a significantly higher affinity for IGFBPs than for its receptor, enabling IGFBPs to exert precise control over IGF-1's actions. Among the six IGFBPs expressed in the brain, IGFBP2 is the most abundant one, and plays a particularly pivotal role in synaptic plasticity (Burgdorf et al., 2023; Khan et al., 2019; Russo et al., 2005; W. Sun et al., 2024).

Initially thought to inhibit IGF signalling by sequestering IGFs, IGFBP2 is now recognized as both a buffer and facilitator of localized IGF signalling. By increasing IGF-1 local availability for IGF1R, IGFBP2 enhances receptor-mediated effects (Guan et al., 1996; Russo et al., 1999). This regulatory function, however, requires proteolytic cleavage of IGFBPs to release IGFs for receptor interaction (Forbes et al., 2012). MMPs are among the primary enzymes involved in IGFBP processing, with MMP-3, MMP-9, and pregnancy-associated plasma protein-A (PAPP-A) specifically implicated in IGFBP2 cleavage. This proteolysis facilitates IGF-1 release and enhances its downstream signalling effects (Fowlkes et al., 1995; Rorive et al., 2008).

The structure of IGFBPs includes three key domains: an N-terminal IGF binding domain (IGF BD1), a linker region, and a C-terminal IGF binding domain (IGF BD2). Proteolytic cleavage sites are localized within the flexible linker region, where IGF-IGFBP2 binding

further increases accessibility to proteases (Jaipuria et al., 2022). Cleavage in this region reduces the affinity of IGFBP2 for IGF, allowing IGF-1 to interact more readily with IGF1R. This finely tuned mechanism underscores the complexity and specificity of IGFBP-mediated regulation in IGF-1 signalling but still requires investigation to identify whether it is directly involved in IGF1R activation during sLTP.

AIMS AND OBJECTIVES

The aim of this thesis was to elucidate the role of MMP-9 activity in the structural long-term potentiation on a single dendritic spine and to identify its key substrates involved in this process.

Objectives:
To achieve this aim, the following objectives were established:

1. Induction of sLTP: Induce sLTP under conditions excluding MMP-9 and analyse the timing of the resulting effects.

2. MMP-9 Release: Determine the precise timing of MMP-9 release induced by activation.

3. BDNF/TrkB Signalling: Investigate the role on MMP-9 and its activity in BDNF/TrkB signalling.

4. IGF1/IGF1R Signalling: Assess whether IGF1/IGF1R signalling is modulated by MMP-9 activity.

5. Role of IGFBPs: Validate the role of IGFBPs in sLTP and IGF1/IGF1R signalling pathways.

6. Dominant IGFBP Identification: Identify the dominant IGFBP expressed in the hippocampus.

7. IGFBP2 as an MMP-9 Substrate: Identify whether IGFBP2 serves as a substrate for MMP-9.

8. IGFBP2 Localization: Confirm the localization of IGFBP2 at synapses.

MATERIALS AND METHODS

Molecular cloning

The cloning procedure description exclude routine steps, such as DNA purification and transformation and culturing of competent bacteria, which were conducted following standard methods: PCR reactions were performed using Q5® High-Fidelity 2X Master Mix (NEB, #M0492), and molecular construct assembly (vector + inserts) was achieved with NEBuilder® HiFi DNA Assembly, following the manufacturer's instructions (NEB, #E2621).

DNA purification after PCR or restriction digestion was carried out using Syngen Gel/PCR Mini Kit (Syngen Biotech, #SY201010), Zymoclean Gel DNA Recovery Kit (Zymo Research, #D4001), or DNA Clean & Concentrator-5 (Zymo Research, #D4004). Chemically competent bacteria (NEB, #C3040, #C2987) were transformed and cultured following the respective manufacturer's protocol.

Plasmid DNA for cloning and sequencing applications was isolated using miniprep kits (A&A Biotechnology, #020-50). For applications involving dissociated neuronal cultures and gene gun transfection, plasmid DNA was purified with the NucleoBond Xtra Maxi kit (MACHEREY-NAGEL, #740414) or EndoFree Plasmid Maxi Kit (QIAGEN, #12362).

The concentration and purity of plasmid DNA were measured using a NanoDrop 1000 spectrophotometer (Thermo Scientific). DNA concentration was determined by absorbance at $\lambda = 260$ nm, assuming an absorbance of 1.0 corresponds to 50 µg/ml. Purity was assessed via the A260/A280 ratio, with values between 1.8 and 2.0 indicating high purity.

Generation of Enzymatically Inactive pCMV MMP-9 E402A Variant

The enzymatically inactive MMP-9 E402A variant was generated using site-directed mutagenesis on the murine MMP-9 template under a CMV promoter (Addgene #121172). A single point mutation at nucleotide 1205 was introduced, replacing adenine (A) with cytosine (C). This nucleotide change altered the codon from GAG (glutamate) to GCG

(alanine) at position 402 of the MMP-9 amino acid sequence, rendering the protein enzymatically inactive (Michaluk et al., 2009).

Mutagenesis Primers:

- o **Forward Primer**:
  5' TGGCAGCGCACGCGTTCGGCCATGC 3'
- o **Reverse Primer**:
  5' GCATGGCCGAACGCGTGCGCTGCCA 3'

Generation of pCAG MMP-9 and pCAG MMP-9 E402A Constructs

To enhance expression levels, the pCAG promoter was utilized to replace the original promoter in the constructs. The Addgene vector pCAG-mEGFP (#127389) served as the backbone for this process.

1. **Vector Preparation**: The vector pCAG-mEGFP was digested with *EcoRI* and *SalI* to generate a 4720 bp fragment. The digested fragment was purified for subsequent HiFi DNA assembly.
2. **Insert Preparation**: Inserts were amplified by PCR from either the pCMV MMP-9 E402A or pCMV MMP-9 templates. The primers used for amplification of 2218 bp fragments were as follows:
   - o **Forward Primer**:
     5' TGTCTCATCATTTTGGCAAGGTGGTGGAATTCATGAGTC 3'
   - o **Reverse Primer**:
     5' CAGAGGGAAAAAGATCCGTCGACTTAAGCGTAATCTGGAA CATC 3'
3. **Construct Assembly**: HiFi DNA Assembly was employed to integrate the PCR-amplified inserts into the linearized pCAG vector, resulting in the pCAG MMP-9 and pCAG MMP-9 E402A constructs.
4. **Applications**:
   - o **pCAG MMP-9**: Used in MMP-9 rescue experiments and IGFBP2 cleavage assays.
   - o **pCAG MMP-9 E402A**: Designed to study the non-enzymatic roles of MMP-9 and served as a negative control in MMP-9 rescue experiments.

Generation of fluorescent pH-Sensitive MMP-9 E402A (pCAG MMP-9 E402A SEP)

To visualize MMP-9 release events from vesicles, I fused it with a pH-sensitive variant of GFP (SEP) that becomes quenched in low pH environments. This design allows detection of release events as the fluorescence signal increases upon exposure to the neutral extracellular pH.

1. **Vector Preparation**: The vector pCAG MMP-9 E402A was linearized by digestion with the *NotI* restriction enzyme.
2. **Insert Preparation**: The SEP insert was amplified by PCR from the pZac2.1gfaABC1D_VAMP2_SEP template provided by Dr. Piotr Michaluk. The following primers were used for 717 bp fragment amplification:
   - **Forward Primer**:
     5' CCATACGATGTTCCAGATTACGCTATGAGTAAAGGAGAAGA ACTTTTCACTGG 3'
   - **Reverse Primer**:
     5' GTTTAAACGGGCCCTCTAGACTCGAGCGGCCGCTTATTTGT ATAGTTCATC 3'
3. **Construct Assembly**: The linearized vector and amplified SEP insert were assembled using the HiFi DNA Assembly method to produce the final pCAG MMP-9 E402A SEP construct.
4. **Applications**: Used in Expansion microscopy study on localisation of MMP-9 vesicles, TIRF and 2p imaging of MMP-9 release

Generation of fluorescent pH-Stable MMP-9 E402A (pCAG MMP-9 E402A Gamillus)

To ensure visualization of MMP-9 regardless of its localization, we fused it with Gamillus, a pH-stable variant of GFP. This approach mitigates the limitations of conventional GFP, due to its insensitivity to low pH, thereby enabling reliable imaging across various cellular environments.

1. **Vector Preparation**: The vector pCAG MMP-9 E402A was linearized by digestion with the *NotI* restriction enzyme.

2. **Insert Preparation**: The SEP insert was amplified by PCR from the pZac2.1gfaABC1D_VAMP2_SEP template provided by Dr. Piotr Michaluk. The following primers were used for 717 bp fragment amplification:
   - o **Forward Primer**:
     5' CCATACGATGTTCCAGATTACGCTATGAGTAAAGGAGAAGA ACTTTTCACTGG 3'
   - o **Reverse Primer**:
     5' GTTTAAACGGGCCCTCTAGACTCGAGCGGCCGCTTATTTGT ATAGTTCATC 3'
3. **Construct Assembly**: The linearized vector and amplified SEP insert were assembled using the HiFi DNA Assembly method to produce the final pCAG MMP-9 E402A SEP construct.

Applications: Used in 2p imaging of MMP-9 release as control.

Generation of pCAG HA IGFBP2 FLAG

To facilitate the purification of full-length IGFBP2, an HA tag was introduced at the N-terminus of the protein. Additionally, a FLAG tag was added at the C-terminus to enable the detection of cleaved variants.

1. **Vector Preparation**: The vector pCAG-mEGFP was digested with *EcoRI* and *SalI* and 4720 bp fragment was purified.
2. **Inserts Preparation**: The murine IGFBP2 sequence was amplified from brain homogenate cDNA. HA tag was introduced between signal sequence and N-terminal of mature IGFBP2 and FLAG tag sequence was introduced at the C-terminus of the protein. The following primers were used for amplification of two inserts:
   1. **Signalling sequence** 156 bp:
      - o **Forward Primer:**
        5' TCATTTTGGCAAGGTAGTGGAATTCGCCAACATGCTGCC GAGATTG 3'
      - o **Reverse Primer containing HA sequence:**
        5' TAATCTGGAACATCGTATGGGTAGGCGCGCACCCCGGGG CC 3'
   2. **IGFBP2** 886 bp:

- o **Forward Primer containing HA sequence:**
  5' CCATACGATGTTCCAGATTACGCTGAGGTGCTGTTCCGCT
  GCCC 3'
- o **Reverse Primer containing FLAG sequence:** 5'
  GGCAGAGGGAAAAAGATCTTACTTATCGTCGTCATCCTTGT
  AATCCTGCACACTTTGGGCATGG 3'

3. **Construct Assembly:** HiFi DNA Assembly was employed to integrate the PCR-amplified inserts into the linearized pCAG vector, resulting in the pCAG HA IGFBP2 FLAG construct.

4. **Applications**: Used in IGFBP2 cleavage assay

MMP-9 Cleavage Assay with IGF1-IGFBP2 Complexes

HEK293 cells were cultured in Dulbecco's Modified Eagle Minimum Essential Medium (DMEM) containing 10% fetal bovine serum (FBS) at 37 ˚C in a 5% CO_2 atmosphere. Cells were transfected with plasmids encoding pCAG HA IGFBP2 FLA and pCAG IGF1 (Ratio 3:2); pCAG MMP-9; pCAG MMP-9 E402A or pCAG mCherry for control media. Transfections were performed using TurboFect™ Transfection Reagent (Thermo Scientific, #R0533) according to the manufacturer's protocol. After four hours, the transfection medium was replaced with serum-free optimem medium supplemented with pyruvate. Media were collected following overnight expression.

To prepare the collected media for the cleavage assay, 1M HEPES buffer was added to a final concentration of 20 mM, along with a EDTA-free protease inhibitor cocktail (Roche, #04693132001), $ZnCl_2$ (final 1 µM), and $CaCl_2$ (final 5 mM). 200 µl of media containing IGF1-IGFBP2 complexes were incubated with 10 µL of HA-tagged agarose resin for 30 minutes at room temperature with gentle rocking. After incubation, the resin was centrifuged gently for 5 seconds, and the supernatant was discarded. The resin was washed three times with unconditioned medium buffered with HEPES to remove non-specific proteins.

To assess cleavage, the IGF1-IGFBP2 complexes bound to the HA resin were exposed to various media conditions. 200 µl of media from HEK293 cells expressing pCAG MMP-9, pCAG MMP-9 E402A, or pCAG mCherry were added to the resin. Additionally, recombinant catalytic domain of MMP-9 (400 ng/µL) or unconditioned medium

(negative control) was used in parallel. Activation of MMP-9 was achieved by adding APMA (final concentration 1 mM), while DMSO was used as a control (All variants presented on the Figure 8). All reaction mixtures were incubated for six hours at 37 ˚C with gentle rocking. Following incubation, the resin was centrifuged, and the supernatant was collected for further analysis.

Western Blot Analysis for Cleavage Assay

Supernatants collected from the cleavage assay were mixed with 4x loading dye containing 20 mM BondBreaker TCEP solution (Thermofisher #77720) and 20 mM EDTA. The samples were heated at 95 °C for 5 minutes to denature proteins, followed by rapid cooling on ice. Twenty microliters of each sample were loaded onto Any kD™ Mini-PROTEAN TGX Precast Protein Gels (Bio-Rad) for SDS-PAGE.

Protein separation was performed using SDS electrophoresis, and proteins were subsequently transferred onto a PVDF membrane (Trans-Blot Turbo Mini 0.2 µm PVDF, Bio-Rad, #1704156) using the Trans-Blot Turbo Transfer System, following the manufacturer's protocol.

The PVDF membrane was blocked with EveryBlot Blocking Buffer (Bio-Rad) for 10 minutes at room temperature to prevent non-specific binding. The primary antibody rat anti-FLAG (#MA1-142, Invitrogen), diluted 1:1000 in the blocking buffer was applied overnight at 4 °C. Secondary antibody, HRP-conjugated anti-rat (Invitrogen, #31470), diluted 1:5000 in blocking buffer, was applied for 1 hour at room temperature. Protein detection was performed using the SuperSignal Chemiluminescent substrate (Thermo Fisher, #34580).

Images of the detected proteins were captured using ChemiDoc imaging equipment and analysed using Image Lab software.
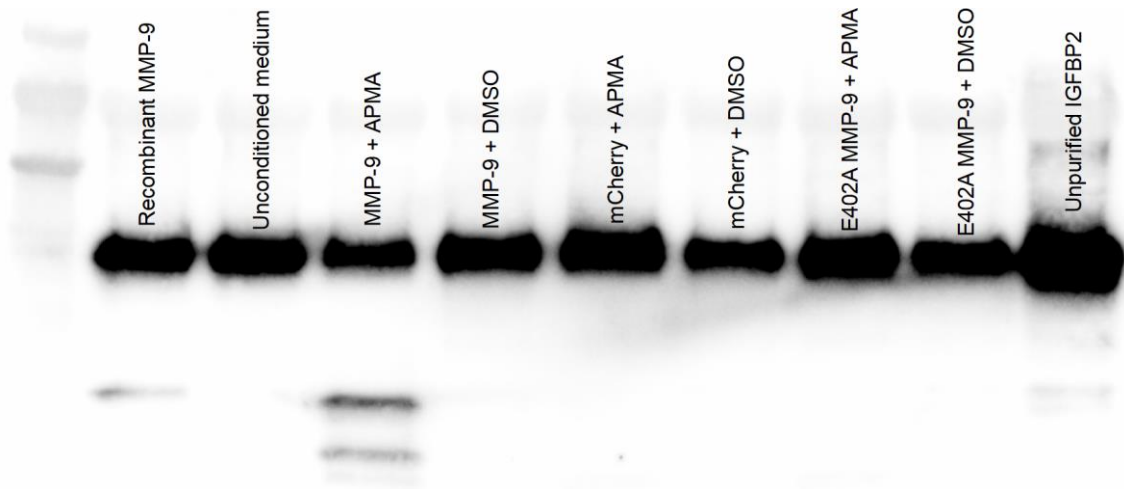
Figure 8. Exemplary western blot of IGFBP2 cleavage under different experimental conditions

Conditions list: line 1-8 supernatants of IGF1-IGFBP2-complexes bound to the HA resin in following conditions; line 1 - Recombinant MMP-9 – unconditioned media with MMP-9 catalytic domain 400 ng/μL; line 2 - Unconditioned media, line 3 – media conditioned by HEK cells expressing MMP-9 with addition of APMA; line 4 - media conditioned by HEK cells expressing MMP-9 with addition of DMSO; line 5 - media conditioned by HEK cells expressing mCherry with addition of APMA; line 6 - media conditioned by HEK cells expressing mCherry with addition of DMSO; line 7 - media conditioned by HEK cells expressing E402A MMP-9 with addition of APMA; line 8 - media conditioned by HEK cells expressing E402A MMP-9 with addition of DMSO; line 9 – media conditioned by HEK cells expressing IGFBP2 and IGF1.

For the clarity purpose in the result section I am presenting only variants treated with MMP-9 activated by APMA or DMSO as a control. Reactions were repeated for all variants on separate conditioned HEK-cell media four times.

Animals

All animal procedures were approved by the Max Planck Florida Institute for Neuroscience, and Use Committees and were conducted in accordance with the NIH Guide for the Care and Use of Laboratory Animals, as well as with the Animal Protection Act of Poland (directive 2010/63/EU). In this study I used 4-8 days-old mice of both sexes. C57BL/6J mice were obtained from Charles River and MMP-9$^{-/-}$ (B6.FVB(Cg)-Mmp9tm1Tvu/J) were purchased from Jackson Laboratory. B6.FVB(Cg)-Mmp9tm1Tvu/J mice have been maintained by mating heterozygotes MMP-9$^{+/-}$. The genotype of each animal used was verified before preparing slices using PCR of genomic

DNA isolated from the tail. For experiments we used MMP-9$^{-/-}$ mice and their wild-type (WT) littermates. Primers used for genotyping B6.FVB(Cg)-Mmp9tm1Tvu/J:

Common Forward: 5' TCC TCC ATC CAC AGG CAT AC 3'
Wild type Reverse: 5' TCC CAC TTG AGG CCT TTG A 3'
Mutant Reverse: 5' CCT TCT ATC GCC TTC TTG ACG 3'

Additionally, I utilized MMP-9 conditional knockout (MMP-9$^{fl/fl}$) mice generated by the Yasuda Lab. These mice were created on a C57BL/6J genetic background and harbour a conditional knockout of the *mmp9* gene. The targeted *mmp9* locus includes loxP sites flanking exon 7 and exon 8, which encode the catalytic domain of MMP-9. This design enables precise deletion of the catalytic domain upon Cre recombinase expression, allowing for tissue-specific or temporally controlled knockout of MMP-9.

Primary Hippocampal Neuronal Culture and Transfection

Glass coverslips pretreatment:

Glass coverslips (#1.5, Ø 18 mm, Hecht Assistent®) were cleaned, sterilized, and coated for cell seeding. Coverslips were rinsed with distilled water, treated with 2 M sodium hydroxide, and cleaned ultrasonically. After rinsing and immersion in 96% ethanol, they were sterilized at 180°C for 3 hours.

Two days before seeding, coverslips were coated with poly-D-lysine (100 µg/ml) in borate buffer (pH 8.5) and incubated overnight at room temperature. After rinsing with sterile water, they were coated with laminin (10 µg/ml in PBS with MgCl$_2$ and CaCl$_2$) and stored at 4°C until use.

Primary culture preparation:

Neurons for primary hippocampal cultures were obtained from postnatal day 0 (P0) Wistar rat pups. The pups were subjected to hypothermia by placing them on ice, followed by decapitation. The brains were carefully removed and placed in cold DM/Ky solution (1 mM Kynurenic acid, 10 mM MgCl^2 in dissociation medium, DM). Hippocampi were dissected out and washed three times in cold DM/Ky. The tissues were digested through two successive incubations in warm papain solution (37°C for 15 minutes each). The

enzymatic reaction was stopped by washing the tissues three times in MEM supplemented with FBS.

The tissues were mechanically dissociated using a 1 ml Pasteur pipette to achieve a single-cell suspension. The suspension was centrifuged once at 1,000 rpm for 5 minutes at room temperature. After removing the supernatant, the cell pellet was resuspended in MEM/FBS. The cell density was determined using a Bürker chamber, and cells were seeded onto pre-prepared coverslips at a density of 150,000 cells per coverslip. After 3 hours of incubation to facilitate adhesion, the medium was replaced with Neurobasal-A medium supplemented with B27. Cultures were maintained in an incubator at 37°C with 5% CO_2.

Transfection of primary culture:

Mixed primary neuronal cultures, were transfected between DIV7 and DIV9 using Lipofectamine® 3000 (Invitrogen®, #L3000008). DNA-Lipofectamine complex was prepared according to manufacturer protocol.

The conditioned growth medium (750 µl) was removed from the well and mixed 1:1 with fresh medium. The DNA-Lipofectamine complex was added dropwise to the well, and the cultures were incubated at 37°C for 1 hour. After incubation, the medium containing the transfection reagent was replaced with the prepared conditioned medium to support long-term neuronal growth.

Hippocampal organotypic culture and transfection

Organotypic hippocampal slices were prepared from postnatal day 4–8 (P4–P8) mouse pups of various genotypes, including C57BL/6J, MMP-9+/+, MMP-9-/-, and MMP-9fl/fl. Animals were anesthetized with isoflurane, decapitated, and the brains quickly removed under sterile conditions. Hippocampi were dissected and sliced into 350–400 µm thick transverse sections using a McIlwain tissue chopper (Ted Pella, Inc.).

Slices were transferred to hydrophilic PTFE membranes (Millicell, Merck, Cat# PICMORG50) positioned at the air-medium interface. Cultures were maintained in Minimal Essential Medium (MEM; Life Technologies) supplemented with: 20% heat-inactivated horse serum, 12.9 mM D-glucose, 5.2 mM $NaHCO_3$, 30 mM HEPES buffer,

2 mM MgSO$_4$, 1 mM CaCl$_2$, 1 mM L-glutamine, 0.075% ascorbic acid and 1 μg/ml insulin. Slices were incubated at 37°C with 5% CO$_2$. Half of the medium was replaced every 2–3 days to maintain culture health.

After 7–13 days in vitro, hippocampal slices were transfected using the GeneGun method (BioRad).

Plasmid-coated gold particles (1.0 μm; 8–12 mg of gold beads) were prepared as previously described (Woods & Zito, 2008). Briefly, to prepare DNA-coated gold beads, 3.5 ml of dilute PVP solution was made by mixing 5 μl of 20 mg/ml PVP stock with 3.5 ml of 100% ethanol. Approximately 30 inches of tubing was dried using N$_2$ gas for at least 20 minutes. 1.0 μm gold beads (6-8 mg) were combined with 100 μl of 0.05 M spermidine and sonicated for 20 seconds. Next, 50 μl of DNA was added to the gold/spermidine mixture and vortexed, followed by the addition of 100 μl of 1 M CaCl$_2$ and a brief sonication. After 10 minutes of precipitation, the beads were washed three times with 1 ml of ethanol. The gold/DNA was resuspended in the PVP solution, and the mixture was aspirated into dried tubing using a syringe, leaving 2 inches dry at each end. Gold was allowed to sediment at the bottom of the tubing and the solution was aspirated to the syringe. The tubing was dried while rotating with N$_2$ gas for 5 minutes. Finally, the tubing was cut, and the cartridges were stored in labelled scintillation vials with desiccation pellets at 4°C.

Slices were transfected through shooting high pressure (180 PSI) helium gas through cartridges.

Specific DNA compositions for gene gun bullets included constructs such as:

- structural change experiments
    - pCAG GFP 30 μg DNA
    - pCAG GFP and pCAG Cre ratio 3:2 50 μg DNA (Imaged 4-7 days from transfection to ensure gene knockout and clearance of MMP-9 mRNA and protein),
    - pCAG GFP and pCAG MMP-9 ratio 3:2 50 μg DNA,
    - pCAG GFP and pCAG MMP-9 E402A ratio 3:2 50 μg DNA,
- MMP-9 release experiments

44

- o pCAG MMP-9 E402A SEP and pCAG mCherry ratio 1:1 50 μg DNA,

- o pCAG MMP-9 E402A Gamillus with pCAG mCherry ratio 1:1 50 μg DNA,

- o pCAG MMP-9 E402A SEP and pCAG mCherry IRES TeTx 1:1 50 μg of DNA,

- TrkB activation experiment (Imaged within 12-48 hours after transfection due to increased cell death upon prolonged TrkB overexpression)

- o pCAG TrkB GFP and pCAG PLC RFP in ratio 1:3 50 μg DNA,

- IGF1R activation experiment

- o pCAG IGF1R GFP and pCAG p58 mCherry in ratio 1:3 50 μg DNA,

- o pCAG IGF1R GFP, pCAG p58 mCherry, pCAG MMP-9 in ratio 1:3:1 50 μg DNA,

- o pCAG IGF1R GFP, pCAG p58 mCherry, pCAG MMP-9 E402A in ratio 1:3:1 50 μg DNA,

After the transfection, slices were returned to the incubator and allowed to express the transfected plasmids. Imaging experiments were conducted 1-7 days after transfection unless indicated differently.

Two-Photon Fluorescence Lifetime Imaging Microscopy (2pFLIM)

Fluorescence lifetime imaging was performed using a custom-built two-photon fluorescence lifetime imaging microscope, following previously established protocols (Harward et al., 2016; Murakoshi et al., 2011). A Ti-sapphire laser (Coherent, Chameleon) tuned to a wavelength of 920 nm provided excitation, with laser power adjusted to 1.2–1.6 mW. The emitted fluorescence was collected using a 60× water immersion objective (numerical aperture 0.9, Olympus) and split with a dichroic mirror (565 nm). The green channel emission was filtered with a 510/70 nm band-pass filter (Chroma), and the red channel with a 620/90 nm band-pass filter (Chroma). Photon detection for both channels was performed using low transfer time spread photoelectron multiplier tubes (H7422-40p; Hamamatsu), enabling precise fluorescence lifetime measurements.

Photon counting was achieved using a time-correlated single-photon counting board (Time-harp 260; Pico-Quant) and processed using the FLIMage software package developed in C# (https://github.com/ryoheiyasuda/FLIMage_public). Imaging parameters were optimized based on the experiment type. For measurements of relative spine volume and sensor activation, images were acquired at 128×128 pixels at a frame rate of 7.8 Hz, with 24-frame averaging. Spine volume was quantified using mEGFP fluorescence. For MMP-9 SEP release imaging, 64×64 pixel frames were collected at the same frame rate but without frame averaging to capture dynamic release events with high temporal resolution.

Two-Photon Glutamate Uncaging

Two-photon glutamate uncaging was performed using a second Ti-sapphire tuneable laser (Coherent, Chameleon) set to a wavelength of 720 nm. The laser delivered a train of 6 ms pulses with an intensity of 2.7–3.0 mW, repeated 30 times at 0.5 Hz. These pulses were targeted approximately 0.5 µm away from the spine of interest, as previously described (Colgan et al., 2018; Murakoshi et al., 2011). The power and length of the pulses were calibrated on neurons expressing calcium sensor GCaMP6f to ensure precise single spine stimulation (Figure 9).
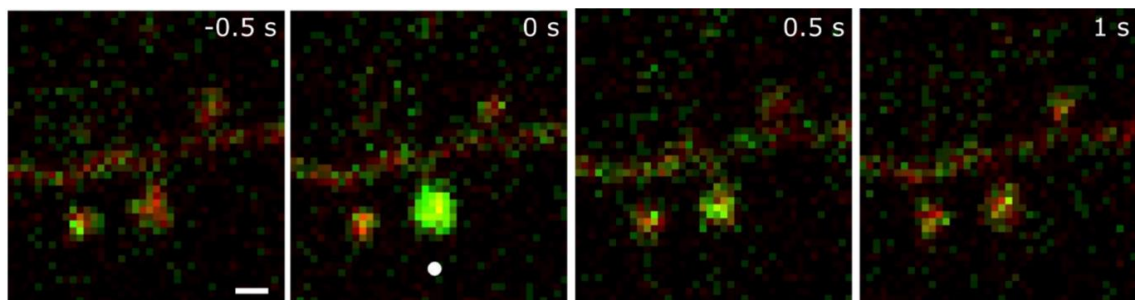
Figure 9. Demonstration of accuracy of glutamate uncaging
Time series of images of dendrite from neuron expressing cytoplasmic mCherry and GCaMP6f (calcium sensor increasing its fluorescence upon Ca^{2+} binding). Upon 720 nm laser pulse (indicated by white dot) at time 0 s, GCaMP6f temporarily increase fluorescence locally at stimulated spine. Scale bar – 0.5 µm.

Organotypic hippocampal slices were maintained in Mg^{2+}-free artificial cerebrospinal fluid (ACSF) containing 127 mM NaCl, 2.5 mM KCl, 4 mM $CaCl_2$, 25 mM $NaHCO_3$, 1.25 mM NaH_2PO_4, and 25 mM glucose, supplemented with 1 µM tetrodotoxin (TTX; Tocris) and 2 mM 4-Methoxy-7-nitroindolinyl-caged-L-glutamate (MNI-caged

glutamate; Tocris). The ACSF was aerated with a carbogen gas mixture (95% O_2 and 5% CO_2) to maintain pH balance. Experiments were conducted at room temperature (24–26°C).

Spine volume change measurements

Spines of GFP-expressing pyramidal neurons in CA1 subfield of hippocampus were imaged sequentially up to four spines located on separate secondary apical dendrites. For treatment, slices were perfused in ACSF (see above) with either DMSO (for control; final concentration 0.08%), MMP-9/MMP-13 Inhibitor I (Cat: 444252, Calbiochem) in DMSO final concentration 5 μM or broad spectrum MMPs inhibitor GM6001 (Cat: 364205, Sigma-Aldrich) in DMSO final concentration 10 μM for 30 minutes before the start of sLTP protocol.

For the spines of CA1 neurons from MMP-9$^{-/-}$ animals expressing: GFP, GFP and MMP-9 or GFP and E402 MPP-9, images were collected simultaneously up to four dendritic spines located on separate secondary apical dendrites.

For the spines of CA1 neurons from MMP-9$^{fl/fl}$ animals expressing: GFP or GFP and CRE recombinase, images were collected simultaneously up to four dendritic spines located on separate secondary apical dendrites.

For the IGFBPs inhibition experiment slices were pre-treated in culture media for 2 hours with either DMSO (for control; final concentration 0.08%) or IGFBPs inhibitor (NBI-31772) in DMSO final concentration 10 μM. Next spines of GFP-expressing pyramidal neurons in CA1 subfield of hippocampus were imaged simultaneously up to four spines located on separate secondary apical dendrites. Slices were perfused in ACSF with either DMSO or IGFBPs inhibitor in DMSO final concentration 10 μM.

All experiments were repeated on organotypic cultures from at least three different dissections.

MMP-9 release 2P imaging

Spines were imaged sequentially from distinct proximal secondary dendrites of pyramidal cells in CA1 co-expressing MMP9-SEP and mCherry, or MMP9-SEP and mCherry-

IRES-TTX, or MMP-9 Gamillus and mCherry. Additionally for obtaining specificity of observed effects to NMDAR signalling, group of neurons co-expressing MMP9-SEP and mCherry was perfused in ACSF with AP5 (d-2-amino-5-phosphonovalerate) at final concentration 100 μM.

Two-photon FLIM data analyses

The analysis of FRET sensor activation was performed as previously described (Harward et al., 2016). To measure the fraction of a donor bound to an acceptor, I fit a fluorescence lifetime curve summing all pixels over a whole image with a double exponential function convolved with the Gaussian pulse response function:

$$F(t) = F_0[P_D H(t, t_0, \tau_D, \tau_G) + P_{AD} H(t, t_0, \tau_{AD}, \tau_G)]$$

F_0 - peak fluorescence before convolution
P_D - fraction of free donor and
P_{AD} - fraction of donor bound with acceptor
τ_D - fluorescence lifetime of the free donor
τ_{AD} - fluorescence lifetime of donor bound with acceptor
τ_G - width of the Guassian pulse response function
t_0 - time offset
$H(t)$ - fluorescence lifetime curve with a single exponential function convolved with the Gaussian pulse response function:

$$H(t, t_0, \tau_D, \tau_G) = \frac{1}{2} \exp\left(\frac{\tau_G^2}{2\tau_D^2} - \frac{t - t_0}{\tau_D} \right) \mathrm{erfc}\left(\frac{\tau_G^2 - \tau_D(t - t_0)}{\sqrt{2}\,\tau_D \tau_G} \right)$$

erfc - complementary error function.

I fixed τ_D to the fluorescence lifetime obtained from free eGFP (2.6 ns). To generate the fluorescence lifetime image, I calculated the mean photon arrival time, $\langle t \rangle$, in each pixel as:

$$\langle t \rangle = \int t F(t) dt / \int F(t) dt$$

then, the mean photon arrival time is related to the mean fluorescence lifetime, $\langle \tau \rangle$, by an offset arrival time, t_0, which is obtained by fitting the whole image:

$$\langle \tau \rangle = \langle t \rangle - t_0$$

For small regions-of-interest (ROIs) in an image (spines or dendrites), I calculated the binding fraction (P_{AD}) as:

$$P_{AD} = \tau_D(\tau_D - \langle \tau \rangle)(\tau_D - \tau_{AD})^{-1}(\tau_D + \tau_{AD} - \langle \tau \rangle)^{-1}$$

TrkB and IGF1R activation measurements

FLIM images were collected simultaneously for up to four ROI located on distinct secondary apical dendrites of CA1 pyramidal neurons co-expressing: TrkB-GFP and PLC-RFP; IGF1R-GFP and p58 mCherry; IGF1R-GFP, p58 mCherry, MMP-9 or IGF1R-GFP, p58 mCherry, E402A MMP-9. Cells included in experiment had average initial binding fraction not higher than 45%. Slices were treated with either DMSO, Inhibitor I or IGFBPs Inhibitor as described above. Experiments were repeated on organotypic cultures from at least three different dissections.

Total internal reflection fluorescence imaging

Dissociated neuronal cultures transfected with mCherry and either MMP-9 SEP or BDNF SEP were imaged using total internal reflection fluorescence (TIRF) microscopy between 19–21 DIV. Imaging was performed in an extracellular solution (ES buffer) at pH 7.4, containing: 145 mM NaCl, 2.5 mM KCl, 10 mM D-(+)-glucose, 10 mM HEPES, 0.4 mM Trolox, 1 µM TTX, 4 mM $CaCl_2$.

Recordings were analyzed using Suite2p software (Pachitariu et al., 2017), which enabled automatic detection of events and fluorescence extraction. Fluorescent traces were then further processed with a MATLAB script to extract information about the timing of event occurrence.

Immunostaining of Neuronal Cultures

Three-week-old primary mixed neuronal cultures grown on glass slides were fixed in PBS containing 4% paraformaldehyde and 4% sucrose for 8 minutes at 37°C. Following fixation, the cells were washed three times with PBS containing 4% sucrose and permeabilized with 0.25% Triton X-100 for 2 minutes.

Blocking was performed in PBS with 3% BSA and 0.1% Triton X-100 for 1 hour at room temperature. The cultures were then incubated overnight at 4°C with primary antibodies (see antibody details in Table 1). After three washes with PBS, secondary antibodies were applied for 1 hour at room temperature.

Following secondary antibody incubation, the cultures were washed three times with PBS and stained with Hoechst 33342 (0.1 μg/ml) for 5 minutes. After an additional PBS wash, samples were mounted on glass slides using Fluoromount-G mounting medium (#00-4958-02). Images were collected with confocal microscope (Inverted Axio Observer Z.1, 40× objective with Airyscan). The acquired images were processed using the Zen (Zeiss) and analysed with the ImageJ (http://rsbweb.nih.gov/ij/).

	Primary antibody	Secondary antibody
Identification of IGFBP2 signal localization astrocytes vs neurons	anti-GFAP (1:100, #13-0300)	anti Rat Alexa 488-conjugated (1:500, #A21208)
Identification of IGFBP2 signal localization astrocytes vs neurons	Mouse anti-MAP2 (1:1000 #AB5622)	Anti Mouse Alexa 568-conjugated (1:500, #A32727)
Identification of IGFBP2 signal localization astrocytes vs neurons, Identification of IGFBP2 signal localization on dendritic spines	Rabbit anti-IGFBP2 (1:1000, #AB188200)	anti Rabbit Alexa 647-conjugated (1:500, #A21244)
Identification of IGFBP2 signal localization on dendritic spines, Expansion Microscopy	Rat anti-RFP (1:500 #M11217)	anti Rat Alexa 568-conjugated (1:500 #A11077)
Expansion Microscopy	Chicken anti-GFP (1:500, #13970)	anti Chicken Alexa 488-conjugated (1:500 #A11039)

Table 1. List of Antibodies and Their Applications

Expansion Microscopy of Rat Hippocampal Neuronal Cultures

Rat hippocampal neuronal cultures were transfected with plasmids encoding tdTomato (for visualizing dendritic spine morphology) and either MMP-9-SEP or BDNF-SEP. Following paraformaldehyde fixation, the samples were immunolabeled (see immunostaining protocol) and expanded using Basic Protocol 1: proExM for Cultured Cells (Asano et al., 2018).

Gelation Process: Fixed cells were incubated in 0.1 mg/ml Acryloyl-X SE (AcX) in PBS for 2–3 hours at room temperature. After two 15-minute PBS washes, coverslips with cultured cells were placed in a gelation chamber constructed with spacers and a small amount of gelation solution. The gelation solution contained sodium acrylate (8.6 g/100 ml), acrylamide (2.5 g/100 ml), N,N′-methylenebisacrylamide (0.15 g/100 ml), sodium

chloride (11.7 g/100 ml), TEMED (0.2 g/100 ml), and ammonium persulfate (APS, 0.2 g/100 ml) in PBS. The solution was kept chilled on ice to prevent premature polymerization. Additional gelation solution was applied to ensure even coverage, and the chamber was sealed with a lid. The chamber was incubated at 37°C for 1 hour to allow gelation.

Digestion and Expansion: After gelation, the chamber was carefully opened, and the gel was trimmed around the immunolabeled cells using a 3D-printed cutter. The gel, along with the cell culture substrate, was immersed in digestion buffer containing Proteinase K (8 U/ml) for at least 2–3 hours at room temperature. The gel was gently detached from the glass slide using a fine brush and incubated overnight in digestion buffer to ensure complete digestion. Following digestion, the gel was washed with PBS.

For expansion, the gel was sequentially immersed in fresh water for three 20-minute intervals, resulting in approximately 4× expansion and optical clarity. The gel was then trimmed to focus on regions containing immunolabeled cells and transferred to an appropriate container for immediate imaging.

Imaging and Analysis: Expanded samples were imaged using a confocal microscope (Cell Discoverer 7, 50× objective with Airyscan 2). Images of vesicles and neuronal morphology were reconstructed using Imaris Image Analysis Software. The expansion factor for each sample was determined by dividing the average area of nuclei (Hoechst signal) post-expansion by the pre-expansion area.

cLTP Stimulation and Collection of Organotypic Hippocampal Slices for RNA Analysis

Three-week-old organotypic hippocampal slice cultures were maintained on PTFE inserts and prepared for stimulation as follows: Inserts were rinsed with ES solution (composition described previously) and then incubated for 10 minutes in a stimulation buffer containing 20 µM Bicuculline, 200 µM Glycine, 3 µM Strychnine, and 4 mM $CaCl_2$ in ES.

After stimulation, the inserts were rinsed with fresh ES solution containing 2 mM $MgCl_2$ and 2 mM $CaCl_2$ and then returned to the culture medium. Time point 0 hour was

collected immediately following the ES rinse, while additional groups were collected after 6 and 24 hours.

Collection for RNA Analysis: At each time point, slices were scraped from the inserts using a sterile scalpel, placed into RNAlater solution, and stored at 4°C. Samples were processed within two weeks of collection.

RNA Isolation, Reverse Transcription, and Quantitative PCR (RT-qPCR)

RNA Isolation: Total RNA was isolated from hippocampal organotypic slices using the RNeasy Mini Kit (Qiagen, Cat# 74104), following the manufacturer's protocol. Tissue homogenization was performed in a QIAzol Lysis Reagent (QUIAGEN, #79306) using an IKA Ultra-Turrax T8 homogenizer (IKA). Genomic DNA contamination was eliminated by DNase treatment using the RNase-Free DNase Set (Qiagen, Cat# 79254). RNA concentration and purity were measured using a NanoDrop 2000 spectrophotometer (Thermo Fisher Scientific).

Reverse Transcription: Complementary DNA (cDNA) synthesis was performed using the SuperScript IV VILO with ezDNAse kit (Thermo Fisher Scientific, Cat# 11766050) according to the manufacturer's instructions.

Quantitative PCR: Gene expression analysis was conducted using TaqMan probes (TaqMan Gene Expression Assay, Thermo Fisher Scientific, Cat# 4331182; probe identifiers provided in (Table 2) and TaqMan Fast Advanced Master Mix (Thermo Fisher Scientific, Cat# 4444557). Quantitative PCR (qPCR) was performed on a StepOne Real-Time PCR System (Thermo Fisher Scientific). Relative mRNA expression levels were calculated using the comparative $2^{-\Delta\Delta Ct}$ method and normalized to the reference gene GAPDH as an endogenous control.

Gene	Probe identifier	Gene	Probe identifier
GAPHD	Mm99999915_g1	IGFBP4	Mm00494922_m1
IGFBP2	Mm00492632_m1	IGFBP5	Mm00516037_m1
IGFBP3	Mm01187817_m1	IGFBP6	Mm00599696_m1

Table 2. List of the TaqMan® Gene Expression Assays ID.

Data analyses

Spine volume change was calculated using formula $\Delta F/F0 = (F-F0)/F0$ where F is a sum of fluorescence in a given time from the ROI containing the spine of the interest and F0 represents average of F from the baseline of first 5-7 time points (before sLTP protocol).

MMP-9 SEP release was calculated using traces from 13 spines, where normalized intensity was calculated using formula $\Delta F/F0 = \frac{(F-F0)}{F0}$, where F_0 corresponds to average fluorescence of frames preceding the uncaging pulse and frames of uncaging pulse. Later the results from uncaging pulses 2-18 were averaged. Same analysis was performed for data collected from red channel corresponding to cytoplasmic mCherry treated as spine volume.

Binding fraction (P_{AD}) was normalized by subtracting averaged baseline binding fraction (P_{AD0}; before sLTP protocol) with a formula $P_{AD} - P_{AD0}$.

Cleavage Site Prediction, and Structural Modelling of Protein Interactions

Protein sequences were retrieved from the UniProt Knowledgebase (UniProt KB) for the following proteins:

- IGFBP2: P47877, residues 35-305
- MMP-9: P41245, residues 108-456
- IGF1: P05017, residues 49-118

Cleavage site predictions for IGFBP2 were performed using Prosperousplus (Li et al., 2023), employing a pretrained model for MMP-9 (M10.004). The analysis utilized IGFBP2 amino acid sequence (indicated above). Additionally, Procleave (Li et al., 2020) was applied to an AlphaFold-generated structural model of IGFBP2 (based on the same sequence). For both tools, results were ranked by cleavage probability, with a threshold cut-off set at 0.75. Sites exceeding this cut-off were prioritized for further analysis.

Predictive structural modelling of IGF-IGFBP2-MMP-9 interactions was performed using ColabFold: AlphaFold2 with MMseqs2 (v1.2) (Evans et al., 2022; Jumper et al.,

2021). Both monomeric and multimeric configurations were evaluated, and the models with the highest prediction quality scores were selected for further analysis.

Molecular graphics images and minimal distance measurements between protein atoms were generated using PyMOL Molecular Graphics System (v2.6.0a0, Schrödinger, LLC). Protein-protein interaction interfaces were analysed using PDBsum (Laskowski et al., 2018), which provided details on residue interactions across the interfaces and calculated the interaction surfaces between IGFBP2 and MMP-9.

Statistical analyses

All data are presented as mean ± SEM unless otherwise specified. The number of independent measurements (n-spines) is provided in the figure legends. Statistical comparisons between two independent samples were performed using an unpaired two-tailed Student's t-test. For grouped datasets, two-way ANOVA followed by multiple comparison tests was used (Prism 10, GraphPad).

Data showing clear signs of poor cellular health, such as dendritic blebbing or spine collapse, were excluded from the analyses.

.

RESULTS

Dendritic spine-head enlargement during sLTP depends on MMP-9 activity

The aim of this study is to investigate the contribution of MMP-9 to structural long-term potentiation (sLTP) on a single dendritic spine. As outlined in the Introduction, dendritic spines undergo rapid remodelling in response to strong stimulation, characterized by a transient volume increase followed by stabilization at a volume larger than the original.

Whereas the significance of MMP-9 for the fLTP has been established (Nagy et al., 2006; Wang et al., 2008), possible role of this enzyme in sLTP remained unknown. I suspected MMP-9 to be responsible for facilitation of signaling cascades involved in spine structural reorganization. This assumption was based on its potential role in BDNF maturation and BDNF being linked to sLTP. To address this issue, I investigated volume changes in dendritic spines under conditions of MMP-9 inhibition, aiming to determine whether its activity is required for either the transient or sustained spine volume changes. In my experiments, I focused on CA1 subfield of hippocampus, as it is a model structure for studying LTP. Murine hippocampal organotypic cultures were transfected with GFP-encoding plasmid and pyramidal neurons in CA1 region were imaged using two-photon (2P) microscopy. In order to achieve single-spine sLTP stimulation, I used 2P glutamate uncaging protocol (see Materials and Methods; Figure 10A). As discussed in the Introduction, this established experimental paradigm allows for single spine stimulation with simultaneous imaging of its volume and it is the most advanced method for the studies of molecular processes dynamics during sLTP (Figure 10B).

To investigate a role of MMP-9, I measured spine volume changes during sLTP in the presence of either 10 μM GM6001 (a broad-spectrum MMP inhibitor) or 5 μM Inhibitor I (which specifically targets MMP-9/-13), and compared these groups to control spines treated with DMSO (Figure 10C).

In the control condition, spines rapidly increased in volume following glutamate uncaging, reaching peak volume increase by 330% at 2 minutes post-stimulation. Following this initial peak, spine volume reached sustained phase at 100% increase above a baseline around 15 minutes after stimulation.

Spines in slices treated with GM6001 also grew in response to stimulation, however, to a markedly lesser degree than in control conditions, average observed growth reached 120%. Similarly to the broad spectrum inhibition, treatment with more specific Inhibitor I resulted in a smaller than control group volume peak, on average reaching 170% increase in volume.

For statistical analysis, I divided the spine volume changes into three distinct time periods (Figure 10D):1-3 minutes, corresponding to the transient phase; 9-11 minutes, representing early sustained phase and 15-20 minutes, marking the sustained phase of sLTP. The early sustained phase was separated in order to allow for event timeline comparison between volume changes and receptors activation measurements described in following sections. At each of these time periods, the volume change differences between the DMSO-treated and inhibitor-treated groups were statistically significant, highlighting an essential role of proteolytic activity during the early stages of sLTP. The absence of significant differences between the broad-spectrum inhibitor and the MMP-9/13-specific inhibitor further suggests that MMP-9 is likely the primary protease involved in regulating these early volume changes.
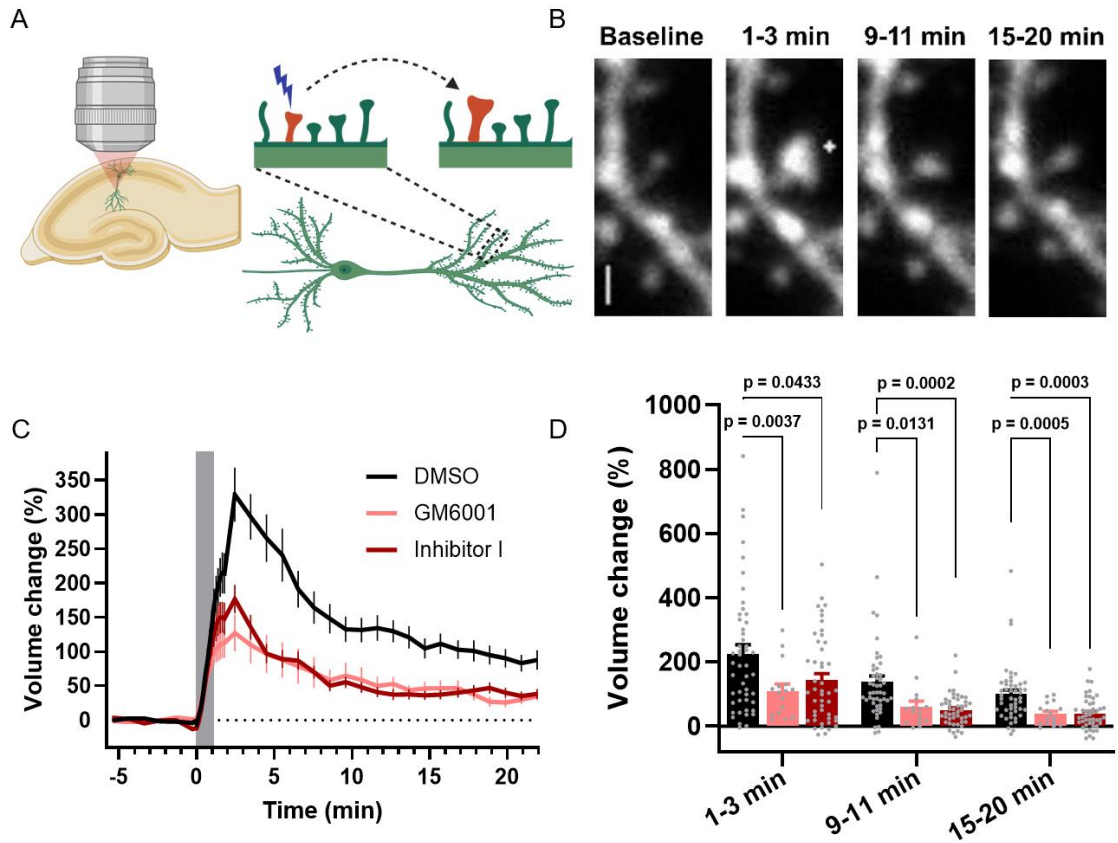
Figure 10. Dendritic Spine Growth During sLTP Depends on MMP Activity

A. Experimental arrangement: GFP-expressing neuron in CA1 subfield of hippocampus. Individual spine in secondary dendrites were stimulated using sLTP protocol leading to the spine enlargement.

B. Representative dendrite expressing GFP, at various time points from the onset of stimulation. Cross indicates uncaging spot. Scale bar - 1 μm.

C. Average spine volume changes over time for groups treated with DMSO in black (n=49), GM6001 light pink (n=16), and Inhibitor I in red (n=46). Data are mean ± SEM, the grey box indicates duration of the uncaging protocol.

D. Statistical analysis of the data in panel C. Data is shown for three time periods: 1–3 minutes (peak of spine volume change), 9–11 minutes (early sustained phase), and 15–20 minutes (sustained phase). Grey dots represent individual values. Bars are means ± SEM (colours are the same as in B). Repeated-measures two-way ANOVA followed by Tukey's multiple comparisons test.

There are over twenty subtypes of MMPs and their substrate specificity largely overlap (Cieplak & Strongin, 2017; Fields, 2015). Apparently for that reason, no fully specific, MMP-9 inhibitors are available. Importantly, both inhibitors might unspecifically affect other proteases. Therefore, to confirm my hypothesis that MMP-9 is the major MMP involved in structural plasticity, I monitored spine volume change during the sLTP protocol in GFP-expressing neurons in slices obtained from MMP-9 knockout (*MMP-9⁻/⁻*) mice and their *MMP-9⁺/⁺* littermates (Figure 11A). In *MMP-9⁺/⁺* animals, I observed

an average peak increase in spine volume change by 220%, which stabilized at 75% enlargement. In contrast, neurons from $MMP\text{-}9^{-/-}$ mice exhibited a reduced peak increase reaching only 130%, with a sustained phase at only 50% increase. Interestingly, the differences between $MMP\text{-}9^{+/+}$ and $MMP\text{-}9^{-/-}$ cells were statistically significant during both the peak (1-3 min) and early sustained (9-11 min) phases but did not reach significance during the sustained phase (15-20 min; Figure 11B).

Next, I wanted to determine whether the phenotype of decreased structural plasticity observed in $MMP\text{-}9^{-/-}$ animals can be rescued by overexpression of MMP-9. Therefore, I used $MMP\text{-}9^{-/-}$ slices and co-transfected them with the GFP plasmid together either with the full-length MMP-9 or an inactive mutant, MMP-9 (E402A) (Figure 11C). In cells expressing the MMP-9, I observed an increase in spine volume change by 230% at peak and by 70% at sustained phase closely resembling the WT profile. In contrast, in cells expressing inactive MMP-9 (E402A) I did not observe a phenotype rescue. Spines showed an increase by only 130% at peak phase and only by 35% at sustained phase. Statistically significant differences between the MMP-9 and MMP-9 (E402A)-expressing cells were observed at all three measured time points (Figure 11D).

In order to identify if the lack of the sustained phase volume deficits of sLTP in $MMP\text{-}9^{-/-}$ mice is not an effect of compensatory mechanisms, such as those dependent on other enzymes, I performed additional experiment on inducible MMP-9 knockout animal (MMP-9$^{fl/fl}$), which have been recently developed for the purpose of this project (see Materials and Methods). Neurons from organotypic hippocampal slices obtained from MMP-9$^{fl/fl}$ mice, were transfected only with GFP (Cre-) or co-transfected with GFP and Cre recombinase (Cre+) plasmids. Indeed I observed that acute knock down of MMP-9 leads to significant reduction of all sLTP phases in comparison to control conditions (Figure 11E). Spines in Cre- group reached 200% volume increase and stabilization at 50% whereas Cre+ achieved only 50% increase of the volume and stabilization at 13%. The differences between Cre+ and Cre- cells were statistically significant in all tested time periods (Figure 11F).

These findings further shown that MMP-9 proteolytic activity is crucial for both, early and sustained phase of sLTP.
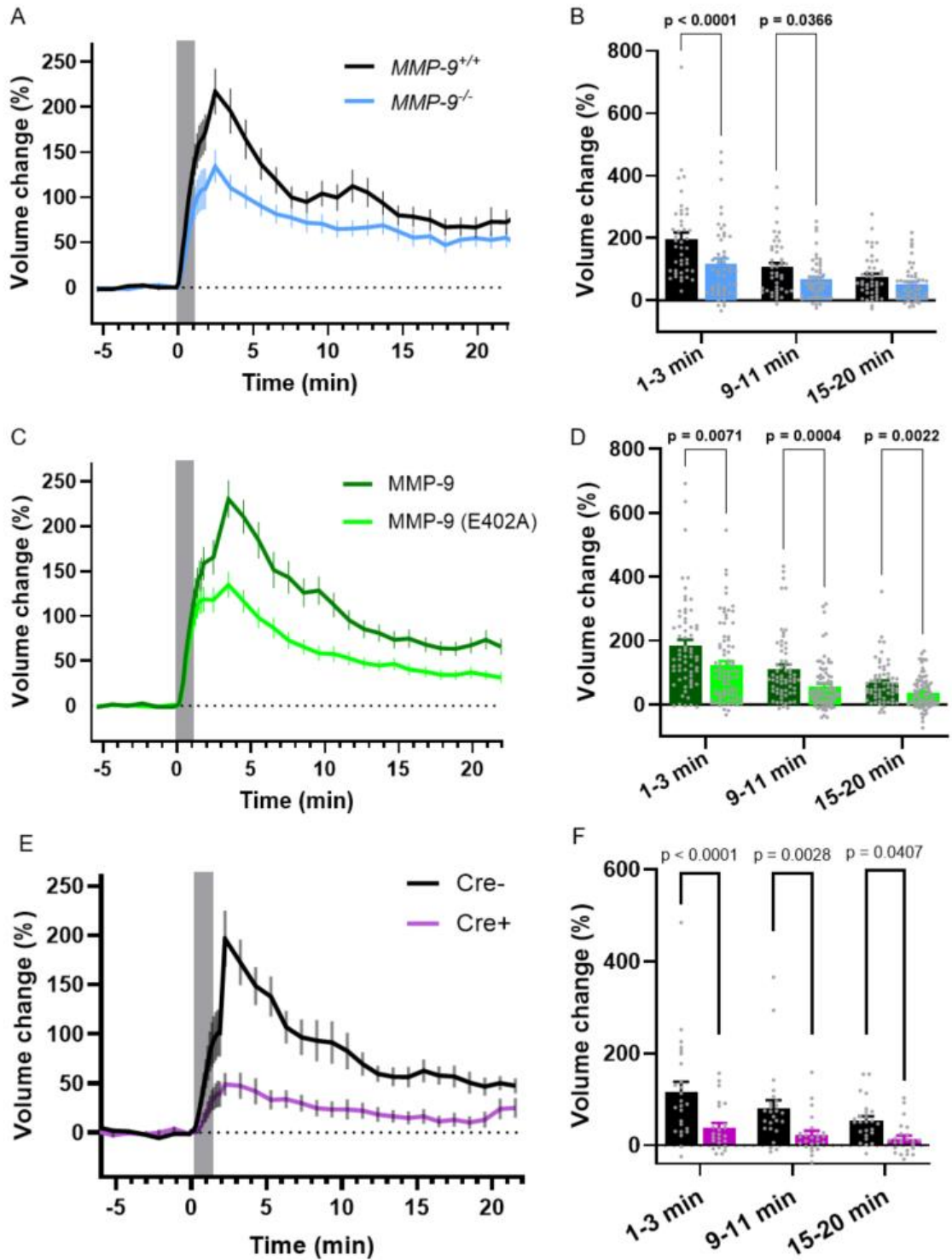
Figure 11. Dendritic Spine Growth During sLTP Is Disrupted in MMP-9^{-/-} and MMP-9^{fl/fl} Cre+, but Can Be Rescued by Overexpression of MMP-9

A. Averaged spine volume changes over time in MMP-9^{-/-} animals (blue, n=49) and in their MMP-9^{+/+} littermates (black, n=41). Data are mean ± SEM, the grey box indicates duration of the uncaging protocol. B. Statistical analysis of the data in panel A. Data is shown for three time periods: 1–3 minutes, 9-11 minutes, and 15–20 minutes. Grey dots represent individual values. Bars are means ± SEM (colours are the same as in A). Repeated-measures two-way ANOVA followed by Tukey's multiple comparisons test.

C. Averaged spine volume changes over time in MMP-9$^{-/-}$ neurons with overexpression of either MMP-9 (dark green, n=64), or inactive MMP-9 (E402A) (light green, n=82).

D. Statistical analysis of the data in panel C. Data is shown for three time periods: (1–3 minutes, 9–11 minutes, 15–20 minutes). Repeated-Measures two-way ANOVA followed by Tukey's multiple comparisons test.

E. Averaged spine volume changes over time in MMP-9$^{fl/fl}$ neurons in control conditions (Cre-; black, n=25), or in presence of Cre recombinase (Cre+; magenta, n=24).

F. Statistical analysis of the data in panel

E. Data is shown for three time periods: (1–3 minutes, 9–11 minutes, 15–20 minutes). Repeated-Measures two-way ANOVA followed by Tukey's multiple comparisons test.

Localization of vesicles carrying BDNF and MMP-9 within dendritic spines and their release upon stimulation

The above results indicate that MMP-9 is crucial for structural plasticity during sLTP at individual spines, even very early after stimulation (around 1-3 minutes) that indicate the involvement in transient phase. From the previously published data (Michaluk et al., 2007; Wilczynski et al., 2008) we know that MMP-9 is localized at postsynaptic site. However, the detailed information on where and when it can be released after stimulation was lacking. Such early involvement in sLTP, requires most probably a pre-existing MMP-9 to be present at the synapse, to be released shortly after the stimulation occurs. To address this, I decided to characterize the MMP-9 vesicles location. As a positive control I used localization of BDNF-containing vesicles, which are known to be released from spines during sLTP (Harward et al., 2016). BDNF is present in dense core vesicles that are being transported to the axonal and dendritic terminals where they undergo secretion upon increased neuronal activity (Dean et al., 2012; Harward et al., 2016; Lin et al., 2018; Zakharenko et al., 2003). Based on that I was expecting to observe similar distribution of vesicles containing BDNF and MMP-9 in dendritic spines.

To determine if MMP-9-containing vesicles can be present directly in a dendritic spine, I used expansion microscopy in dissociated neuronal cultures transfected with tdTomato and MMP-9 fused with a pH-sensitive GFP variant (superecliptic pHluorin, SEP) (Ng et al., 2002). I used this method since there are no reliable antibodies enable to detect rodent MMP-9. Expansion microscopy enables high-resolution imaging by physically

expanding the sample, achieving single-vesicle resolution and capturing the complex morphology of dendrites (Figure 12). I identified vesicles containing green fluorescence from an anti-GFP antibody (antibody successfully recognizing SEP protein) within dendrites and dendritic spines, indicating MMP-9 localization in these regions.

In parallel, I imaged cells expressing BDNF-SEP. I observed vesicles carrying BDNF within dendritic spines and shafts, supporting the postsynaptic release site for BDNF. Those results show that both proteins are localized within dendritic compartments, where they are available for rapid release in response to synaptic activity.
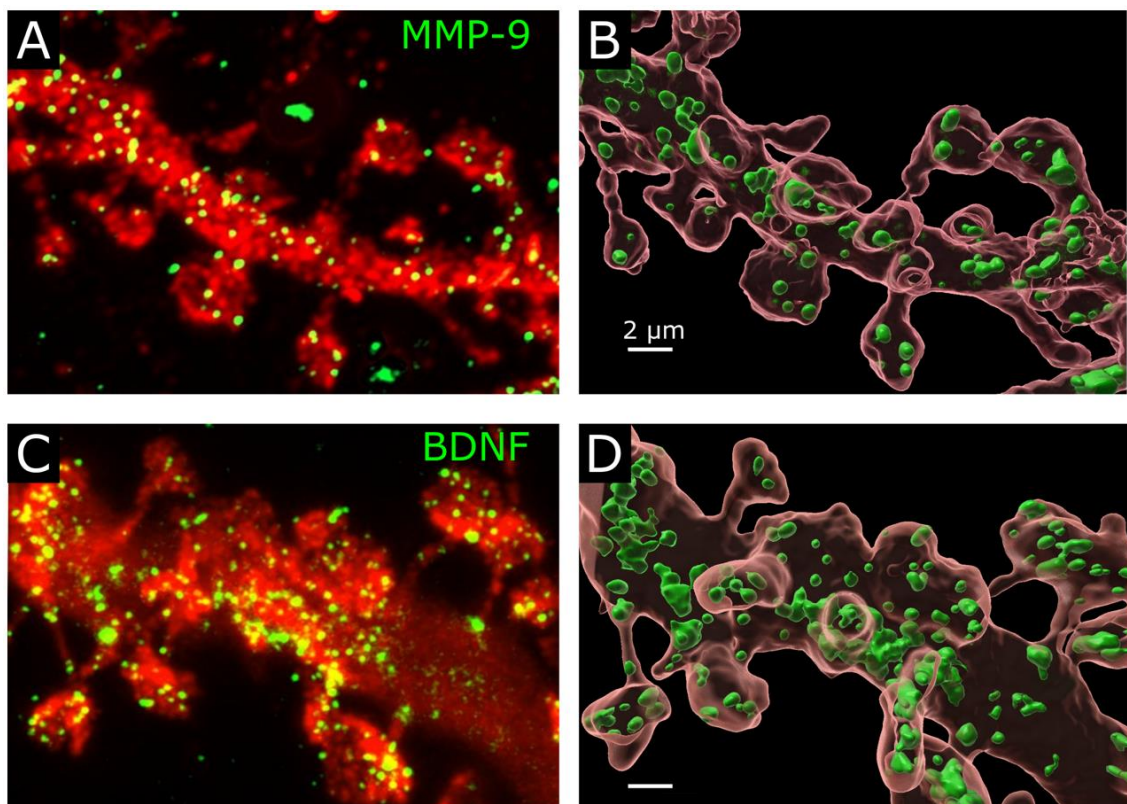
Figure 12. BDNF and MMP-9 Vesicles Localize in Dendrites and Dendritic Spines

A. Exemplary image of a dendrite expressing MMP-9 SEP (green) and cytoplasmic tdTomato (red), expanded 4x and imaged using confocal microscopy, maximum z-projection.

B. Reconstruction of the dendritic surface and vesicles carrying MMP-9. Scale bar – 2 μm (corresponding to 0.5 μm before expansion).

C. Exemplary image of a dendrite expressing BDNF SEP (green) and cytoplasmic tdTomato (red), expanded 4x and imaged using confocal microscopy, maximum z-projection.

D. Reconstruction of the dendritic surface and vesicles carrying BDNF. Scale bar – 2 μm (corresponding to 0.5 μm before expansion).

To investigate whether MMP-9 vesicles can be released in response to neuronal stimulation, I imaged dissociated neurons expressing MMP-9-SEP or BDNF-SEP (which would serve as a positive reference). BDNF has been shown to be released rapidly in response to stimulation, playing an immediate role in synaptic plasticity; however, the timing and dynamics of MMP-9 release in neurons have not been previously studied in detail.

I imaged dissociated hippocampal culture using Total Internal Reflection Fluorescence (TIRF) microscopy, which allows for high-speed imaging with decreased background fluorescence. The use of dissociated hippocampal culture in these experiments was necessary, because TIRF microscopy allows only for imaging of the cell surface close to the coverslip on which they are cultured 100-300nm from the surface of the glass.

Since SEP fluorescence is quenched at the low pH inside vesicles, the increase in pH upon membrane fusion makes release events detectable as sudden spots of increased fluorescence with exponential decay (Figure 13A-B). I was able to detect release events in both, MMP9-SEP and BDNF-SEP transfected cells. On average decay time for MMP-9 vesicles was 1.88 s and was longer than average decay time of BDNF vesicles 0.9 s (Figure 13D). This may suggest slower diffusion rate for MMP-9, which could be explained by bigger molecular size and presence of fibronectin and hemopexin domains that interact with a variety of proteins.

During imaging in solution free of Mg^{2+}, I applied electrical stimulation at a frequency resembling that of sLTP uncaging protocol. For each imaged cell, I quantified exocytosis frequency before, and after the onset of stimulation. I observed a significant increase in a vesicle release rate in response to electrical stimulation in both BDNF-SEP (Figure 13G,H) and MMP-9-SEP expressing neurons (Figure 13I). BDNF baseline release was detected at an average frequency of 0.08 Hz, which increased to 0.6 Hz during stimulation. For MMP-9, baseline release had an average frequency of 0.04 Hz, rising to 0.1 Hz during stimulation. I also measured the time between electrical stimulation and release events and presented them as relative frequency distribution for both MMP-9 and BDNF (Figure 13J). 80% of the BDNF events occurred within 0-40 s time window whereas for MMP-9 maximum release with 70% of the events occurred within 10-50 s time window.

These results demonstrate that both MMP-9 and BDNF vesicles are rapidly released in response to neuronal stimulation, suggesting that MMP-9 exocytosis may occur at similar timescales to BDNF. This strongly supports my previous results showing involvement of MMP-9 even in transient phase of sLTP. Additionally, the significant increase in vesicle release frequency supports the hypothesis that MMP-9 release is tightly regulated by LTP-related processes.
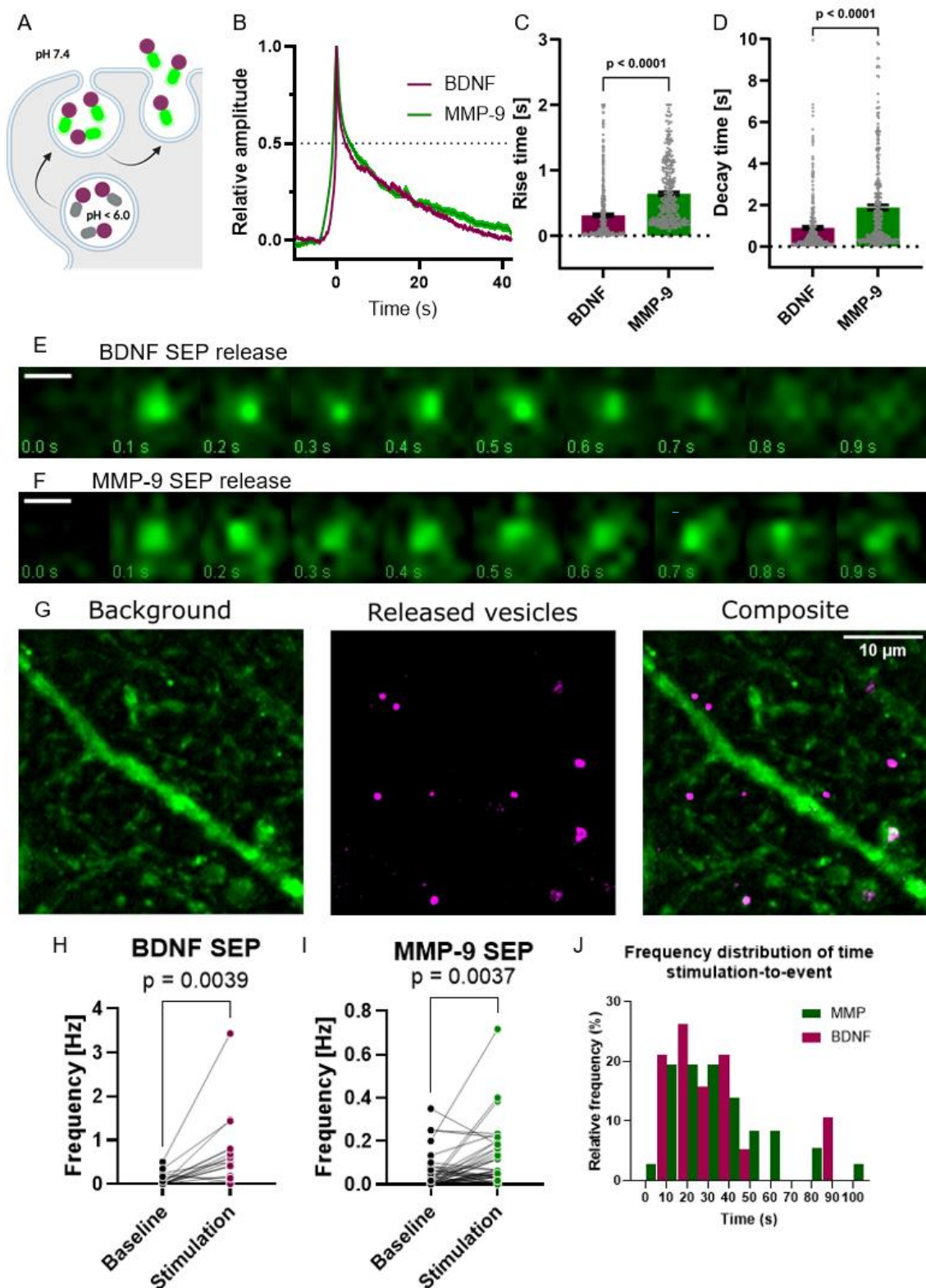
Figure 13. BDNF and MMP-9 Release During Electrical Stimulation

A. Schematic representation of SEP-tagged molecule release from dendritic spine. SEP is quenched inside vesicles with a pH < 6.0. Once the vesicles fuse with the cell membrane the pH equilibrates with the extracellular space, allowing for SEP fluorescence to become detectable.

B. Average trace of fluorescence of released vesicles aligned by peak fluorescence as t=0 (BDNF-SEP in purple and MMP-9-SEP in green).

C. Statistical analysis of vesicle fluorescence rise time for BDNF-SEP and MMP-9-SEP. t-test

D. Statistical analysis of vesicle fluorescence decay time for BDNF-SEP and MMP-9-SEP t-test.

E. Exemplary vesicle release images of the BDNF SEP, scale bar 1um.

F. Exemplary vesicle release images of the MMP-9 SEP, scale bar 1um.

G. Exemplary dendrite of BDNF SEP with a background fluorescence in green and released vesicles in magenta.

H. Statistical analysis of BDNF SEP release event frequency at the baseline and stimulation periods, using a paired t-test (p=0.0.039).

I. Statistical analysis of MMP-9 SEP release event frequency at the baseline and stimulation periods, using a paired t-test (p=0.0.037).

J. Histogram showing the frequency distribution of times of occurrence of successfully evoked BDNF-SEP (magenta) and MMP-9-SEP (green) events. Times of release after electrical stimulation were binned into 10-second intervals.

Since field electrical stimulation relies on backpropagating action potential and is not limited to a single dendritic spine, I aimed to confirm whether MMP-9 release events could be detected at individual spines during the initial stages of sLTP. To investigate this, I used two-photon (2P) microscopy combined with uncaging to determine whether release events occur near a single stimulated spine (Figure 14A). Again, I employed the MMP-9-SEP fusion protein to image released MMP-9 and mCherry for a reference dye to monitor the spine volume. I co-transfected neurons from hippocampal organotypic cultures using two plasmids – MMP-9-SEP and mCherry, and imaged dendritic spines from CA1 pyramidal neurons.

Unlike with TIRF microscopy, I could not detect discrete single-vesicle release events, but I observed a gradual increase in fluorescence of both the SEP and cytoplasmic mCherry channels. The signal in mCherry channel increased gradually upon the stimulation, indicating spine growth, while the SEP signal also increased but less pronounced than mCherry signal. Therefore, the fluorescence increase could not be solely attributed to volume changes but could be a result of mixed effect of vesicle release and recruitment of vesicles from the dendritic shaft into the spine (M. Park et al., 2006). For additional controls, I stimulated cells either in the presence of the NMDA receptor antagonist, AP5 or in neurons co-expressing Tetanus Toxin, which prevents vesicular release. In both cases, no fluorescence increase was observed in either channel (Figure

14B-C) indicating that volume change and MMP-9 release depends on NMDA receptor activation and vesicular release from postsynaptic site.

To further assess the fast kinetics of MMP-9 release after each uncaging pulse, I divided imaging data of SEP fluorescence in an activated spine, into blocks of 16 frames (2.048 s, Figure 14D), corresponding to uncaging intervals in sLTP-inducing protocol. The blocks were positioned vertically (in columns) and stacked as a rectangle in such a way that the uncaging pulse was always applied during the second frame (aligned to the second row) of the block (Figure 14D). The fluorescence data were normalized to the first two averaged frames in each block. The first seven columns represent a baseline fluorescence acquired without stimulation. This procedure allowed me to visualize the averaged fluorescence changes normalized to fluorescence before uncaging (averaged over 2 frames) as a heat map (Figure 14D). Visually brighter pixels in the heat map, indicating increases in the dendritic spine fluorescence, are located between 16th and 56th second of imaging which corresponds to the 2nd and 22nd uncaging pulse (and 2-42 s from the time of first uncaging pulse). After that period the fluorescence was back to the baseline level (Figure 14D). Therefore, for some uncaging pulses there were rapid and stable increases in fluorescence coming from SEP (Figure 14E).

To better visualize the rapid release of MMP-9 upon uncaging, I averaged the relative fluorescence changes for the 2nd -18th uncaging pulses, averaged them and plotted over time alongside fluorescence for mCherry (Figure 14E,F). While mCherry fluorescence showed a slow increase, reflecting the stimulated spine gradual volume changes, MMP-9-SEP fluorescence had a faster onset, consistent with rapid MMP-9 release in response to each uncaging pulse. Within the 0.128-0.384 second time bin (three frames after uncaging pule), the SEP signal was significantly higher than the corresponding mCherry signal in the same spines (Figure 14F).

To confirm, that MMP-9-SEP fluorescence increases were due to pH changes associated with vesicular MMP-9 release, rather than simply an increase in vesicular transport into the spine or by increased volume of the spine, I performed similar experiment using a pH-stable GFP variant, Gamillus, fused to MMP-9 (Shinoda et al., 2018). Next, I performed the same kind of analysis as for MMP-9-SEP, and I did not observe any fluorescence increase in the MMP-9-Gamillus heat map (Figure 14G). The analysis of fluorescence

changes for the 2nd-18th uncaging pulses for mCherry vs MMP-9-Gamillus fluorescence also did not reveal any significant differences (Figure 14H, I).

This analysis allowed me to distinguish volume/vesicle trafficking-related fluorescence from vesicle release, indicating that MMP-9 release is most likely to occur during the initial phase of sLTP stimulation. Thus, any effects observed after the first minute may be attributed to locally released MMP-9 in response to stimulation, providing insight into the timing of MMP-9's role in early synaptic plasticity.
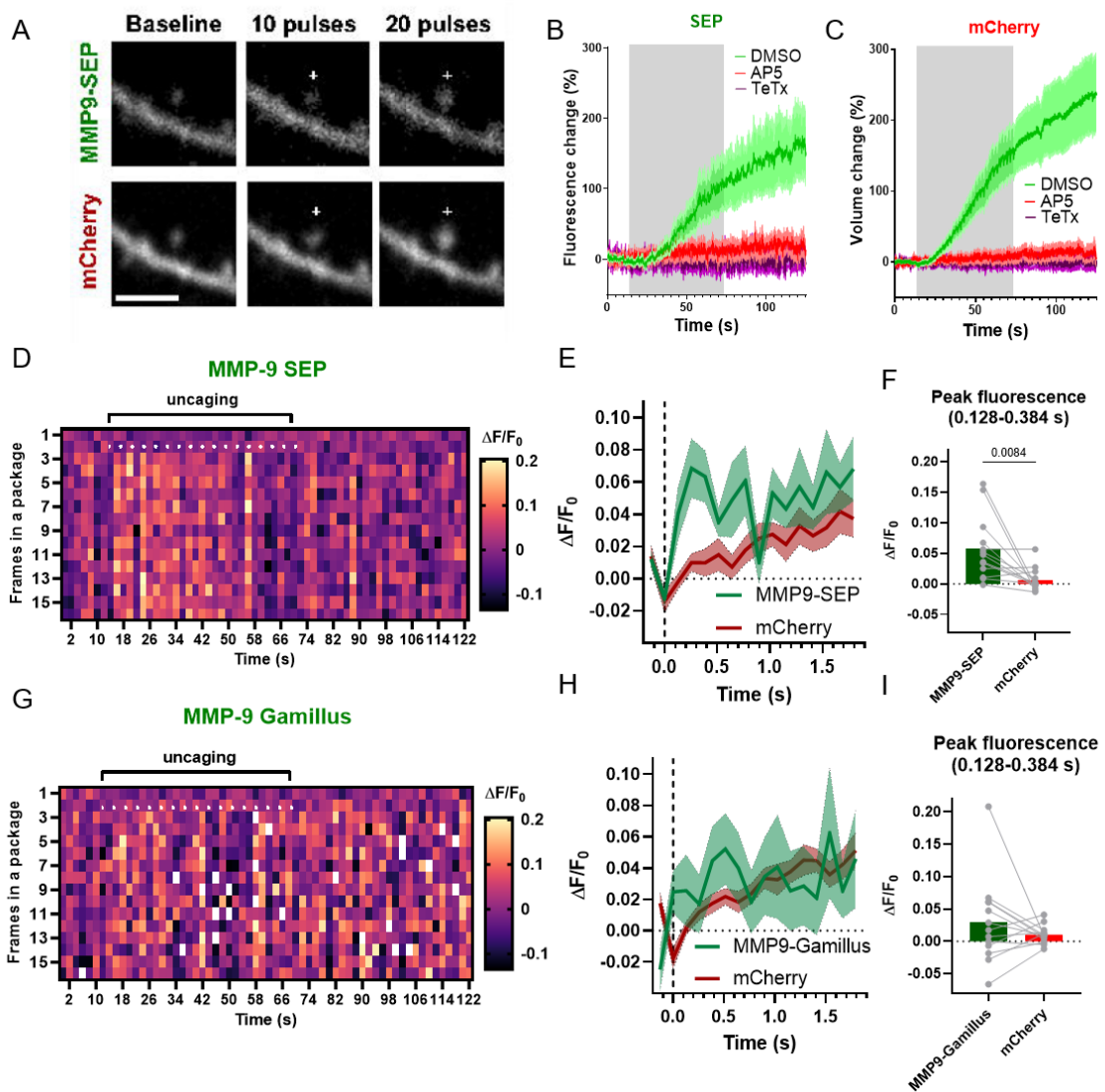

Figure 14. MMP-9 Release During sLTP

A. Representative images of a dendritic spine from a neuron co-expressing cytoplasmic mCherry and MMP-9 SEP, shown before stimulation and after 10 and 20 pulses. Scale bar – 1 μm.

B. Averaged time course of fluorescence intensity changes in the SEP channel. Data are mean ± SEM; DMSO in green n=13, AP5 in red n=13, and TeTx in violet n=12. The grey-shaded area indicates the period of stimulation.

C. Average time course of fluorescence intensity changes in the mCherry channel, for same dataset as in panel B.

D. Heat map representation of the spine MMP-9-SEP signal in the DMSO. Each coloured rectangle represents averaged relative fluorescence intensity of SEP in stimulated spines (n=13). Imaging data were divided into blocks (columns) of 16 frames matching uncaging frequency, so that uncaging pulse always occurs in a second frame of the block. sLTP protocol starts after recording baseline of 7 blocks (~ 14 s) and lasts for 60 seconds (30 pulses, 0.5 Hz). White dots represent uncaging laser pulse which occurs always during the second frame in a block during sLTP-evoking protocol.

E. Averaged data from the MMP-9 SEP in green (D) and mCherry in red signals, with binned values for 2nd-18th uncaging pulses. Shaded area represents ±SEM.

F. Statistical analysis of MMP-9 SEP and mCherry fluorescence (E) at the peak SEP fluorescence time (three frames after uncaging pulse: 0.128–0.384 s) using a paired t-test (p=0.0084).

G. Heat map representation of the spine MMP-9 Gamillus signal analogous to panel D

H. Averaged data from MMP-9 Gamillus in green (G) and mCherry in red signals, with binned values for 2nd-18th uncaging pulses. Shaded area represents ±SEM.

I. Statistical analysis of MMP-9 Gamillus and mCherry fluorescence (J) at the time corresponding to panel I, using a paired t-test (p=0.3130).

BDNF/TrkB signalling depends on MMP-9 in sLTP

 Above experiments have shown that structural plasticity depends on MMP-9 activity and that MMP-9 can be released from dendritic spines within the same time frame as BDNF. As described in the Introduction, proBDNF is released rapidly into extracellular space upon the dendritic spine stimulation, where it has to be converted into its mature form (mBDNF) in order to stimulate its receptor TrkB within seconds from the onset of the stimulation. The effects of MMP-9 inhibition reported herein have similar impact on spine growth reduction as $BDNF^{fl/fl}$Cre+ or TrkB inhibition demonstrated by Harward et al. (2016). It was also shown that MMP-9 could cleave proBDNF to convert it into mBDNF (Legutko et al., 2023). Based on that observations I decided to measure TrkB activation during sLTP while inhibiting activity of MMP-9. That would answer the question if MMP-9 activity is required for BDNF/TrkB pathway activation and would provide the mechanistic explanation of MMP-9 inhibition effects on reduced spine growth. Measurement of TrkB activation is possible with TrkB FRET sensor (Harward et al., 2016), which is composed of two fusion proteins TrkB-GFP and RFP-PLCγ-RFP (Figure 15A). Upon mBDNF binding TrkB-GFP autophosphorylates in the same way as

endogenous TrkB, allowing for recruitment of SH2 domain to the phosphorylated site. In this sensor, SH2 domain of phospholipase Cγ1 (PLCγ) is fused with two RFP proteins. Upon RFP-PLCγ-RFP recruitment, the distance between GFP and RFP becomes small enough to allow for energy transfer between the donor (GFP) and the acceptor (RFP). This interaction can be measured as a decrease in GFP photon emission time using FLIM (Fluorescence Lifetime Imaging Microscopy). The change in fluorescence lifetime can be used to calculate a binding fraction that represent percentage of the donor molecules interacting with the acceptor. In this case binding fraction convey into the percentage of activated TrkB. This method allows for high spatiotemporal resolution of receptor activation.

To assess TrkB activation in sLTP, I expressed a TrkB FRET-based sensor in neurons of hippocampal organotypic slices. Dendritic spines of CA1 subfield were imaged using FLIM during sLTP (Figure 15B).

In the control group treated with DMSO, TrkB activation increased rapidly during the uncaging phase, reaching 7% peak at 2 minutes post-stimulation, followed by stabilization at 4.5% after 3 minutes from stimulation onset. In the Inhibitor I-treated group, TrkB activation peaked immediately at 5% and after 3 minutes returned to the baseline (Figure 15C).

For statistical analysis, I compared TrkB activation levels at 1-3 minutes (transient phase) and 9-11 minutes (early sustained phase). In both phases, the TrkB activation levels in the Inhibitor I-treated group were significantly lower than those observed in DMSO-treated spines (Figure 15D).

Similarly to my previous experiments on MMP-9 involvement in sLTP I decided to assess specificity of this result to MMP-9. For that purpose I measured TrkB activation in organotypic hippocampal slice derived from $MMP-9^{-/-}$ and $MMP-9^{+/+}$ mice.

In $MMP-9^{-/-}$ cells, TrkB activation increases rapidly post-stimulation by 4.5%, but this drops to baseline by 2 minutes. By comparison, cells from $MMP-9^{+/+}$ littermates show more pronounced increase by 5.5%, followed by a sustained phase 3.5% above initial activation levels (Figure 15E). Averaging the activation levels across the peak and stable

phases revealed lower TrkB activation in *MMP-9*$^{-/-}$ cells compared to *MMP-9*$^{+/+}$ littermates (Figure 15F).

These results indicate that TrkB activation is dependent on MMP-9 activity. The dependence of TrkB activation on MMP-9 activity suggests that MMP-9 plays a role in enhancing BDNF/TrkB signalling pathway necessary for facilitation of sLTP.
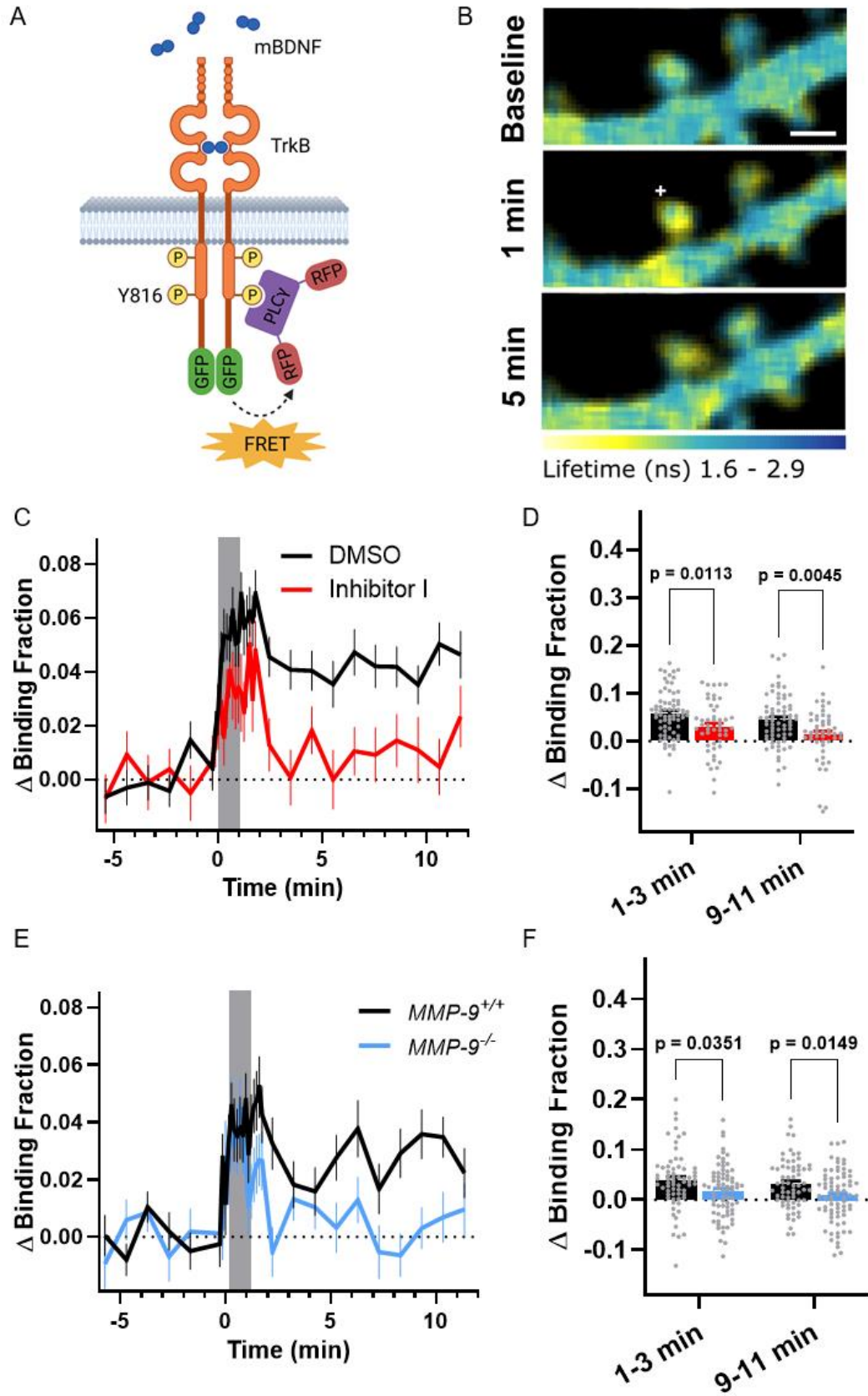
Figure 15. TrkB Activation During sLTP Depends on MMP-9 Activity

A. TrkB FRET sensor scheme.

B. Fluorescence lifetime images of representative dendrite expressing TrkB FRET at various time points from the onset of stimulation, colours indicate TrkB activation levels (blue = less active, yellow = more active). Scale bar = 1 µm.

C. Average spine TrkB activation changes over time for groups treated with DMSO in black (n=70) and Inhibitor I in red (n=49). Data are mean ± SEM, the grey box indicates duration of the uncaging protocol.

D. Statistical analysis of the data in panel C. Data is shown for two time periods: 1–3 minutes (transient), 9–11 minutes (early sustained). grey dots represent individual values. Bars are means ± SEM (colours are the same as in C). Repeated-Measures two-way ANOVA followed by Šídák's multiple comparisons test.

E. Average spine TrkB activation changes over time for spines of MMP-9$^{-/-}$ animals in blue (n=73) and their MMP-9$^{+/+}$ littermates in black (n=66). Data are mean ± SEM, the grey box indicates duration of the uncaging protocol.

F. Statistical analysis of the data in panel E. Data is shown in the same two time periods: 1–3 min, 9–11 min. grey dots represent individual values. Bars are means ± SEM (colours are the same as in E). Repeated-Measures two-way ANOVA followed by Šídák's multiple comparisons test.

IGF1R Function in sLTP is controlled by MMP-9 activity

As discussed in the Introduction, MMP-9 targets several proteins related to synapse reorganization and LTP maintenance. My previous results have revealed that pre-existing MMP-9 is released immediately upon the sLTP stimulation and acts by enhancing TrkB signalling that contribute to spine growth.

Apart from neurotrophins, where BDNF is a primary example, synaptic plasticity is often influenced by a broader group of proteins – neurotrophic factors, which have also significant role in neuronal development, survival, and regeneration. Among the latter, IGF1 emerges to be an interesting example, whose action in synaptic plasticity, has been recently described (Nuñez et al., 2023; Tu et al., 2023). The activation of IGF1R by IGF1 in sLTP is temporally similar to that of BDNF/TrkB. Interestingly, MMP-9 was demonstrated to induce IGF1R activation in other models (Chattopadhyay & Shubayev, 2009; Furuta et al., 2023; Rorive et al., 2008). Therefore, I hypothesized that IGF1/IGF1R signalling pathway might be controlled by MMP-9 activity during sLTP, similarly to BDNF/TrkB pathway. To assess whether this hypothesis is correct, I measured an activation of IGF1R FRET sensor using FLIM, in a manner similar to the TrkB activation experiment.

Neurons from hippocampal organotypic cultures were transfected with two plasmids coding IGF1R sensor: IGF1R-GFP (FRET donor) and mCherry-p58-mCherry (FRET

acceptor). Successfully transfected pyramidal cells from CA1 region were imaged with FLIM during sLTP. To measure relevance of MMP-9 enzymatic activity for IGFIR activation I performed experiments in the presence of either Inhibitor I or DMSO (for control).

In the DMSO-treated group, IGF1R activation rapidly increased within seconds post-stimulation by 6% and remain elevated for the time of the recording. In the Inhibitor I-treated group, IGF1R activation was greatly reduced with an average increase around 2% (Figure 16A).

To statistically compare these conditions, I selected three time points: 1-3 minutes as the initial receptor activation (transient phase), 9-11 minutes (early sustained phase) and 15-20 minutes (sustained phase).

In all time periods, the Inhibitor I-treated spines had lower IGF1R activation levels compared to the DMSO-treated group (Figure 16B).

To assess the specificity of MMP-9 effect on IGF1R activation, I conducted similar experiment using neurons from $MMP-9^{-/-}$ mice and their $MMP-9^{+/+}$ littermates. In $MMP-9^{+/+}$ cells, IGF1R activation increased by 5% post-stimulation and remain elevated. In $MMP-9^{-/-}$ cells I observed IGF1R activation by 2% similarly to previous condition (Figure 16C). At all time periods, $MMP-9^{-/-}$ cells exhibited lower IGF1R activation than $MMP-9^{+/+}$ cells (Figure 16D).

To determine if MMP-9 overexpression could rescue IGF1R activation levels in $MMP-9^{-/-}$ cells, I conducted additional experiments with organotypic cultures overexpressing either MMP-9 or the inactive MMP-9 (E402A) mutant as a control. In the MMP-9 expressing group, IGF1R activation levels increased rapidly by 7.5% in response to stimulation. In the MMP-9 (E402A) expressing group, activation was less pronounced oscillating around 2% (Figure 16E).

Consistent with previous results, the group expressing MMP-9 had significantly higher IGF1R activation compared to the MMP-9 (E402A) group (Figure 16F). Together, these results indicate that MMP-9 regulate more than one signalling pathway and that IGF1R

activation relies predominantly on MMP-9 activity throughout all stages of sLTP. This receptor activation dependence on MMP-9 apparently cannot be explained by processing of proIGF1 similarly to proBDNF since it was demonstrated that proIGF1 is capable of activating IGF1R (Durzynska et al., 2013). Therefore, a different mechanism should be involved. The most common control of the IGF/IGF1R signalling occur through IGFBPs and their proteolytic cleavage as a mechanism of IGF release and IGF1R activation. Importantly, IGFBPs are cleaved mainly by extracellular metalloproteinases (Fowlkes et al., 1995). Therefore, I have hypothesized that MMP-9 is driving IGF-1 release from its carrier proteins (IGFBPs), thereby evoking signalling required for dendritic spine plasticity.
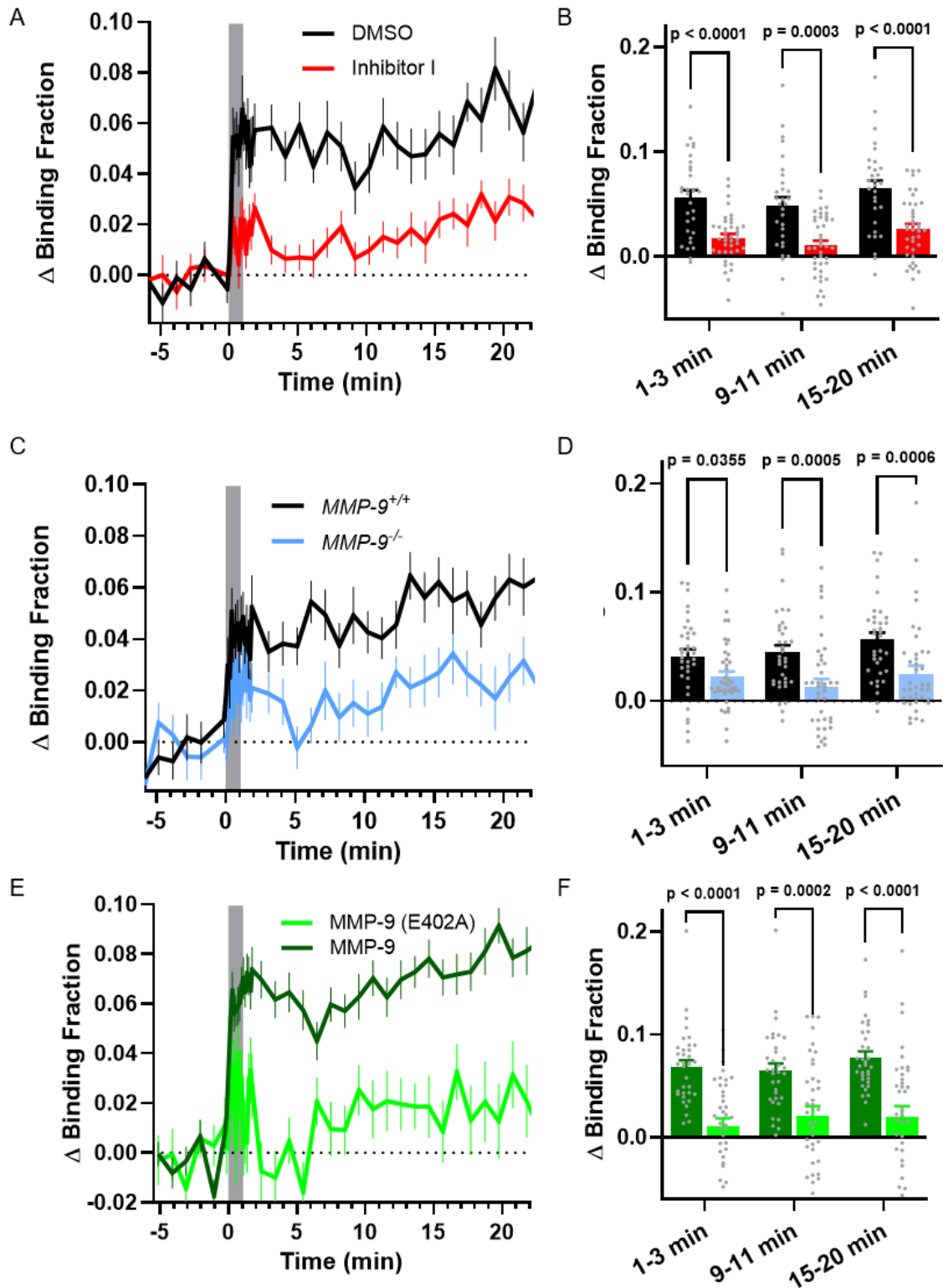
Figure 16. IGFIR Activation During sLTP Depends on MMP-9 Activity

A. Average spine IGFIR activation changes over time for groups treated with DMSO in black (n=31) and Inhibitor I in red (n=39). Data are mean ± SEM, the grey box indicates duration of the uncaging protocol. B. Statistical analysis of the data in panel A. Data is shown for three time periods: 1–3 min, 9–11 min and 15-20 min. Grey dots represent individual values. Bars are means ± SEM (colours are the same as in A). Repeated-Measures two-way ANOVA followed by Tukey's multiple comparisons test.

C. Average spine IGR1R activation changes over time for spines of MMP-9$^{-/-}$ animals in blue (n=40) and their MMP-9$^{+/+}$ littermates in black (n=35). Data are mean ± SEM, the grey box indicates duration of the uncaging protocol.

D. Statistical analysis of the data in panel C. Data is shown in the same three time periods: 1–3 min, 9–11 min and 15-20 min. Grey dots represent individual values. Bars are means ± SEM (colours are the same as in C). Repeated-Measures two-way ANOVA followed by Tukey's multiple comparisons test.

E. Average spine IGR1R activation changes over time for spines from MMP-9$^{-/-}$ neurons with overexpression of MMP-9 in dark green (n=34) and inactive MMP-9 (E402A) in light green (n=39). Data are mean ± SEM, the grey box indicates duration of the uncaging protocol.

F. Statistical analysis of the data in panel E. Data is shown in the same three time periods: 1–3 min, 9–11 min and 15-20 min. Grey dots represent individual values. Bars are means ± SEM (colours are the same as in E). Repeated-Measures two-way ANOVA followed by Tukey's multiple comparisons test.

IGFBP-IGF1 complexes are primary source of IGF1 during sLTP

Next to verify if IGFBPs are involved in IGFIR signalling I decided to block their ability to form complexes with IGF1. By blocking their ability to bind and store IGF1 we should be able to observe the effect on the spine growth. The effect will be dependent on their intrinsic function in the IGF1 signalling system. We might either expect increased IGF1 availability since IGF1 released from dendritic spines will bind directly to IGFIR promoting spine plasticity or in case IGFBPs serving as IGF1 reservoir at the cellular membrane, we might expect to observe decreased plasticity, since IGF1 pool would be depleted.

Firstly, I decided to block all IGFBPs using a broad-spectrum IGFBP inhibitor, small non-peptide ligand of IGFBPs (C. Chen et al., 2001). This inhibitor displaces IGF1 from IGF1-IGFBP complex but does not interact with IGF1R. Either the Inhibitor (10 μM final concentration) or DMSO as a solvent were applied in into the culture media 2 hours before the experiment, to ensure sufficient depletion of IGF1-IGFBP complexes and prevent IGF1 release from those complexes during experiment. Next, I performed sLTP protocol on dendritic spines from CA1 neurons transfected with GFP plasmid and measured spine growth in response to stimulation.

DMSO treated spines had classical response to sLTP stimulation showing initial peak of the volume by 120% followed by sustained phase 50% above the baseline level. In

contrast, the IGFBP inhibitor-treated group exhibited a 40% peak in response to stimulation that was followed by return to the baseline volume (Figure 17A). Statistical analysis showed a significant decrease in plasticity in the IGFBP inhibitor-treated group at all tested time periods (Figure 17B).

To confirm that observed effects in reduced spine plasticity come from IGF1 related function of IGFBPs as a follow up experiment I measured IGF1R activation in sLTP in presence of broad-spectrum IGFBPs inhibitor. Experiments were conducted on neurons expressing IGF1R FRET sensor in exact conditions as described above. For dendritic spines in DMSO condition I observed rapid stable activation of IGF1R by 10% while in IGFBPs inhibitor treated spines I observed much smaller responses around 4% stabilizing around 2% (Figure 17C). All tested time periods (transient, early sustained and sustained) were significantly lower in the IGFBP-inhibitor-treated group than those in DMSO group (Figure 17D).

These results underscore the role of IGFBPs in sLTP, with IGFBPs acting as a reservoir of IGF1, making it available for IGF1R activation during sLTP.
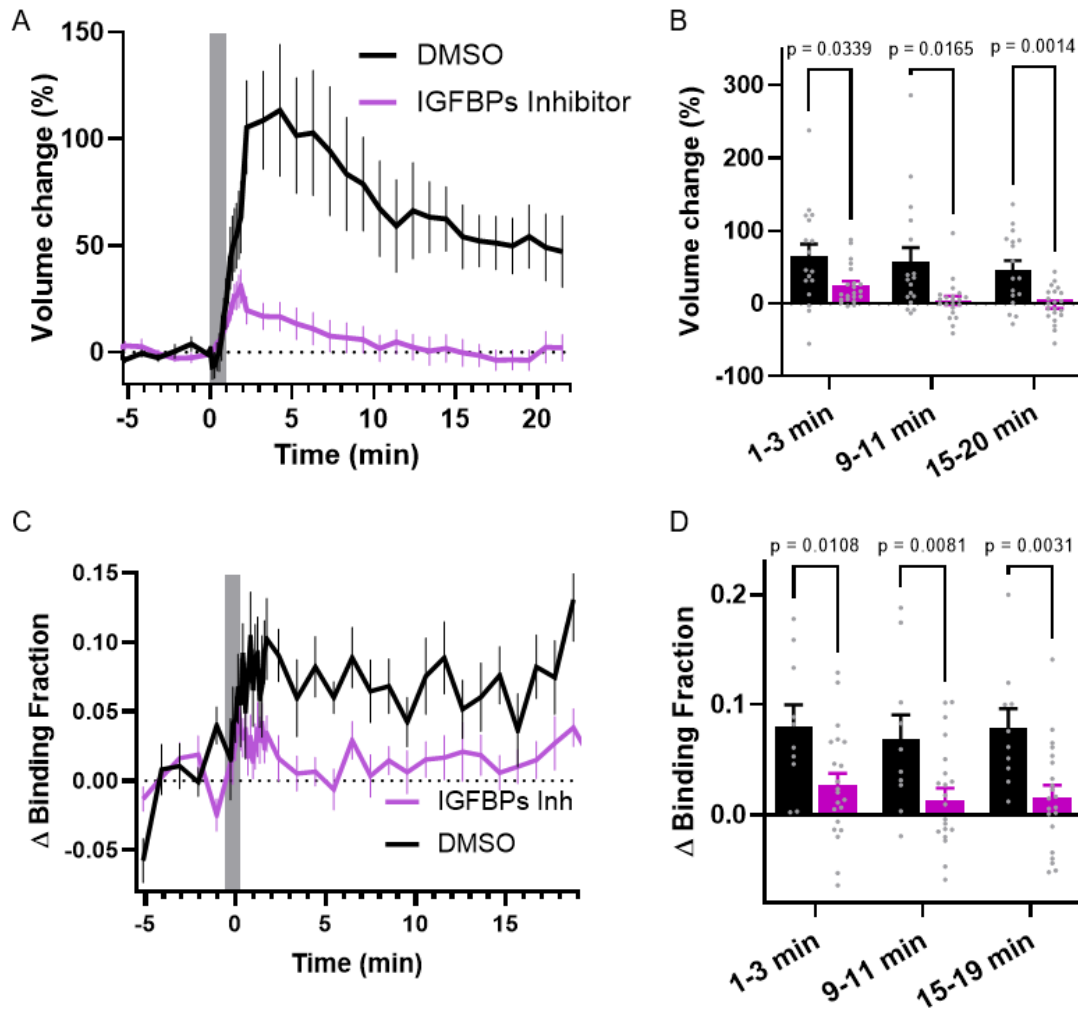
Figure 17. Blocking of IGFBPs Inhibits sLTP and IGFIR Activation

A. Average spine volume changes over time for groups treated with DMSO in black (n=18) and IGFBPs inhibitor in purple (n=22). Data are means ± SEM, the grey box indicates uncaging protocol.

B. Statistical analysis of the data in panel A. Data is shown for three time periods: 1–3 minutes (transient), 9–11 minutes (early sustained), and 15–20 minutes (sustained). grey dots represent individual values. Bars are means ± SEM (colours are the same as in A). Repeated-Measures two-way ANOVA followed by Tukey's multiple comparisons test: DMSO vs IGFBPs Inhibitor.

C. Average spine IGFIR activation changes over time for groups treated with DMSO in black (n=10) and IGFBPs Inhibitor in purple (n=22). Data are mean ± SEM, the grey box indicates uncaging protocol.

D. Statistical analysis of the data in panel C. Data is shown for three time periods: 1–3 min, 9–11 min and 15-19 min. grey dots represent individual values. Bars are means ± SEM (colours are the same as in A). Repeated-Measures two-way ANOVA followed by Tukey's multiple comparisons test.

IGFBP2 mRNA is the predominant and upregulated transcript in response to cLTP

Out of 6 IGFBPs all except IGFBP1 can be found in the brain at mRNA levels. Their localization pattern differ in terms of brain areas and cell types. In hippocampus dominant IGFBPs are IGFBP2, expressed mostly by astrocytes, IGFBP4 mostly expressed in neurons and IGFBP5 found in both astrocytes and neurons (Cembrowski et al., 2016; Chai et al., 2017; X. Chen et al., 2024; Srinivasan et al., 2016).

To identify which IGFBPs might be involved in sLTP, I analysed RNA expression data from a hippocampal synaptoneurosome database. mRNAs were sequenced using nanopore method (Dziembowska, unpublished). Five out of six IGFBPs were detected, with the highest expression levels observed for IGFBP2, IGFBP5, and IGFBP4 (Figure 18A). Many genes coding for the proteins engaged in synaptic plasticity become upregulated in response to LTP-like stimulation. To investigate whether transcription of IGFBPs change in response to synaptic plasticity, I induced chemical LTP (cLTP) on organotypic hippocampal slices and measured mRNA levels of IGFBPs at two time points post-stimulation.

I observed increase in IGFBP2 mRNA levels at 6 hours post-stimulation (one-way ANOVA with Dunnett's test, $p = 0.0243$) (Figure 18B). IGFBP3 mRNA also increased at the 6-hour mark ($p < 0.0001$) and remained elevated at 24 hours ($p = 0.033$) (Figure 18C). In contrast, IGFBP4 mRNA levels decreased at 24 hours post-cLTP ($p = 0.0103$) (Figure 18D). No significant changes were detected for IGFBP5 or IGFBP6 (Figure 18E-F).

Based on literature findings on involvement of IGFBP2 in neuronal plasticity (Burgdorf et al., 2023; Khan, 2019; Russo et al., 2005; W. Sun et al., 2024), supported by RNA databases and my findings on RNA levels increase in response to cLTP I selected IGFBP2 as potential candidate for further investigation of its involvement in MMP-9 mediated IGF1/IGF1R signalling pathway.
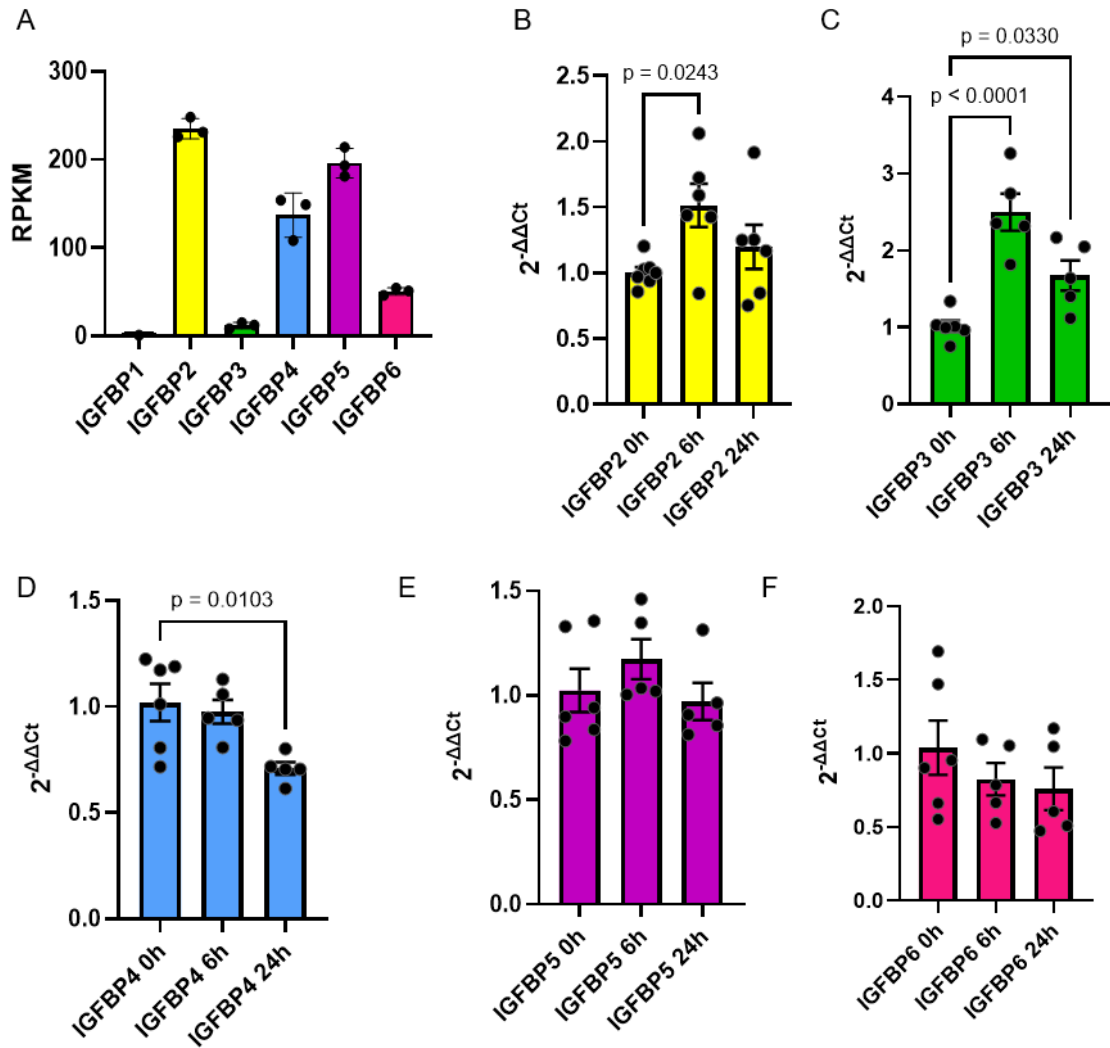
Figure 18. IGFBPs RNA Levels in Hippocampus

A. Average number of Reads Per Kilobase per Million mapped reads (RPKM) for each IGFBP RNA from hippocampal synaptoneurosomes. Bars represent means ± SD. Black dots indicate individual values (n=3 animals).

B-F. RT-PCR analysis of the IGFBP RNA levels in hippocampal organotypic slices at various time points following cLTP stimulation. Coloured dots represents individual samples. Bars represent means ± SEM. Statistical analysis was performed using a one-way ANOVA, followed by Dunnett's multiple comparisons test. n=6 animals.

B. IGFBP2 (yellow): 0h vs 6h, p=0.0243, C. IGFBP3 (green): 0h vs 6h, p<0.0001; 0h vs 24h, p=0.033. D. IGFBP4 (blue): 0h vs 24h, p=0.0103. E. IGFBP5 (purple): no significant differences. F. IGFBP6 (magenta): no significant differences.

IGFBP2 is a substrate for MMP-9

MMP-9 was reported to increase IGF availability through IGFBP2 cleavage (Fowlkes et al., 1995; Rorive et al., 2008). Some studies indicate that proteolytic cleavage occurs within linker domain of IGFBP2 (Jaipuria et al., 2022). All IGFBPs structurally compose of two IGF Binding Domains (IGF BD) that separately have decreased affinity for IGF1 that indicates that free IGF will more likely bind to its receptor than individual IGF BDs, however it is not clear whether the complex of IGF-IGFBP can diffuse upon the cleavage of the linker. Therefore, I decided to identify location of MMP-9 cleavage sites within IGFBP2 sequence. MMP-9 does not have just single consensus cleavage sequence. The most common one is composed of PXX † Hy(S/T) (X represents any residue; Hy represents a hydrophobic residue; cleavage site marked as †). I aimed to determine MMP-9 potential cleavage site within IGFBP2 through a bioinformatics analysis of its amino acid sequence. The ProsperousPlus (Li et al., 2023) is a tool designed for protease cleavage site prediction. I employed pertained model for MMP-9 cleavage site prediction on amino acid sequence of IGFBP2. In result (Table 3) I obtained prediction scores for each cleavage site. The cleavage site is presented as +/- 4 amino acids - P4-P4' starting from N-terminus, where hydrolysis occurs between amino acids: P1 and P1'. The prediction values varies between 0-1 where scores closer to 1 are indicating higher cleavage site probability. Prediction scores were plotted against the cleavage site position in amino acid sequence (Residue Position). To filter out less probable results I set the threshold at 0.75 obtaining 7 potential residues with a score value >0.75 (Figure 19A, Table 3). This information itself does not fully answer my question since some of those sequences may be unavailable for proteolytic cleavage due to secondary structure of the protein. IGFBP2 contains two IGF BD with complex secondary structure and flexible linker that connects both of them. To test if folded IGFBP2 contain any of the potential cleavage sites, I employed second cleavage prediction model Procleave (Li et al., 2020). Procleave utilizes both amino acid sequence and 3D structure of protein of interest ranking cleavage sites in analogue way to previously described model. In result of applying 0.75 score threshold, I obtained two cleavage sites (P1) at residue R47 and K197 that were also present in ProsperousPlus analysis. (Figure 19B, Table 4).
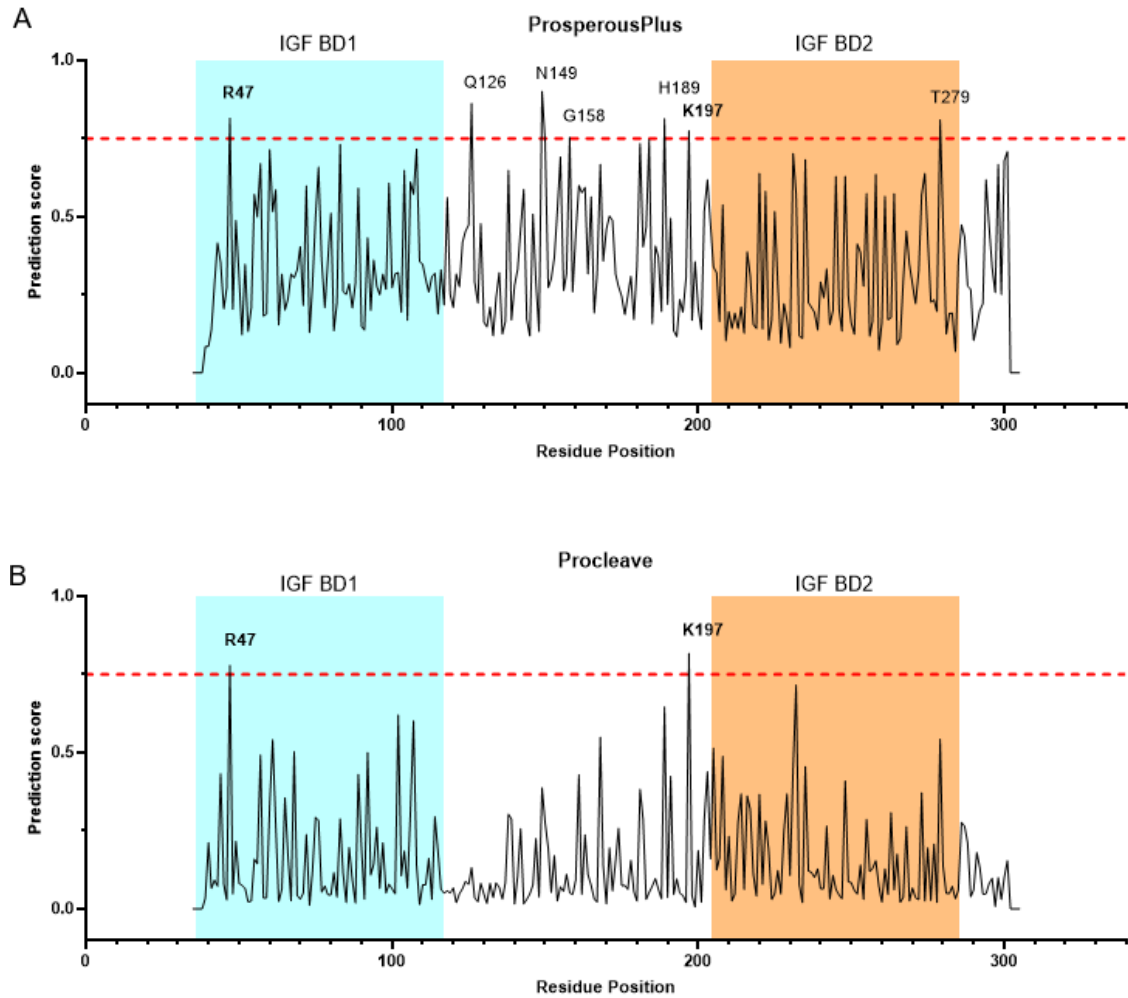
Figure 19. Predicted MMP-9 Cleavage Sides in IGFBP2

   A. *ProsperousPlus model prediction results presented as prediction score values plotted against amino acid P1 (Residue Position). Residues with scores above 0.75 (red dashed line) were labelled. IGF BDs are marked in teal (IGF BD1) and orange (IGF BD2).*

   B. *Procleave model prediction results presented same as in A.*

Rank	Position	P4-P4' Site	IGFBP2 Domain	Score
1	149	GTMN † MLGG	Linker	0.901
2	126	TPQQ † VADS	Linker	0.862
3	47	TPER † LAAC	IGF Binding Domain I	0.815
4	189	GAKH † LSLE	Linker	0.813
5	279	GAPT † IRGD	IGF Binding Domain II	0.810
6	197	EPKK † LRPP	Linker	0.775

Table 3. ProsperousPlus – Prediction of MMP-9 Cleavage Sites P4-P4'in IGFBP2 Based on Amino Acid Sequence. Position refers to residue P1 position in amino acid chain of IGFBP2. Results above 0.75 score threshold were sorted by highest to lowest score.

Rank	Position	P4-P4' Site	IGFBP2 Domain	Score
1	197	EPKK † LRPP	Linker	0.817
2	47	TPER † LAAC	IGF Binding Domain I	0.779

Table 4. Procleave – Prediction of MMP-9 Cleavage Sites P4-P4' in IGFBP2 Based on 3D Structure. Position refers to residue P1 position in amino acid chain of IGFBP2. Results above 0.75 score threshold were sorted by highest to lowest score.

Next, to further evaluate how IGFBP2 can interact with active site of MMP-9, I used AlphaFold2 to model complexes between these proteins. AlphaFold was originally designed as protein structure prediction tool, however, it has also been demonstrated to predict protein-protein interactions (Bryant et al., 2022). One of the top five ranked models generated by AlphaFold2 revealed an interaction between the MMP-9 active site and the TPERLAAC sequence of IGFBP2 (Figure 20A-D). This sequence was previously identified as potential cleavage site by both cleavage site prediction models. Using the model obtained, I analysed the interaction between IGFBP2 and the MMP-9 active site, identifying 8 hydrogen bonds, 2 salt bridges, and 80 non-bonded contacts. The total interface area measured 899 Å² for MMP-9 and 952 Å² for IGFBP2. The multiple

hydrogen bonds and extensive non-bonded contacts suggest a strong and stable interaction, indicating that MMP-9 active site may effectively recognize IGFBP2 at TPERLAAC side.

Additionally, I detected a weak 3.6 Å interaction between crucial amino acid for enzymatic activity E402 of MMP-9 and E46 of IGFBP2 that localize in TPERLAAC sequence.

Figure 20. IGFBP2 and MMP-9 Interaction Site
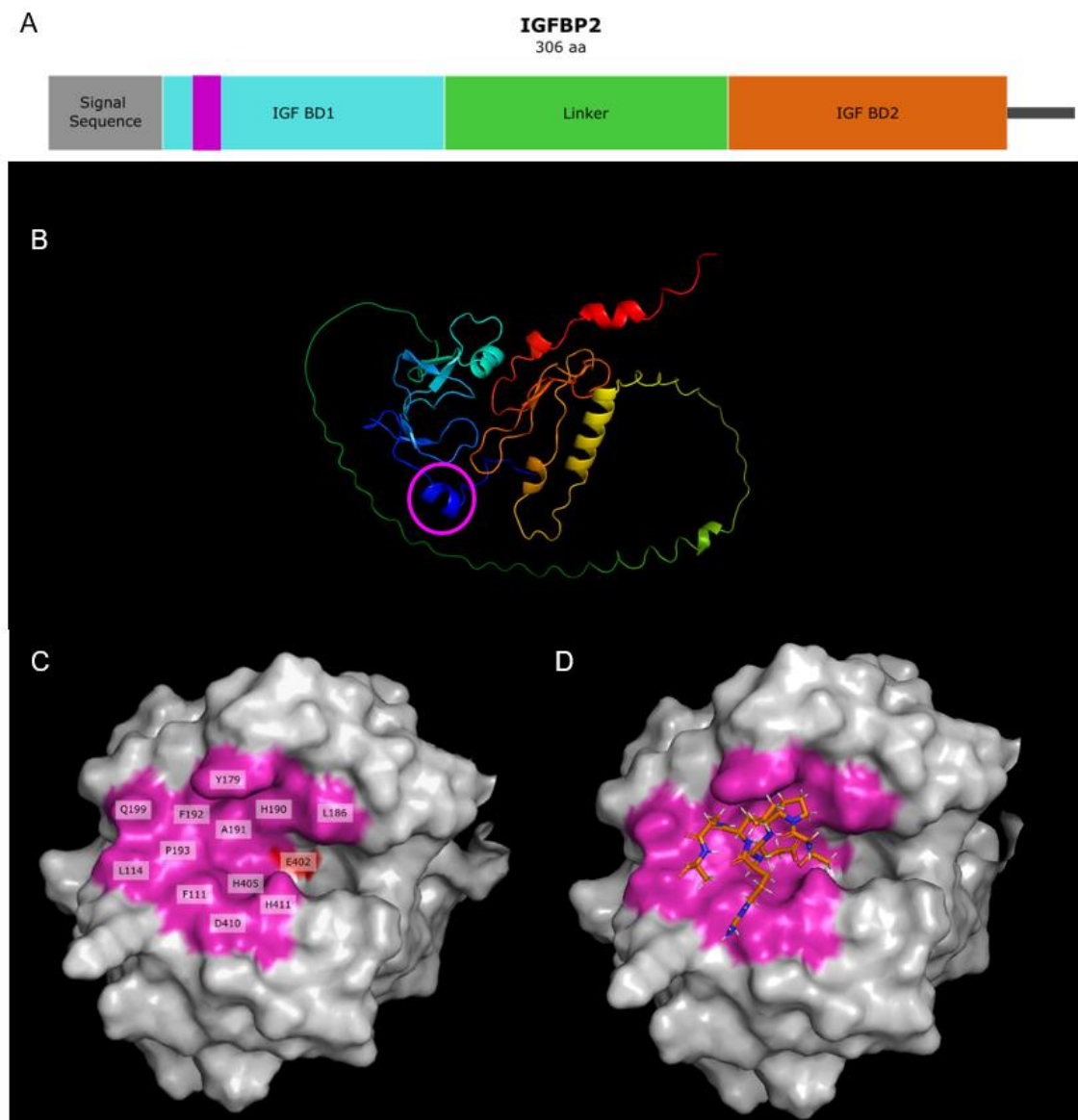*A. IGFBP2 domain structure, showing the propeptide sequence in grey, IGF BD1 in teal, IGF BD2 in orange and linker in green. A novel potential MMP-9 cleavage site identified within IGF BD1 (magenta).*
B. 3D model of the IGFBP2 protein, rainbow-colored from N-terminal to C-terminal, with the helical structure corresponding to the TPERLAAC sequence marked by magenta circle.

C. Surface model of the MMP-9 active site. Amino acids interacting with the TPERLAAC sequence are coloured in magenta and red. The red region corresponds to Glutamic acid 402, the catalytic site of the MMP-9.

D. TPERLAAC of IGFBP2 model fitted into the active site of MMP-9, generated by AlphaFold2.

My *in silico* analysis identified potential MMP-9 cleavage sites within IGFBP2. To validate these findings experimentally, I conducted an enzymatic cleavage assay using recombinant IGFBP2 and MMP-9. For this, HA-IGFBP2-FLAG and MMP-9 were individually expressed in HEK cells, and the media containing the secreted proteins were collected. IGFBP2 was immobilized on anti HA-Agarose.

The immobilized IGFBP2 was then incubated with media containing MMP-9 and 4-aminophenylmercuric acetate (APMA), a known activator of MMP-9 (Okada et al., 1992). As a control, identical IGFBP2-binding beads were incubated with media containing MMP-9 and DMSO instead of APMA. After a 6-hour incubation, the supernatant was collected, and proteins were separated via SDS-PAGE. The cleavage products were analysed by western blot, using an anti-FLAG antibody targeting the C-terminal FLAG tag of the recombinant IGFBP2 protein (Figure 21A).

The presence of lower molecular weight bands at 20 kDa and 15 kDa in samples treated with active MMP-9 suggests that IGFBP2 undergoes cleavage in at least two sites within the linker. To quantify this, I compared the band intensity ratio between the 20 kDa and 38 kDa bands across all experimental conditions. On average, the 20 kDa band accounted for 54% of the intensity in samples treated with MMP-9 activated with APMA, compared to 13% in the DMSO-treated group. Statistical analysis using a t-test revealed a significant difference, with $p=0.0232$ (Figure 21B).
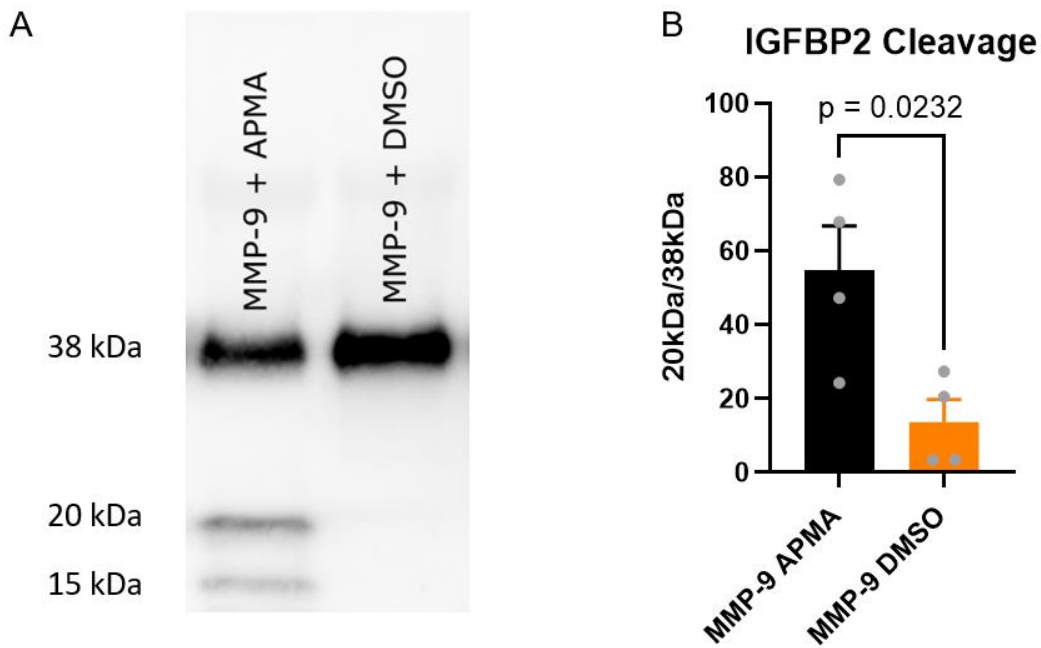
Figure 21. Cleavage of IGFBP2 by MMP-9

A. Representative immunoblot demonstrating the cleavage of IGFBP2 by MMP-9. Two experimental conditions are shown: IGFBP2 + MMP-9 (APMA-activated) and IGFBP2 + MMP-9 (vehicle-treated). Cleavage products are visible in the APMA-activated MMP-9-treated lane.

B. Quantification: Four independent Western blots were quantified, showing the intensity of the full-length IGFBP2 (~38 kDa) and the cleaved product (~20 kDa) in both conditions. Grey dots represent the individual ratios between the 20 kDa and 38 kDa band intensity values from each experiment. Bars indicate means ± SEM. Statistical analysis was performed using a t-test.

Together my results confirm that MMP-9 is able to cleave IGFBP2, which is a primary mechanism for IGF release from IGF-IGFBP complexes.

IGFBP2 localizes in astrocytes and neurons

So far, I provided mechanistic insight into IGF1/IGF1R activation by MMP-9. Next step was to confirm localization of IGFBP2 protein in neuronal cultures that could help me to identify a source of this protein in my experimental model. Some reports indicate that IGFBP2 is a astrocytic protein (Caldwell et al., 2022; W. Sun et al., 2024). Therefore, I performed immunostaining on 2-week-old dissociated neuronal cultures, to determine which cell types contain IGFBP2. I observed a concentrated IGFBP2 signal in astrocytic cell bodies as well as a more diffused signal in astrocytic protrusions, neuronal cell bodies

and neurites (Figure 22A). Quantification of IGFBP2 intensity showed that neurons contain, on average, 40% less IGFBP2 signal compared to astrocytes (Figure 22B). This suggests that astrocytes may serve as a major source of IGFBP2, potentially secreting it in proximity of synapses to support nearby neuronal plasticity.
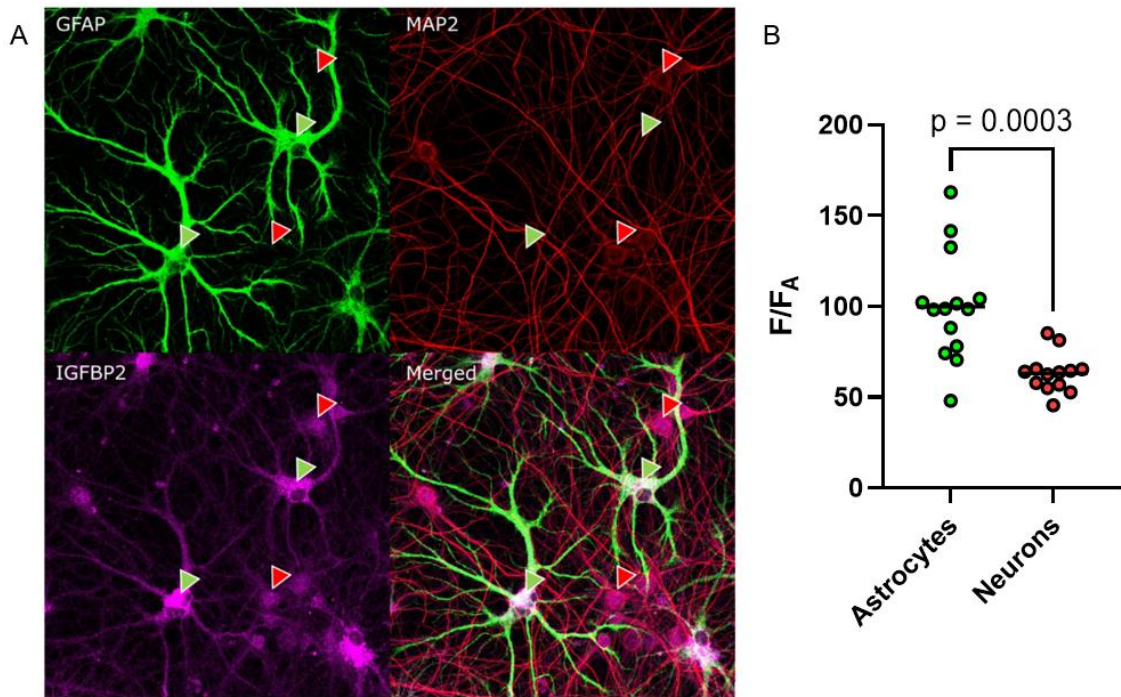

Figure 22. Localization of IGFBP2 in Astrocytes and Neurons in Dissociated Neuronal Culture
A. Immunostaining of dissociated neuronal culture showing IGFBP2 localization in both astrocytes and neurons. Astrocytes are labelled with an antibody against GFAP (green), neurons with an antibody against MAP2 (red), and IGFBP2 is detected with an antibody in magenta. Green arrows indicate astrocytic cell bodies, while red arrows indicate neuronal cell bodies.
B. Quantification of IGFBP2 signal intensity in astrocytic (n=14) and neuronal cell bodies (n=13) presented as F/FA where F is and average cell fluorescence in IGFBP2 channel and FA is average IGFBP2 fluorescence in astrocytes, t-test p=0.0003.

Additionally, I performed IGFBP2 immunostaining on dissociated neuronal cultures that were transfected with tdTomato under a neuronal promoter to visualize the morphology of neurons and identify dendritic spines. This enabled me to assess the localization of the IGFBP2 signal in relation to dendritic spines (Figure 23). My findings confirmed that IGFBP2 frequently localizes within dendritic spines and along dendrites, supporting its potential role in the sLTP related processes.
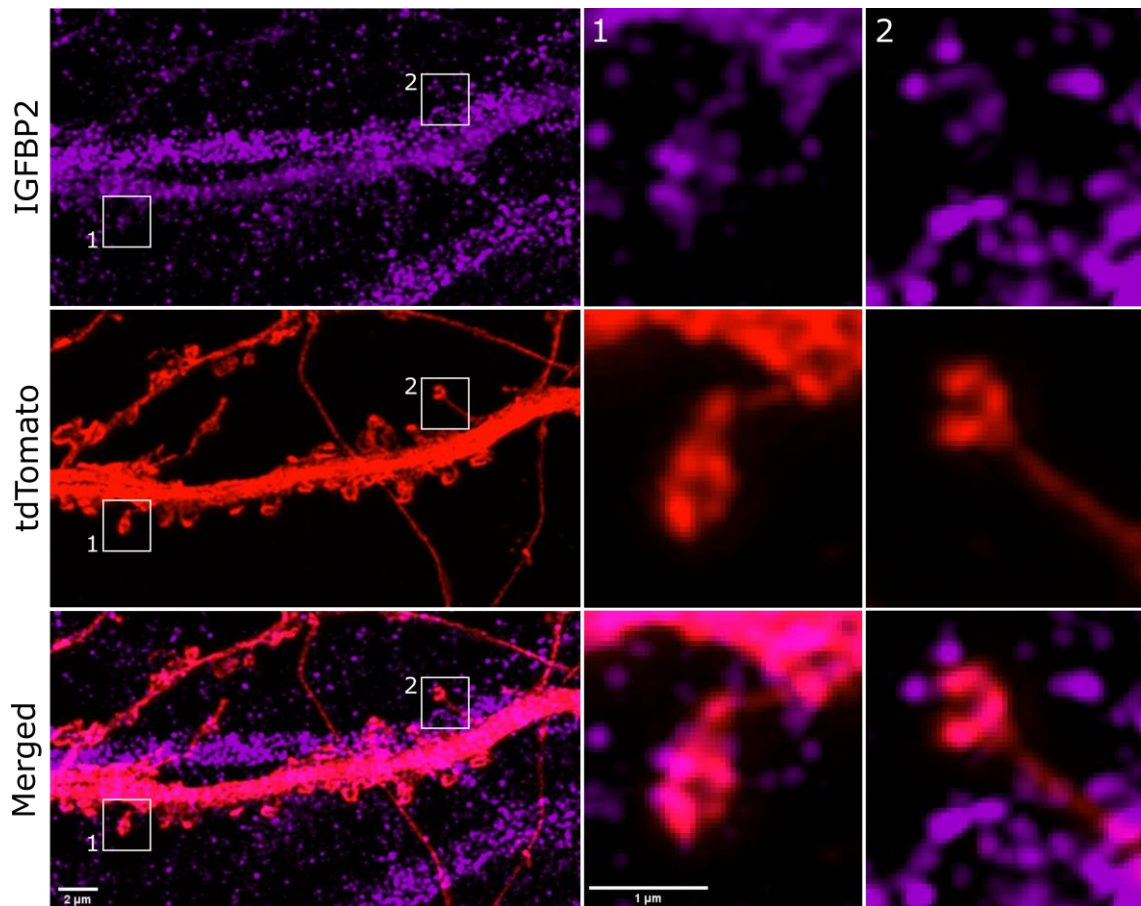
Figure 23. Localization of IGFBP2 in the Proximity of Dendritic Spines

The confocal images presenting immunostaining of a dissociated neuronal culture and highlighting IGFBP2 (magenta) near dendritic spines. Neurons were transfected with tdTomato (red) as a cytoplasmic dye to visualize dendritic morphology, including dendritic spines. Scale bar- 2 µm. On the left side panels view on exemplary dendrite with two spines marked as white squares presented with magnification on the right hand side panels, provide detailed visualization of IGFBP2 localization within the spine vicinity. Scale bar - 1 µm.

Collectively, these results demonstrate that MMP-9 is intricately involved in multiple pathways supporting sLTP. Through its release at dendritic spines, MMP-9 may modulate the availability of neurotrophins like mBDNF, or neurotrophic factors such as IGF-1, ultimately influencing their receptor activation and promoting structural plasticity.

DISCUSSION

The major findings reported in this dissertation provide new insights into the molecular mechanisms underlying structural long-term potentiation (sLTP). In particular:

1) Both, transient and sustained phase of sLTP depends on MMP-9 activity
2) MMP-9 is released from postsynaptic site within seconds from stimulation onset
3) BDNF/TrkB signalling relies on MMP-9 activity during sLTP
4) IGR1R activation during sLTP depends on MMP-9 activity
5) IGFBPs are required for structural plasticity and IGF1R activation in transient and sustained phase of sLTP
6) IGFBP2 is a major IGFBP in the hippocampus and is cleaved by MMP-9 in linker region and potentially within IGF1-binding domain
7) IGFBP2 is mainly astrocytic and localizes close to the dendritic spines

Together, these findings establish a multifaceted role for MMP-9 in regulating sLTP through its interaction with signalling pathways and substrate processing.

Both, transient and sustained phase of sLTP depends on MMP-9 activity

It is particularly interesting that my results demonstrate MMP-9 involvement in the initial spine enlargement - transient sLTP, as well as sustained phase of sLTP. My results from sLTP protocol on dendritic spines show typical rapid spine enlargement that, for control conditions, this is consistent with published findings. Notably, some variability between experiments in the rate of transient and sustained spine volume is typical and usually ranges from 200% to 300% increase in transient phase and sustained between 50% to 100% (Colgan et al., 2018; Harward et al., 2016; Murakoshi et al., 2017; Patterson et al., 2010; Tu et al., 2023). My results of pharmacological inhibition of MMPs and MMP-9/MMP-13 specific inhibition on spine growth during sLTP show reduction in initial spine growth and following sustained volume is decreased as compared to control conditions with un-inhibited enzymatic activity. This means that metalloproteases activity is required already for the transient spine volume increase. The lack of significant differences between broad spectrum MMP inhibitor and more specific MMP-9/13 inhibitor might suggest that either MMP-9 or 13 are responsible for observed effects. Of those two metalloproteases, only MMP-9 has been implicated in dendritic spine shape

rearrangements (Magnowska et al., 2016; Michaluk et al., 2011), whereas MMP-13 is primarily associated with the nervous tissue response to hypoxia, with no clear evidence supporting its involvement in dendritic spine remodelling (Cuadrado et al., 2009; Hohjoh et al., 2020; Nagel et al., 2005).

Further support for MMP-9 involvement in early phase of sLTP came from my experiments on genetic ablation of MMP-9. The results from MMP-9$^{-/-}$ model indicate that initial spine growth during sLTP is MMP-9 dependent, though this effect becomes less pronounced at later time points. The sustained phase of sLTP (15-20 min post-stimulation) does not show significant differences between MMP-9$^{+/+}$ and MMP-9$^{-/-}$ animals. The involvement of MMP-9 in the sustained phase of sLTP in MMP-9$^{-/-}$ animals remains unclear and suggests the presence of compensatory mechanisms regulating sLTP.

This notion appears to be well supported by experiment with conditional MMP-9 KO in cultures derived from MMP-9$^{fl/fl}$ animals. In these experiments, I demonstrated that acute knockout of the MMP-9 gene, induced by Cre recombinase not earlier than five days prior to the experiment, significantly reduces sLTP in both its transient and sustained phases.

To minimize misinterpretation and account for compensatory changes, it should be considered to employ conditional MMP-9$^{fl/fl}$ models developed for the purpose of this study, where the induction of MMP-9 KO can be temporally controlled. This approach limits the extent of compensatory adaptations and provide clearer insights into MMP-9's role in synaptic plasticity.

To my best knowledge, this is a first study, where MMP-9 involvement in structural plasticity is tested in all-optical protocol of sLTP. My results show that MMP-9 is pivotal for dendritic spine enlargement in response to optical glutamate uncaging producing sLTP. Chemical inhibition of MMP-9 resulted in impairment of dendritic spine growth as early as 1-3 min. post-stimulation and lasting at least over 9-11 min. This early spine volume impairment suggests the potential for MMP-9 to be involved in LTP processes much earlier than previously assumed. By employing high-resolution sLTP tracking, I achieved the temporal and spatial precision needed to identify the exact timing of MMP-9 involvement at the scale of individual dendritic spines. This approach fills a critical gap in our understanding, addressing the limitations of prior methods and, therefore, providing new insights into MMP-9 role in LTP.

MMP-9 has previously been implicated in morphological changes of spines and its role in functional LTP (fLTP). However, most studies addressing MMP-9 involvement in structural plasticity have focused on the application of recombinant MMP-9 to dissociated cultures (Magnowska et al., 2016; Michaluk et al., 2011; Szepesi et al., 2014). Studies in context of LTP focused mostly on fLTP, established MMP-9's involvement in L-LTP (Gorkiewicz et al., 2015; Nagy et al., 2006; Wang et al., 2008; Wiera et al., 2013). On the other hand, MMP-9 role in LTP induction has not been directly addressed.

In this context the Wang et al. (2008) study is particularly important as they addressed the question of structural plasticity by tracking spines volume and EPSP during LTP. Their findings emphasized the importance of MMP-9 in sustained spine volume. Wang et al. (2008) concluded that MMP-9 activity must occur within minutes post stimulation as first effects of MMP-9 inhibition were observed at 10-15 minutes from the LTP induction for both sLTP and EPSP amplitude. However, their conclusions relied on an LTP-evoking protocol involving electrical stimulation paired with depolarization of a patch-clamped postsynaptic neuron. This approach resulted in multi-spine activation, limiting its utility for dissecting molecular aspects of structural plasticity (Kasai, 2023). Moreover, their imaging protocol had low temporal resolution (spine images were collected every 5-10 minutes), and likely missed the transient phase of spine enlargement. Hence, this study was not in position to assess the involvement of MMP-9 in the early stages of sLTP.

Additionally, my findings bring more insight to the timing of MMP-9 activity required for dendritic spine plasticity as previous report indicate cleavage of MMP-9 substrates to be detectable 5 minutes post-stimulation (Dziembowska et al. 2012). Moreover those authors demonstrated rapid local translation of MMP-9, which, together with pre-existing MMP-9, contributed to increased substrate cleavage within this early timeframe. Although I did not verify whether MMP-9 related effects come from pre-existing or locally translated MMP-9, it seems that especially for the transient and sustained phase of spine volume changes local protein translation is most likely not essential (Bosch et al., 2014).

Nagy et al. (2006) findings on MMP-9$^{-/-}$ animals provide additional insights, indicating large scale fLTP impairment when compared to effects obtained by pharmacological MMP-9 inhibition. As in their model of pharmacological inhibition of MMP-9 only

L-LTP was compromised whereas MMP-9$^{-/-}$ displayed general impairment in LTP induction. Furthermore, it has been shown that although dendritic spine morphology appears unaffected in MMP-9$^{-/-}$ models, there is significant increase in spine turnover (Kelly et al., 2015). Kelly et al., (2015) demonstrated that greater spine loss over spine gain proportion typical for primary somatosensory cortex during adolescence was disrupted in MMP-9$^{-/-}$ animals, which displayed similar rate of spine gain and loss. This observations together with my own observation points to complex compensatory mechanisms, that result in abnormal plasticity processes having differential effects on fLTP and sLTP. Nevertheless, by overexpressing MMP-9 in MMP-9$^{-/-}$ cells, I demonstrated that the observed effects can be reversed, leading to robust spine growth in transient phase and enhanced sustained phase.

In summary, I demonstrate that MMP-9 is the primary matrix metalloproteinase involved in sLTP. Its early engagement within the first minutes following stimulation is crucial for driving robust dendritic spine growth and facilitating the transient phase of sLTP.

MMP-9 is released from postsynaptic site within seconds from stimulation onset

I have demonstrated that both MMP-9 and BDNF vesicles localize within dendritic spines. My results with overexpression of MMP-9 and BDNF constructs, analysed using expansion microscopy, enabled the identification of individual vesicles containing MMP-9 and BDNF within the dendritic spine volume. Unlike traditional confocal microscopy, which lacks the resolution to distinguish individual vesicles and produces a blurred signal that appears colocalized with the spine, expansion microscopy—a super-resolution technique—provided the necessary clarity. This approach confirmed that the observed signals originated from distinct vesicular structures and demonstrated their localization within dendritic spines for both MMP-9 and BDNF.

The localization of MMP-9 is consistent with earlier electron microscopy studies on the endogenous protein, which revealed its presence in small dendritic spines (Michaluk et al., 2007; Wilczynski et al., 2008). Similarly, the localization of BDNF vesicles observed in this study aligns with findings from both endogenous protein studies (Andreska et al., 2014; Helm et al., 2021) and overexpression models (Harward et al., 2016).

Moreover, I demonstrated that both MMP-9 and BDNF are released in response to membrane depolarization, following a similar time course. By application of repetitive electrical stimulation I observed the MMP-9 and BDNF release events from neurons in dissociated neuronal cultures. However, based on those results I could not identify whether the MMP-9 and BDNF release occurred specifically at dendritic spines. TIRF imaging, though effective for observing dynamic processes, is limited by its restricted evanescent field penetration depth, requiring observed events to occur near the glass surface. This poses challenges in pinpointing release sites accurately, as neuronal cultures typically consist of astrocytes spreading flat on the glass slide with neuronal protrusions layered above. Consequently, precise identification of release sites becomes difficult. To address this, I employed two-photon (2p) imaging combined with single spine uncaging protocol, which offers restricted single spine stimulation, but as laser-scanning microscopy has lower temporal resolution and a reduced signal-to-noise ratio. Consequently, we were unable to capture individual vesicle release events and instead relied on data processing to extract averaged release patterns for single dendritic spines. The 2p imaging combined with glutamate uncaging protocol, has confirmed that such release events can occur at dendritic spines during sLTP—a critical aspect of this investigation. This release occurs within a similar timeframe to the release of BDNF (Harward et al., 2016) and insertion of AMPA receptors into the membrane (Patterson et al., 2010). These findings suggest that the initial phase of sLTP is characterized by a rapid increase in exocytosis, involving the release of MMP-9.

MMP-9 release was previously addressed by Michaluk et al (2007) who demonstrated MMP-9 levels increase in culture media in response to enhanced neuronal activity. Although this method had limited spatiotemporal resolution, it demonstrated that MMP-9 levels significantly increased within 5 minutes of stimulation (Michaluk et al., 2007), whereas earlier time points were not investigated. Therefore, my results bring insight into dynamics of this process and provide experimental confirmation for our hypothesis that MMP-9 involvement in induction of sLTP requires its rapid release that is triggered by NMDA signalling.

BDNF/TrkB signalling relies on MMP-9 activity during sLTP

My results provide compelling evidence that MMP-9 and BDNF release are closely coordinated during synaptic plasticity. Additionally, my subsequent experiments offered

direct evidence of MMP-9 activity contributing to BDNF/TrkB activation during sLTP. The measurements of TrkB FRET sensor activation under control conditions revealed a rapid increase in TrkB activation at the stimulated spine, consistent with findings previously reported by Harward et al. (2016). Under control conditions, TrkB activation is maintained for at least 10 minutes post-stimulation. Meanwhile, results obtained in the presence of an MMP-9 inhibitor and in MMP-9$^{-/-}$ conditions showed a reduced, yet detectable, TrkB activation during sLTP induction, which diminished at later time points.

Similar effect was observed in BDNF$^{fl/fl}$ where in Cre+ group exhibited reduced TrkB activity in response to sLTP stimulation, though not completely abolished (Harward et al., 2016). This reduction also led to impaired spine growth, closely resembling the sLTP outcomes observed in MMP-9$^{fl/fl}$ Cre+ neurons in my study.

Transient TrkB activation indicates that availability of mBDNF beyond first two minutes relies on MMP-9 activity. The initial TrkB activation may be driven by the release of recycled mBDNF captured by dendritic spines (Santi et al., 2006). Meanwhile, the absence of MMP-9 significantly impairs sustained TrkB activation, implicating vesicles containing unprocessed proBDNF as reservoirs requiring MMP-9-mediated cleavage to maintain receptor activity.

The resemblance of conditional knockout of BDNF and MMP-9 effects for structural plasticity is further substantiated by direct evidence demonstrating the dependence of BDNF/TrkB signalling on MMP-9 activity. These findings align with prior studies emphasizing MMP-9 role in facilitating BDNF maturation and enhancing TrkB signalling (Hwang et al., 2005; Kaminari et al., 2017; Mizoguchi et al., 2011), as well as my results showing MMP-9-mediated cleavage of proBDNF to mBDNF (Legutko et al., 2023).

These results underscore the critical role of MMP-9 in sustaining TrkB activation and highlight extracellular BDNF maturation as a pivotal mechanism for prolonged TrkB signalling. Furthermore, they contribute to the ongoing debate regarding whether BDNF is released in its mature or pro-form (Sasi et al., 2017), supporting the hypothesis of both forms of BDNF being released.

Additional validation of these findings is necessary. For instance, applying MMP-9 inhibitors after sLTP induction could provide insights into how long-lasting TrkB

activation is achieved. A similar question was addressed by Pang et al. (2016), who demonstrated that the tPA/plasmin-mediated processing of BDNF is critical only during the initial stages of LTP. Beyond 20 minutes post-stimulation, extracellular processing of BDNF appears to be unnecessary for LTP maintenance. It remains to be determined whether MMP-9 acts downstream of plasmin in proBDNF conversion or if it functions independently.

IGR1R activation during sLTP depends on MMP-9 activity

In addition to establishing a functional link between MMP-9 involvement in sLTP and TrkB activation, I identified a second receptor, IGF1R, whose activation during sLTP is also dependent on MMP-9 activity. I measured IGF1R FRET sensor activation during sLTP. Observed IGF1R activity rapidly increased in response to sLTP stimulation in control conditions in similar manner to reported IGF1R activation (Tu et al., 2023).

Meanwhile, the absence of MMP-9 activity, achieved either through chemical inhibition or gene knockout, significantly reduces the rate of IGF1R activation during sLTP. This impairment persists for over 20 minutes. This indicates that MMP-9 activity is necessary for induction of IGF1R activation during sLTP, unlike the TrkB receptor that in early time points was partially independent of MMP-9.

Furthermore, I measured IGF1R activation in MMP-9 rescue model, showing that the observed deficits in IGF1R activation in MMP-9 [-/-] neurons can be reversed by MMP-9 overexpression. This finding confirms the specificity of MMP-9 in mediating IGF1R activation.

To my knowledge, this is the first investigation linking MMP-9 activity to IGF1R activation in the context of synaptic plasticity. While IGF1R activation dependency on MMP-9 activity has been previously reported in other cellular contexts, such as Schwann cell proliferation (Chattopadhyay & Shubayev, 2009), myelin formation (Larsen et al., 2006) astrocytoma's growth and motility (Rorive et al., 2008) and cancer progression (Egeblad & Werb, 2002; Lacalle et al., 1999; Mañes et al., 1999), the role of MMP-9 mediating IGF1R in neuronal plasticity had not been explored before.

IGFBPs are required for structural plasticity and IGF1R activation in transient and sustained phase of sLTP

My findings on the dependence of IGF1R activation on MMP-9 activity suggest that MMP-9 activity facilitates IGF-1 release during sLTP. As discussed in the Introduction IGF-IGFBs complexes may serve as IGF1 reservoir. By chemically inhibiting IGF-IGFBP complex formation, I demonstrated that spine growth was greatly compromised during sLTP induction and that dendritic spines returned to their initial volume shortly after the stimulation. Previously, limited sLTP was also reported in IGF1^{fl/fl} Cre+ model (Tu et al., 2023). The measurements of IGF1R FRET sensor activation during sLTP in the presence of IGFBPs inhibitor revealed no IGF1R activation in response to glutamate uncaging. This result confirmed that observed disruption of sLTP in the presence of IGFBPs inhibitor was a result of lack of IGF1.

My findings indicate that IGFBPs are critical for providing IGF-1 at synaptic sites. If structural changes of dendritic spines relied solely on stimulation-triggered IGF-1 secretion, IGF1R activation would likely occur independently of IGFBPs inhibition. This hypothesis warrants further validation, particularly through examining the localization of IGF-1 to determine whether it is primarily stored in vesicles or as IGF-IGFBP complexes in proximity to synapses.

The IGFBP inhibition approach, however, has certain limitations. Since the inhibitor displaces IGF-1 from the IGF-IGFBP complex, I preincubated the samples for 2 hours prior to the experiment. This could have inadvertently activated IGF1R and its downstream signalling pathways before the experimental sLTP induction. As demonstrated by Noriega-Prieto et al. (2024), the effects of preincubation with IGF-1 on LTP can be bidirectional and depend on IGF-1 concentration, further complicating the interpretation of results.

While these limitations do not undermine the relevance of IGFBPs in IGF1/IGF1R signalling, they highlight the need for further investigation. Future studies should employ more targeted approaches to clarify the role of IGFBPs and explore the dynamics of IGF-1 availability and signalling during sLTP.

IGFBP2 is a major IGFBP in the hippocampus and is cleaved by MMP-9 in linker and potentially within IGF1-binding domain

My next set of experiments was directed towards identifying major IGFBP involved in MMP-9 mediated IGF1 release during sLTP.

All IGFBPs except IGFBP-5 have been demonstrated to serve as substrates for MMP-9 (Fowlkes et al., 1995; Kabir-Salmani et al., 2005; Larsen et al., 2006; Prudova et al., 2010; Rorive et al., 2008). Since the inhibition of MMP-9 activity blocks IGF1R signalling during sLTP, I concluded that it is unlikely that IGFBP-5 is involved in this process.

RNA database analysis indicate that IGFBP2 is highly expressed in the hippocampus. Synaptoneurosome sequencing data supported IGFBP2 as the most prevalent IGFBP within synaptic compartments, suggesting its local translation and release in proximity to dendritic spines. However this has raised the question whether IGFBP2 could originate from postsynaptic compartment or astrocytic protrusions.

Experimentally, I confirmed that IGFBP2 is a substrate of MMP-9. On the Western blot, I detected two products of digestion 20 kDa and 15 kDa (Figure 21), therefore it is possible that there is more than one MMP-9 cleavage site and that both of those sides are located within the linker sequence. One of them is most likely EPKKLRPP identified by the Procleave analysis as it would result in 15kDa C-terminus product. This sequence was previously characterized as being cleaved by MMP-7 (Miyamoto et al., 2007). Additionally, my bioinformatics analysis identified a potential MMP-9 cleavage site within the IGF-binding domain of IGFBP2, specifically within the TPERLAAC sequence. TPERLAAC sequence is present closely to N-terminus therefore, I was not able to detect it, as the expected size of cleaved peptide is around 2kDa. As a result of that cleavage, C-terminus molecular weight difference would be relatively small. Although proximal N-terminus cleavage site has been identified previously for IGFBP2, its effects on IGF binding remain unknown (Forbes et al., 2012; Ho & Baxter, 1997). Future studies will be necessary to confirm TPERLAAC as cleavage site, for example by mass spectrometry and clarify its functional significance. This can be achieved for example, by generating a mutant IGFBP2 variant with an altered TPERLAAC sequence or by measuring the IGF1 affinity of truncated IGFBP2.

Additionally further analysis of purified proteins is necessary to determine the dynamics and efficiency of MMP-9 cleavage process as in our assay we did not control MMP-9 concentration between the trials, as I was investigating the appearance of digestion products not the reaction dynamics, therefore, the concentrated substrate was present in amounts that made it impossible to observe total digestion.

As I cannot exclude the involvement of other IGFBPs in synaptic plasticity, further studies employing acute knockouts of individual IGFBPs will be necessary. Full knockout models of IGFBPs have limited utility due to significant compensatory mechanisms by other IGFBPs (Schneider et al., 2000). A noteworthy approach was demonstrated by Sun et al. (2024), where IGFBP2 was selectively downregulated in astrocytes associated with neurons encoding fear-conditioning memory. This led to compromised memory consolidation, highlighting the role of astrocytic IGFBP2 in cognitive processes. A similar strategy could be applied to organotypic hippocampal slices by selectively downregulating astrocytic or neuronal IGFBP2. This would enable the study of IGF1R activation during sLTP with selective downregulation approach, offering valuable insights into the distinct contributions of astrocytic and neuronal IGFBP2 in synaptic plasticity.

IGFBP2 is mainly astrocytic and localizes close to the synaptic spines

Lastly, I confirmed the localization of IGFBP2 within both astrocytes and neurons through immunolabelling. Measurements of IGFBP2 signal intensity revealed that the majority of the signal originates from astrocytes, though a detectable IGFBP2 signal was also observed in neurons. I also demonstrated that IGFBP2 signal localizes within dendritic spines vicinity. Further investigation like immunostaining without permeabilization is needed to identify exact IGFBP2 location to confirm its extracellular anchoring within proximity of the membrane as suggested by Russo et al., (1997). Moreover additional experiments are required to identify if IGFBP2 protein levels change in response to plasticity and whether astrocytes are capable of local administration of IGFBP2 to the synapse and if this mechanism is engaged in controlling synaptic plasticity. Again targeted downregulation of IGFBP2 in astrocytes could help to answer this question.

Together my findings strongly point to IGFBP2 as a key intermediary linking MMP-9 activity to IGF1R signalling. I propose that IGFBP2 plays a central role in this process. As the most abundant IGFBP in the hippocampus, detectable presence at dendritic spines and targeted by MMP-9, IGFBP2 is uniquely positioned to regulate IGF1 activity in neuronal contexts.

My results also shed light on the astrocyte-neuron axis of interaction, suggesting that astrocyte-secreted IGFBP2 near dendritic spines may fine-tune synaptic plasticity by enhancing local IGF1 storage. This localized reservoir of IGF1 could be strategically positioned for proteolytic cleavage during LTP induction, ensuring its timely availability for receptor activation and synaptic modulation. This mechanism not only underscores the importance of IGFBP2 as a key regulator of IGF1 signalling but also highlights its role in coordinated neuron-glia interactions essential for synaptic plasticity and memory formation (Vignoli et al., 2021).

Summary and conclusion

My findings provide significant new insights into the multifaceted role of MMP-9 in synaptic plasticity, emphasizing its essential contributions to both structural and molecular processes during sLTP. I demonstrate that MMP-9 activity is critical for inducing and maintaining spine growth and facilitating key signalling pathways, including BDNF/TrkB and IGF1/IGF1R activation. Importantly, MMP-9-mediated cleavage of proBDNF and IGFBPs, particularly IGFBP2, emerges as a central mechanism linking extracellular proteolysis to intracellular signalling during LTP.

MMP-9 involvement in LTP begin unexpectedly early, as its availability is detectable within seconds following neuronal stimulation. This early engagement is critical for sLTP induction and is closely tied to the release of BDNF. My data reveal that MMP-9-dependent TrkB activation is essential for sustained receptor signalling, with transient phases potentially relying on recycled mBDNF, while unprocessed proBDNF require MMP-9-mediated cleavage to maintain TrkB activation. This aligns with previous findings on MMP-9's role in BDNF maturation and TrkB signalling and highlights its broader implications for synaptic plasticity.

Beyond its established role in BDNF signalling, I identified a novel role for MMP-9 in regulating IGF1R activation during sLTP. IGF1R activation depends on MMP-9-mediated proteolysis of membrane-bound IGFBPs, with IGFBP2 emerging as the key intermediary. As the most abundant IGFBP in the brain, IGFBP2 regulates local IGF1 availability and is likely translated and released near dendritic spines, fine-tuning IGF1 signalling. Experimentally, I confirmed that IGFBP2 is a substrate of MMP-9 and identified a new potential cleavage site within its IGF-binding domain, providing a molecular basis for its role in synaptic plasticity. Furthermore, my analysis of various databases highlight IGFBP2's astrocytic origin suggesting its involvement in neuron-glia interactions, reinforcing its role in memory consolidation and LTP.

In conclusion, my work positions MMP-9 as a central regulator of synaptic plasticity, bridging extracellular proteolysis with intracellular signalling to orchestrate both structural and functional aspects of LTP. By elucidating its roles in BDNF/TrkB and IGF1/IGF1R signalling pathways, I expand the understanding of how extracellular enzymes regulate synaptic modifications essential for learning and memory (Figure 24).
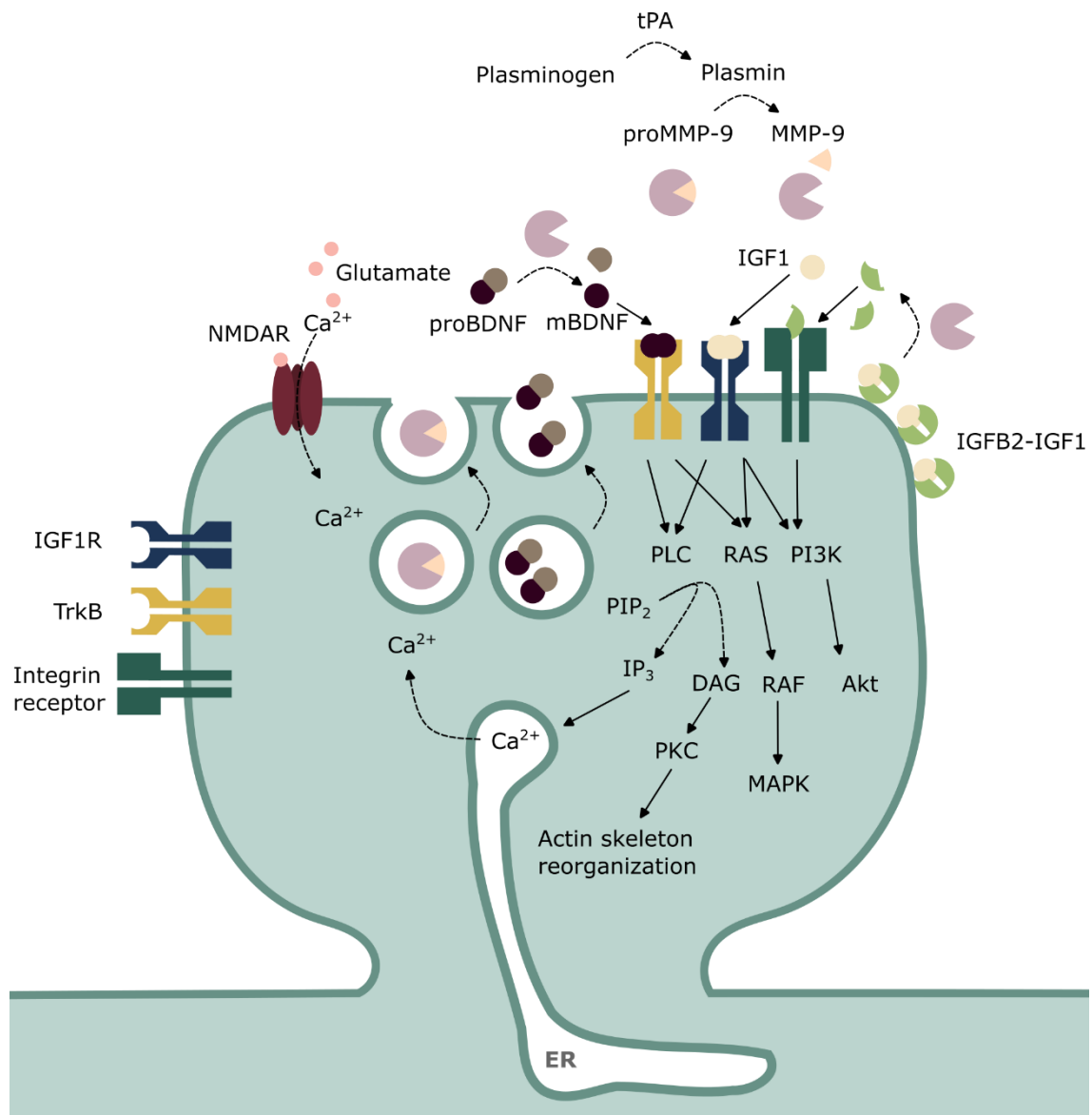
Figure 24. Proposed Mechanism of MMP-9 Involvement in sLTP

The diagram illustrates the proposed role of MMP-9 in structural long-term potentiation (sLTP). Activation of NMDA receptors and the resulting calcium influx trigger the vesicular release of proMMP-9 and proBDNF. ProMMP-9 is activated through a proteolytic cascade involving tPA and plasmin, and active MMP-9 converts proBDNF into mature BDNF (mBDNF).

mBDNF binds to and activates TrkB receptors, initiating intracellular signalling cascades via the PLC and RAS pathways. Additionally, MMP-9 cleaves IGFBP2-IGF1 complexes near the synapse, releasing IGF1 to activate IGF1R. MMP-9 also generates IGFBP2 fragments, which serve as ligands for integrin receptors.

Both IGF1R and integrins activate the PI3K/Akt signalling pathway. Together with TrkB-mediated signalling, these pathways orchestrate the molecular and structural changes required for sLTP, including actin cytoskeleton remodelling and synaptic stabilization.

This schematic highlights the direct role of MMP-9 in neurotrophic factor conversion and its contribution to multiple signalling pathways critical for sLTP.

101

BIBLIOGRAPHY

Ahmad, M., Polepalli, J. S., Goswami, D., Yang, X., Kaeser-Woo, Y. J., Südhof, T. C., & Malenka, R. C. (2012). Postsynaptic Complexin Controls AMPA Receptor Exocytosis during LTP. *Neuron*, *73*(2), 260–267. https://doi.org/10.1016/j.neuron.2011.11.020

An, J. J., Gharami, K., Liao, G. Y., Woo, N. H., Lau, A. G., Vanevski, F., Torre, E. R., Jones, K. R., Feng, Y., Lu, B., & Xu, B. (2008). Distinct Role of Long 3′ UTR BDNF mRNA in Spine Morphology and Synaptic Plasticity in Hippocampal Neurons. *Cell*, *134*(1), 175–187. https://doi.org/10.1016/j.cell.2008.05.045

Andreska, T., Aufmkolk, S., Sauer, M., & Blum, R. (2014). High abundance of BDNF within glutamatergic presynapses of cultured hippocampal neurons. *Frontiers in Cellular Neuroscience*, *8*(1 APR), 1–15. https://doi.org/10.3389/fncel.2014.00107

Asano, S. M., Gao, R., Wassie, A. T., Tillberg, P. W., Chen, F., & Boyden, E. S. (2018). Expansion Microscopy: Protocols for Imaging Proteins and RNA in Cells and Tissues. *Current Protocols in Cell Biology*, *80*(1), 1–41. https://doi.org/10.1002/cpcb.56

Barde, Y. A., Edgar, D., & Thoenen, H. (1982). Purification of a new neurotrophic factor from mammalian brain. *The EMBO Journal*, *1*(5), 549–553. https://doi.org/10.1002/j.1460-2075.1982.tb01207.x

Bauvois, B. (2012). New facets of matrix metalloproteinases MMP-2 and MMP-9 as cell surface transducers: Outside-in signaling and relationship to tumor progression. *Biochimica et Biophysica Acta - Reviews on Cancer*, *1825*(1), 29–36. https://doi.org/10.1016/j.bbcan.2011.10.001

Becker, W. (2012). Fluorescence lifetime imaging - techniques and applications. *Journal of Microscopy*, *247*(2), 119–136. https://doi.org/10.1111/j.1365-2818.2012.03618.x

Bergami, M., Santi, S., Formaggio, E., Cagnoli, C., Verderio, C., Blum, R., Berninger, B., Matteoli, M., & Canossa, M. (2008). Uptake and recycling of pro-BDNF for transmitter-induced secretion by cortical astrocytes. *Journal of Cell Biology*, *183*(2), 213–221. https://doi.org/10.1083/jcb.200806137

Berlucchi, G., & Buchtel, H. A. (2009). Neuronal plasticity: Historical roots and evolution of meaning. *Experimental Brain Research*, *192*(3), 307–319. https://doi.org/10.1007/s00221-008-1611-6

Bliss, T. V. P., & Lømo, T. (1973). Long-lasting potentiation of synaptic transmission in the dentate area of the unanaesthetized rabbit following stimulation of the perforant path. *The Journal of Physiology*, *232*(2), 357–374. https://doi.org/10.1113/jphysiol.1973.sp010274

Borczyk, M., Śliwińska, M. A., Caly, A., Bernas, T., & Radwanska, K. (2019). Neuronal plasticity affects correlation between the size of dendritic spine and its postsynaptic density. *Scientific Reports*, *9*(1), 1–12. https://doi.org/10.1038/s41598-018-38412-7

Bosch, M., Castro, J., Saneyoshi, T., Matsuno, H., Sur, M., & Hayashi, Y. (2014). Structural and molecular remodeling of dendritic spine substructures during long-term potentiation. *Neuron*, *82*(2), 444–459. https://doi.org/10.1016/j.neuron.2014.03.021

Bourguignon, L. Y. W., Gunja-Smith, Z., Iida, N., Zhu, H. B., Young, L. J. T., Muller, W. J., & Cardiff, R. D. (1998). CD44v3,8-10 is involved in cytoskeleton-mediated tumor cell migration and matrix metalloproteinase (MMP-9) association in metastatic breast cancer cells. *Journal of Cellular Physiology*, *176*(1), 206–215. https://doi.org/10.1002/(SICI)1097-4652(199807)176:1<206::AID-JCP22>3.0.CO;2-3

Brew, K., & Nagase, H. (2010). The tissue inhibitors of metalloproteinases (TIMPs): An ancient family with structural and functional diversity. *Biochimica et Biophysica Acta - Molecular Cell Research*, *1803*(1), 55–71. https://doi.org/10.1016/j.bbamcr.2010.01.003

Brigadski, T., Hartmann, M., & Lessmann, V. (2005). Differential vesicular targeting and time course of synaptic secretion of the mammalian neurotrophins. *Journal of Neuroscience*, *25*(33), 7601–7614. https://doi.org/10.1523/JNEUROSCI.1776-05.2005

Bryant, P., Pozzati, G., Zhu, W., Shenoy, A., Kundrotas, P., & Elofsson, A. (2022). Predicting the structure of large protein complexes using AlphaFold and Monte Carlo tree search. *Nature Communications*, *13*(1). https://doi.org/10.1038/s41467-022-33729-4

Burgdorf, J. S., Yoon, S., Santos, M. Dos, Lammert, C. R., Moskal, J. R., & Penzes, P. (2023). An IGFBP2-derived peptide promotes neuroplasticity and rescues deficits in a mouse model of Phelan-McDermid syndrome. *Molecular Psychiatry*, *28*(3), 1101–1111. https://doi.org/10.1038/s41380-022-01904-0.An

Caldwell, A. L. M., Sancho, L., Deng, J., Bosworth, A., Miglietta, A., Diedrich, J. K., Shokhirev, M. N., & Allen, N. J. (2022). Aberrant astrocyte protein secretion contributes to altered neuronal development in multiple models of neurodevelopmental disorders. *Nature Neuroscience*, *25*(9), 1163–1178. https://doi.org/10.1038/s41593-022-01150-1

Cao, P., Maximov, A., & Südhof, T. C. (2011). Activity-dependent IGF-1 exocytosis is controlled by the Ca 2+-sensor synaptotagmin-10. *Cell*, *145*(2), 300–311. https://doi.org/10.1016/j.cell.2011.03.034

Cao, W., Duan, J., Wang, X., Zhong, X., Hu, Z., Huang, F., Wang, H., Zhang, J., Li, F., Zhang, J., Luo, X., & Li, C. Q. (2014). Early enriched environment induces an increased conversion of proBDNF to BDNF in the adult rat's hippocampus. *Behavioural Brain Research*, *265*, 76–83. https://doi.org/10.1016/j.bbr.2014.02.022

Cauwe, B., Steen, P. E. V. Den, & Opdenakker, G. (2007). The biochemical, biological, and pathological kaleidoscope of cell surface substrates processed by matrix metalloproteinases. In *Critical Reviews in Biochemistry and Molecular Biology* (Vol. 42, Issue 3). https://doi.org/10.1080/10409230701340019

Cembrowski, M. S., Wang, L., Sugino, K., Shields, B. C., & Spruston, N. (2016). Hipposeq: A comprehensive RNA-seq database of gene expression in hippocampal principal neurons. *ELife*, *5*(APRIL2016), 1–22. https://doi.org/10.7554/eLife.14997

Chai, H., Diaz-Castro, B., Shigetomi, E., Monte, E., Octeau, J. C., Yu, X., Cohn, W., Rajendran, P. S., Vondriska, T. M., Whitelegge, J. P., Coppola, G., & Khakh, B. S. (2017). Neural Circuit-Specialized Astrocytes: Transcriptomic, Proteomic, Morphological, and Functional Evidence. *Neuron*, *95*(3), 531-549.e9. https://doi.org/10.1016/j.neuron.2017.06.029

Chakraborti, S., Mandal, M., Das, S., Mandal, A., & Chakraborti, T. (2003). Regulation of matrix metalloproteinases. An overview. *Molecular and Cellular Biochemistry*, *253*(1–2), 269–285. https://doi.org/10.1023/A:1026028303196

Chang, J., Parra-Bueno, P., Laviv, T., Szatmari, E. M., Lee, S. R., & Yasuda, R. (2017). CaMKII Autophosphorylation Is Necessary for Optimal Integration of Ca 2+ Signals during LTP Induction, but Not Maintenance. *Neuron*, *94*(4), 800-808.e4. https://doi.org/10.1016/j.neuron.2017.04.041

Chattopadhyay, S., & Shubayev, V. I. (2009). MMP-9 controls Schwann cell proliferation and phenotypic remodeling via IGF-1 and ErbB receptor-mediated activation of MEK/ERK pathway. *Glia*, *57*(12), 1316–1325. https://doi.org/10.1002/glia.20851

Chen, C., Zhu, Y. F., Liu, X. J., Lu, Z. X., Xie, Q., & Ling, N. (2001). Discovery of a series of nonpeptide small molecules that inhibit the binding of insulin-like growth factor (IGF) to IGF-binding proteins. *Journal of Medicinal Chemistry*, *44*(23), 4001–4010. https://doi.org/10.1021/jm010304b

Chen, X., Huang, Y., Huang, L., Huang, Z., Hao, Z. Z., Xu, L., Xu, N., Li, Z., Mou, Y., Ye, M., You, R., Zhang, X., Liu, S., & Miao, Z. (2024). A brain cell atlas integrating single-cell transcriptomes across human brain regions. *Nature Medicine*, *30*(September). https://doi.org/10.1038/s41591-024-03150-z

Chiu, S. L., & Cline, H. T. (2010). Insulin receptor signaling in the development of neuronal structure and function. *Neural Development*, *5*(1), 1–18. https://doi.org/10.1186/1749-8104-5-7

Choquet, D., & Hosy, E. (2020). AMPA receptor nanoscale dynamic organization and synaptic plasticities. *Current Opinion in Neurobiology*, *63*, 137–145. https://doi.org/10.1016/j.conb.2020.04.003

Cieplak, P., & Strongin, A. Y. (2017). Matrix metalloproteinases – From the cleavage data to the prediction tools and beyond. *Biochimica et Biophysica Acta - Molecular Cell Research*, *1864*(11), 1952–1963. https://doi.org/10.1016/j.bbamcr.2017.03.010

Citri, A., & Malenka, R. C. (2008). Synaptic plasticity: Multiple forms, functions, and mechanisms. *Neuropsychopharmacology*, *33*(1), 18–41.

https://doi.org/10.1038/sj.npp.1301559

Colgan, L. A., Hu, M., Misler, J. A., Parra-Bueno, P., Moran, C. M., Leitges, M., & Yasuda, R. (2018). PKCα integrates spatiotemporally distinct Ca 2+ and autocrine BDNF signaling to facilitate synaptic plasticity. *Nature Neuroscience*, *21*(8), 1027–1037. https://doi.org/10.1038/s41593-018-0184-3

Conant, K., Allen, M., & Lim, S. T. (2015). Activity dependent CAM cleavage and neurotransmission. *Frontiers in Cellular Neuroscience*, *9*(AUGUST), 1–15. https://doi.org/10.3389/fncel.2015.00305

Conant, K., Wang, Y., Szklarczyk, A., Dudak, A., Mattson, M. P., & Lim, S. T. (2010). Matrix metalloproteinase-dependent shedding of intercellular adhesion molecule-5 occurs with long-term potentiation. *Neuroscience*, *166*(2), 508–521. https://doi.org/10.1016/j.neuroscience.2009.12.061

Cuadrado, E., Rosell, A., Borrell-Pagès, M., García-Bonilla, L., Hernández-Guillamon, M., Ortega-Aznar, A., & Montaner, J. (2009). Matrix metalloproteinase-13 is activated and is found in the nucleus of neural cells after cerebral ischemia. *Journal of Cerebral Blood Flow and Metabolism*, *29*(2), 398–410. https://doi.org/10.1038/jcbfm.2008.130

Dash, P. K., Hochner, B., & Kandel, E. R. (1990). Injection of the cAMP-responsive element into the nucleus of Aplysia sensory neurons blocks long-term facilitation. *Nature*, *345*(6277), 718–721. https://doi.org/10.1038/345718a0

Davis, G. E., Pintar Allen, K. A., Salazar, R., & Maxwell, S. A. (2001). Matrix metalloproteinase-1 and -9 activation by plasmin regulates a novel endothelial cell-mediated mechanism of collagen gel contraction and capillary tube regression in three-dimensional collagen matrices. *Journal of Cell Science*, *114*(5), 917–930. https://doi.org/10.1242/jcs.114.5.917

Dayer, C., & Stamenkovic, I. (2015). Recruitment of matrix metalloproteinase-9 (MMP-9) to the fibroblast cell surface by lysyl hydroxylase 3 (LH3) triggers transforming growth factor-β (TGF-β) activation and fibroblast differentiation. *Journal of Biological Chemistry*, *290*(22), 13763–13778. https://doi.org/10.1074/jbc.M114.622274

Dean, C., Liu, H., Staudt, T., Stahlberg, M. A., Vingill, S., Bückers, J., Kamin, D., Engelhardt, J., Jackson, M. B., Hell, S. W., & Chapman, E. R. (2012). Distinct subsets of syt-IV/BDNF vesicles are sorted to axons versus dendrites and recruited to synapses by activity. *Journal of Neuroscience*, *32*(16), 5398–5413. https://doi.org/10.1523/JNEUROSCI.4515-11.2012

Denk, W. (1994). Two-photon scanning photochemical microscopy: Mapping ligand-gated ion channel distributions. *Proceedings of the National Academy of Sciences of the United States of America*, *91*(14), 6629–6633. https://doi.org/10.1073/pnas.91.14.6629

Denk, W., & Svoboda, K. (1997). Photon upmanship: Why multiphoton imaging is more than a gimmick. *Neuron*, *18*(3), 351–357. https://doi.org/10.1016/S0896-6273(00)81237-4

Dieni, S., Matsumoto, T., Dekkers, M., Rauskolb, S., Ionescu, M. S., Deogracias, R., Gundelfinger, E. D., Kojima, M., Nestel, S., Frotscher, M., & Barde, Y. A. (2012). BDNF and its pro-peptide are stored in presynaptic dense core vesicles in brain neurons. *Journal of Cell Biology*, *196*(6), 775–788. https://doi.org/10.1083/jcb.201201038

Dragunow, M., Abraham, W. C., Goulding, M., Mason, S. E., Robertson, H. A., & Faull, R. L. M. (1989). Long-term potentiation and the induction of c-fos mRNA and proteins in the dentate gyrus of unanesthetized rats. *Neuroscience Letters*, *101*(3), 274–280. https://doi.org/10.1016/0304-3940(89)90545-4

Dufour, A., Zucker, S., Sampson, N. S., Kuscu, C., & Cao, J. (2010). Role of matrix metalloproteinase-9 dimers in cell migration: Design of inhibitory peptides. *Journal of Biological Chemistry*, *285*(46), 35944–35956. https://doi.org/10.1074/jbc.M109.091769

Durzynska, J., Philippou, A., Brisson, B. K., Nguyen-McCarty, M., & Barton, E. R. (2013). The pro-forms of insulin-like growth factor i (igf-i) are predominant in skeletal muscle and alter igf-i receptor activation. *Endocrinology*, *154*(3), 1215–1224. https://doi.org/10.1210/en.2012-1992

Dyer, A. H., Vahdatpour, C., Sanfeliu, A., & Tropea, D. (2016). The role of Insulin-Like Growth Factor 1 (IGF-1) in brain development, maturation and neuroplasticity. *Neuroscience*, *325*, 89–99. https://doi.org/10.1016/j.neuroscience.2016.03.056

Dziembowska, M., Milek, J., Janusz, A., Rejmak, E., Romanowska, E., Gorkiewicz, T., Tiron,

A., Bramham, C. R., & Kaczmarek, L. (2012). Activity-dependent local translation of matrix metalloproteinase-9. *Journal of Neuroscience*, *32*(42), 14538–14547. https://doi.org/10.1523/JNEUROSCI.6028-11.2012

Egeblad, M., & Werb, Z. (2002). New functions for the matrix metalloproteinases in cancer progression. *Nature Reviews Cancer*, *2*(3), 161–174. https://doi.org/10.1038/nrc745

Ellis-Davies, G. C. R. (2019). Two-Photon Uncaging of Glutamate. *Frontiers in Synaptic Neuroscience*, *10*(January), 1–13. https://doi.org/10.3389/fnsyn.2018.00048

Evans, R., O'Neill, M., Pritzel, A., Antropova, N., Senior, A., Green, T., Žídek, A., Bates, R., Blackwell, S., Yim, J., Ronneberger, O., Bodenstein, S., Zielinski, M., Bridgland, A., Potapenko, A., Cowie, A., Tunyasuvunakool, K., Jain, R., Clancy, E., … Hassabis, D. (2022). Protein complex prediction with AlphaFold-Multimer. *BioRxiv*, 2021.10.04.463034. https://www.biorxiv.org/content/10.1101/2021.10.04.463034v2%0Ahttps://www.biorxiv.org/content/10.1101/2021.10.04.463034v2.abstract

Fields, G. B. (2015). New strategies for targeting matrix metalloproteinases. *Matrix Biology*, *44–46*, 239–246. https://doi.org/10.1016/j.matbio.2015.01.002

Forbes, B. E., McCarthy, P., & Norton, R. S. (2012). Insulin-like growth factor binding proteins: A structural perspective. *Frontiers in Endocrinology*, *3*(MAR), 1–13. https://doi.org/10.3389/fendo.2012.00038

Foscarin, S., Ponchione, D., Pajaj, E., Leto, K., Gawlak, M., Wilczynski, G. M., Rossi, F., & Carulli, D. (2011). Experience-dependent plasticity and modulation of growth regulatory molecules at central synapses. *PLoS ONE*, *6*(1). https://doi.org/10.1371/journal.pone.0016666

Fowlkes, J. L., Thrailkill, K. M., Serra, D. M., Suzuki, K., & Nagase, H. (1995). Matrix metalloproteinases as insulin-like growth factor binding protein-degrading proteinases. *Progress in Growth Factor Research*, *6*(2–4), 255–263. https://doi.org/10.1016/0955-2235(95)00017-8

Furuta, H., Sheng, Y., Takahashi, A., Nagano, R., Kataoka, N., Perks, C. M., Barker, R., Hakuno, F., & Takahashi, S. I. (2023). The IGF-Independent Role of IRS-2 in the Secretion of MMP-9 Enhances the Growth of Prostate Carcinoma Cell Line PC3. *International Journal of Molecular Sciences*, *24*(20). https://doi.org/10.3390/ijms242015065

Ghosh, A., Ginty, D. D., Bading, H., & Greenberg, M. E. (1994). Calcium regulation of gene expression in neuronal cells. *Journal of Neurobiology*, *25*(3), 294–303. https://doi.org/10.1002/neu.480250309

Gibon, J., Buckley, S. M., Unsain, N., Kaartinen, V., Séguéla, P., & Barker, P. A. (2015). proBDNF and p75NTR control excitability and persistent firing of cortical pyramidal neurons. *Journal of Neuroscience*, *35*(26), 9741–9753. https://doi.org/10.1523/JNEUROSCI.4655-14.2015

Gkogkas, C. G., Khoutorsky, A., Cao, R., Jafarnejad, S. M., Prager-Khoutorsky, M., Giannakas, N., Kaminari, A., Fragkouli, A., Nader, K., Price, T. J., Konicek, B. W., Graff, J. R., Tzinia, A. K., Lacaille, J. C., & Sonenberg, N. (2014). Pharmacogenetic Inhibition of eIF4E-Dependent Mmp9 mRNA Translation Reverses Fragile X Syndrome-like Phenotypes. *Cell Reports*, *9*(5), 1742–1755. https://doi.org/10.1016/j.celrep.2014.10.064

Gorkiewicz, T., Balcerzyk, M., Kaczmarek, L., & Knapska, E. (2015). Matrix metalloproteinase 9 (MMP-9) is indispensable for long term potentiation in the central and basal but not in the lateral nucleus of the amygdala. *Frontiers in Cellular Neuroscience*, *9*(March), 1–5. https://doi.org/10.3389/fncel.2015.00073

Gray, K., & Ellis, V. (2008). Activation of pro-BDNF by the pericellular serine protease plasmin. *FEBS Letters*, *582*(6), 907–910. https://doi.org/10.1016/j.febslet.2008.02.026

Guan, J., Williams, C. E., Skinner, S. J. M., Mallard, E. C., & Gluckman, P. D. (1996). The effects of insulin-like growth factor (IGF)-1, IGF-2, and des-IGF-1 on neuronal loss after hypoxic-ischemic brain injury in adult rats: Evidence for a role for IGF binding proteins. *Endocrinology*, *137*(3), 893–898. https://doi.org/10.1210/endo.137.3.8603600

Harvey, C. D., Yasuda, R., Zhong, H., & Svoboda, K. (2008). The spread of Ras activity triggered by activation of a single dendritic spine. *Science*, *321*(5885), 136–140. https://doi.org/10.1126/science.1159675

Harward, S. C., Hedrick, N. G., Hall, C. E., Parra-Bueno, P., Milner, T. A., Pan, E., Laviv, T., Hempstead, B. L., Yasuda, R., & McNamara, J. O. (2016). Autocrine BDNF-TrkB signalling within a single dendritic spine. *Nature*, *538*(7623), 99–103. https://doi.org/10.1038/nature19766

Hawkins, R. D., Abrams, T. W., Carew, T. J., & Kandel, E. R. (1983). A Cellular Mechanism of Classical Conditioning in Aplysia : Activity-Dependent Amplification of Presynaptic Facilitation. *Science*, *219*(4583), 400–405. https://doi.org/10.1126/science.6294833

Hebb, D. O. (1950). The Organization of Behavior; A Neuropsychological Theory. *The American Journal of Psychology*, *63*(4), 633. https://doi.org/10.2307/1418888

Hedrick, N. G., Harward, S. C., Hall, C. E., Murakoshi, H., McNamara, J. O., & Yasuda, R. (2016). Rho GTPase complementation underlies BDNF-dependent homo- and heterosynaptic plasticity. *Nature*, *538*(7623), 104–108. https://doi.org/10.1038/nature19784

Helm, M. S., Dankovich, T. M., Mandad, S., Rammner, B., Jähne, S., Salimi, V., Koerbs, C., Leibrandt, R., Urlaub, H., Schikorski, T., & Rizzoli, S. O. (2021). A large-scale nanoscopy and biochemistry analysis of postsynaptic dendritic spines. In *Nature Neuroscience* (Vol. 24, Issue 8). Springer US. https://doi.org/10.1038/s41593-021-00874-w

Hill, J. W., Poddar, R., Thompson, J. F., Rosenberg, G. A., & Yang, Y. (2012). Intranuclear matrix metalloproteinases promote DNA damage and apoptosis induced by oxygen-glucose deprivation in neurons. *Neuroscience*, *220*, 277–290. https://doi.org/10.1016/j.neuroscience.2012.06.019

Ho, P. J., & Baxter, R. C. (1997). Characterization of Truncated Insulin-Like Growth Factor-Binding Protein-2 in Human Milk*. *Endocrinology*, *138*(9), 3811–3818. https://doi.org/10.1210/endo.138.9.5415

Hohjoh, H., Horikawa, I., Nakagawa, K., Segi-Nishida, E., & Hasegawa, H. (2020). Induced mRNA expression of matrix metalloproteinases Mmp-3, Mmp-12, and Mmp-13 in the infarct cerebral cortex of photothrombosis model mice. *Neuroscience Letters*, *739*(May), 135406. https://doi.org/10.1016/j.neulet.2020.135406

Holtmaat, A., & Svoboda, K. (2009). Experience-dependent structural synaptic plasticity in the mammalian brain. *Nature Reviews Neuroscience*, *10*(9), 647–658. https://doi.org/10.1038/nrn2699

Hruska, M., Cain, R. E., & Dalva, M. B. (2022). Nanoscale rules governing the organization of glutamate receptors in spine synapses are subunit specific. *Nature Communications*, *13*(1). https://doi.org/10.1038/s41467-022-28504-4

Huntley, G. W. (2012). Synaptic circuit remodelling by matrix metalloproteinases in health and disease. *Nature Reviews Neuroscience*, *13*(11), 743–757. https://doi.org/10.1038/nrn3320

Hwang, J. J., Park, M.-H., Choi, S.-Y., & Koh, J.-Y. (2005). Activation of the Trk Signaling Pathway by Extracellular Zinc. *Journal of Biological Chemistry*, *280*(12), 11995–12001. https://doi.org/10.1074/jbc.M403172200

Ishii, C., Shibano, N., Yamazaki, M., Arima, T., Kato, Y., Ishii, Y., Shinoda, Y., Fukazawa, Y., Sadakata, T., Sano, Y., & Furuichi, T. (2021). CAPS1 is involved in hippocampal synaptic plasticity and hippocampus-associated learning. *Scientific Reports*, *11*(1), 1–15. https://doi.org/10.1038/s41598-021-88009-w

Jaipuria, G., Shet, D., Malik, S., Swain, M., Atreya, H. S., Galea, C. A., Slomiany, M. G., Rosenzweig, S. A., Forbes, B. E., Norton, R. S., & Mondal, S. (2022). IGF-dependent dynamic modulation of a protease cleavage site in the intrinsically disordered linker domain of human <scp>IGFBP2</scp>. *Proteins: Structure, Function, and Bioinformatics*, *90*(9), 1732–1743. https://doi.org/10.1002/prot.26350

Janusz, A., Miłek, J., Perycz, M., Pacini, L., Bagni, C., Kaczmarek, L., & Dziembowska, M. (2013). The Fragile X mental retardation protein regulates matrix metalloproteinase 9 mRNA at synapses. *Journal of Neuroscience*, *33*(46), 18234–18241. https://doi.org/10.1523/JNEUROSCI.2207-13.2013

Jaworski, J., Kapitein, L. C., Gouveia, S. M., Dortland, B. R., Wulf, P. S., Grigoriev, I., Camera, P., Spangler, S. A., Di Stefano, P., Demmers, J., Krugers, H., Defilippi, P., Akhmanova, A., & Hoogenraad, C. C. (2009). Dynamic Microtubules Regulate Dendritic Spine Morphology and Synaptic Plasticity. *Neuron*, *61*(1), 85–100.

https://doi.org/10.1016/j.neuron.2008.11.013

Judkewitz, B., Roth, A., & Häusser, M. (2006). Dendritic Enlightenment: Using Patterned Two-Photon Uncaging to Reveal the Secrets of the Brain's Smallest Dendrites. *Neuron*, *50*(2), 180–183. https://doi.org/10.1016/j.neuron.2006.04.011

Jumper, J., Evans, R., Pritzel, A., Green, T., Figurnov, M., Ronneberger, O., Tunyasuvunakool, K., Bates, R., Žídek, A., Potapenko, A., Bridgland, A., Meyer, C., Kohl, S. A. A., Ballard, A. J., Cowie, A., Romera-Paredes, B., Nikolov, S., Jain, R., Adler, J., … Hassabis, D. (2021). Highly accurate protein structure prediction with AlphaFold. *Nature*, *596*(7873), 583–589. https://doi.org/10.1038/s41586-021-03819-2

Jurado, S., Goswami, D., Zhang, Y., Molina, A. J. M., Südhof, T. C., & Malenka, R. C. (2013). LTP Requires a Unique Postsynaptic SNARE Fusion Machinery. *Neuron*, *77*(3), 542–558. https://doi.org/10.1016/j.neuron.2012.11.029

Kabir-Salmani, M., Shimizu, Y., Sakai, K., & Iwashita, M. (2005). Posttranslational modifications of decidual IGFBP-1 by steroid hormones in vitro. *Molecular Human Reproduction*, *11*(9), 667–671. https://doi.org/10.1093/molehr/gah222

Kaczmarek, L., Siedlecki, J. A., & Danysz, W. (1988). Proto-oncogene c-fos induction in rat hippocampus. *Molecular Brain Research*, *3*(2), 183–186. https://doi.org/10.1016/0169-328X(88)90064-2

Kaminari, A., Giannakas, N., Tzinia, A., & Tsilibary, E. C. (2017). Overexpression of matrix metalloproteinase-9 (MMP-9) rescues insulin-mediated impairment in the 5XFAD model of Alzheimer's disease. *Scientific Reports*, *7*(1), 1–12. https://doi.org/10.1038/s41598-017-00794-5

Kang, H., & Schuman, E. M. (1996). A Requirement for Local Protein Synthesis in Neurotrophin-Induced Hippocampal Synaptic Plasticity. *Science*, *273*(5280), 1402–1406. https://doi.org/10.1126/science.273.5280.1402

Kasai, H. (2023). Unraveling the mysteries of dendritic spine dynamics: Five key principles shaping memory and cognition. *Proceedings of the Japan Academy Series B: Physical and Biological Sciences*, *99*(8), 254–305. https://doi.org/10.2183/pjab.99.018

Kelly, E. A., Russo, A. S., Jackson, C. D., Lamantia, C. E. L., & Majewska, A. K. (2015). Proteolytic regulation of synaptic plasticity in the mouse primary visual cortex: Analysis of matrix metalloproteinase 9 deficient mice. *Frontiers in Cellular Neuroscience*, *9*(September), 1–17. https://doi.org/10.3389/fncel.2015.00369

Khan, S. (2019). IGFBP-2 Signaling in the Brain: From Brain Development to Higher Order Brain Functions. *Frontiers in Endocrinology*, *10*(November), 1–14. https://doi.org/10.3389/fendo.2019.00822

Khan, S., Lu, X., Huang, Q., Tang, J., Weng, J., Yang, Z., Lv, M., Xu, X., Xia, F., Zhang, M., Li, Y., Liu, S., Leng, G., Spitzer, N., Du, J., & Chen, X. (2019). IGFBP2 Plays an Essential Role in Cognitive Development during Early Life. *Advanced Science*, *6*(23). https://doi.org/10.1002/advs.201901152

Konorski, J. (1948). Conditioned Reflexes and Neuron Organization. *Cambridge University Press.*, *4*(1), 155–156.

Kuczewski, N., Porcher, C., Ferrand, N., Fiorentino, H., Pellegrino, C., Kolarow, R., Lessmann, V., Medina, I., & Gaiarsa, J. L. (2008). Backpropagating action potentials trigger dendritic release of BDNF during spontaneous network activity. *Journal of Neuroscience*, *28*(27), 7013–7023. https://doi.org/10.1523/JNEUROSCI.1673-08.2008

Lacalle, R. A. N. A., Ma, G., Mira, E., Man, S., & Nez-a, C. M. (1999). Insulin-Like Growth Factor I-Triggered Cell Migration. *Society*, *140*(4), 1657–1664.

Larsen, P. H., DaSilva, A. G., Conant, K., & Yong, V. W. (2006). Myelin formation during development of the CNS is delayed in matrix metalloproteinase-9 and -12 null mice. *Journal of Neuroscience*, *26*(8), 2207–2214. https://doi.org/10.1523/JNEUROSCI.1880-05.2006

Laskowski, R. A., Jabłońska, J., Pravda, L., Vařeková, R. S., & Thornton, J. M. (2018). PDBsum: Structural summaries of PDB entries. *Protein Science*, *27*(1), 129–134. https://doi.org/10.1002/pro.3289

Legutko, D., Kuźniewska, B., Kalita, K., Yasuda, R., Kaczmarek, L., & Michaluk, P. (2023). *BDNF signaling requires Matrix Metalloproteinase-9 during structural synaptic plasticity.*

https://doi.org/10.1101/2023.12.08.569797

Lendvai, B., Stern, E. A., Chen, B., & Svoboda, K. (2000). Experience-dependent plasticity of dendritic spines in the developing rat barrel cortex in vivo. *Nature*, *404*(6780), 876–881. https://doi.org/10.1038/35009107

Li, F., Leier, A., Liu, Q., Wang, Y., Xiang, D., Akutsu, T., Webb, G. I., Smith, A. I., Marquez-Lago, T., Li, J., & Song, J. (2020). Procleave: Predicting Protease-specific Substrate Cleavage Sites by Combining Sequence and Structural Information. *Genomics, Proteomics and Bioinformatics*, *18*(1), 52–64. https://doi.org/10.1016/j.gpb.2019.08.002

Li, F., Wang, C., Guo, X., Akutsu, T., Webb, G. I., Coin, L. J. M., Kurgan, L., & Song, J. (2023). ProsperousPlus: a one-stop and comprehensive platform for accurate protease-specific substrate cleavage prediction and machine-learning model construction. *Briefings in Bioinformatics*, *24*(6), 1–14. https://doi.org/10.1093/bib/bbad372

Lin, P. Y., Kavalali, E. T., & Monteggia, L. M. (2018). Genetic Dissection of Presynaptic and Postsynaptic BDNF-TrkB Signaling in Synaptic Efficacy of CA3-CA1 Synapses. *Cell Reports*, *24*(6), 1550–1561. https://doi.org/10.1016/j.celrep.2018.07.020

Lisman, J. (2017). Glutamatergic synapses are structurally and biochemically complex because of multiple plasticity processes: Long-term potentiation, long-term depression, short-term potentiation and scaling. *Philosophical Transactions of the Royal Society B: Biological Sciences*, *372*(1715). https://doi.org/10.1098/rstb.2016.0260

Liu, S., Yang, X., Yuan, M., Wang, S., Fan, H., Zou, Q., Pu, Y., & Cai, Z. (2024). High salt diet induces cognitive impairment and is linked to the activation of IGF1R/mTOR/p70S6K signaling. *Metabolic Brain Disease*, *39*(5), 803–819. https://doi.org/10.1007/s11011-024-01358-z

Liu, Zhi, Li, N., Diaz, L. A., Shipley, J. M., Senior, R. M., & Werb, Z. (2005). Synergy between a plasminogen cascade and MMP-9 in autoimmune disease. *Journal of Clinical Investigation*, *115*(4), 879–887. https://doi.org/10.1172/JCI23977

Liu, Zhihui, Chen, Z., Shang, C., Yan, F., Shi, Y., Zhang, J., Qu, B., Han, H., Wang, Y., Li, D., Südhof, T. C., & Cao, P. (2017). IGF1-Dependent Synaptic Plasticity of Mitral Cells in Olfactory Memory during Social Learning. *Neuron*, *95*(1), 106-122.e5. https://doi.org/10.1016/j.neuron.2017.06.015

Lledo, P. M., Zhang, X., Südhof, T. C., Malenka, R. C., & Nicoll, R. A. (1998). Postsynaptic membrane fusion and long-term potentiation. *Science*, *279*(5349), 399–403. https://doi.org/10.1126/science.279.5349.399

Lonskaya, I., Partridge, J., Lalchandani, R. R., Chung, A., Lee, T., Vicini, S., Hoe, H. S., Lim, S. T., & Conant, K. (2013). Soluble ICAM-5, a Product of Activity Dependent Proteolysis, Increases mEPSC Frequency and Dendritic Expression of GluA1. *PLoS ONE*, *8*(7), 1–12. https://doi.org/10.1371/journal.pone.0069136

Lu, Y., Christian, K., & Lu, B. (2008). BDNF: A key regulator for protein synthesis-dependent LTP and long-term memory? *Neurobiology of Learning and Memory*, *89*(3), 312–323. https://doi.org/10.1016/j.nlm.2007.08.018

Magnowska, M., Gorkiewicz, T., Suska, A., Wawrzyniak, M., Rutkowska-Wlodarczyk, I., Kaczmarek, L., & Wlodarczyk, J. (2016). Transient ECM protease activity promotes synaptic plasticity. *Scientific Reports*, *6*, 1–14. https://doi.org/10.1038/srep27757

Malenka, R. C., & Bear, M. F. (2004). LTP and LTD: An embarrassment of riches. *Neuron*, *44*(1), 5–21. https://doi.org/10.1016/j.neuron.2004.09.012

Mañes, S., Llorente, M., Lacalle, R. A., Gómez-Moutón, C., Kremer, L., Mira, E., & Martínez-A, C. (1999). The matrix metalloproteinase-9 regulates the insulin-like growth factor-triggered autocrine response in DU-145 carcinoma cells. *Journal of Biological Chemistry*, *274*(11), 6935–6945. https://doi.org/10.1074/jbc.274.11.6935

Matsumoto, T., Rauskolb, S., Polack, M., Klose, J., Kolbeck, R., Korte, M., & Barde, Y.-A. (2008). Biosynthesis and processing of endogenous BDNF: CNS neurons store and secrete BDNF, not pro-BDNF. *Nature Neuroscience*, *11*(2), 131–133. https://doi.org/10.1038/nn2038

Matsuzaki, M., Ellis-Davies, G. C. R., Nemoto, T., Miyashita, Y., Iino, M., & Kasai, H. (2001). Dendritic spine geometry is critical for AMPA receptor expression in hippocampal CA1

pyramidal neurons. *Nature Neuroscience*, *4*(11), 1086–1092. https://doi.org/10.1038/nn736

Matsuzaki, M., Honkura, N., Ellis-Davies, G. C. R., & Kasai, H. (2004). Structural basis of long-term potentiation in single dendritic spines. *Nature*, *255*(5505), 243–244. https://doi.org/10.1038/255243a0

McCusker, R. H., McCrea, K., Zunich, S., Dantzer, R., Broussard, S. R., Johnson, R. W., & Kelley, K. W. (2006). Insulin-like growth factor-I enhances the biological activity of brain-derived neurotrophic factor on cerebrocortical neurons. *Journal of Neuroimmunology*, *179*(1–2), 186–190. https://doi.org/10.1016/j.jneuroim.2006.06.014

Meighan, P., Meighan, S. E., Davis, C. J., Wright, J. W., & Harding, W. (2007). Effects of matrix metalloproteinase inhibition on short- and long-term. *Journal of Neurochemistry*.

Meighan, S., Meighan, P. C., Choudhury, P., Davis, C. J., Olson, M. L., Zornes, P. A., Wright, J. W., & Harding, J. W. (2006). Effects of extracellular matrix-degrading proteases matrix metalloproteinases 3 and 9 on spatial learning and synaptic plasticity. *Journal of Neurochemistry*, *96*(5), 1227–1241. https://doi.org/10.1111/j.1471-4159.2005.03565.x

Mestres, P. (2019). Honoring Santiago Ramón y Cajal (1852-1934),'an exemplary man'. *Eur. J. Anat.*, *23*(August), 1–89. http://www.eurjanat.com/web/paper.php?id=23s10001

Meyer, D., Bonhoeffer, T., & Scheuss, V. (2014). Balance and stability of synaptic structures during synaptic plasticity. *Neuron*, *82*(2), 430–443. https://doi.org/10.1016/j.neuron.2014.02.031

Michaluk, P., Kolodziej, L., Mioduszewska, B., Wilczynski, G. M., Dzwonek, J., Jaworski, J., Gorecki, D. C., Ottersen, O. P., & Kaczmarek, L. (2007). β-Dystroglycan as a target for MMP-9, in response to enhanced neuronal activity. *Journal of Biological Chemistry*, *282*(22), 16036–16041. https://doi.org/10.1074/jbc.M700641200

Michaluk, P., Wawrzyniak, M., Alot, P., Szczot, M., Wyrembek, P., Mercik, K., Medvedev, N., Wilczek, E., De Roo, M., Zuschratter, W., Muller, D., Wilczynski, G. M., Mozrzymas, J. W., Stewart, M. G., Kaczmarek, L., & Wlodarczyk, J. (2011). Influence of matrix metalloproteinase MMP-9 on dendritic spine morphology. *Journal of Cell Science*, *124*(19), 3369–3380. https://doi.org/10.1242/jcs.090852

Miyamoto, S., Nakamura, M., Yano, K., Ishii, G., Hasebe, T., Endoh, Y., Sangai, T., Maeda, H., Shi-chuang, Z., Chiba, T., & Ochiai, A. (2007). Matrix metalloproteinase-7 triggers the matricrine action of insulin-like growth factor-II via proteinase activity on insulin-like growth factor binding protein 2 in the extracellular matrix. *Cancer Science*, *98*(5), 685–691. https://doi.org/10.1111/j.1349-7006.2007.00448.x

Miyawaki, A. (2003). Visualization of the spatial and temporal dynamics of intracellular signaling. *Developmental Cell*, *4*(3), 295–305. https://doi.org/10.1016/S1534-5807(03)00060-1

Mizoguchi, H., Nakade, J., Tachibana, M., Ibi, D., Someya, E., Koike, H., Kamei, H., Nabeshima, T., Itohara, S., Takuma, K., Sawada, M., Sato, J., & Yamada, K. (2011). Matrix metalloproteinase-9 contributes to kindled seizure development in pentylenetetrazole-treated mice by converting pro-BDNF to mature BDNF in the hippocampus. *Journal of Neuroscience*, *31*(36), 12963–12971. https://doi.org/10.1523/JNEUROSCI.3118-11.2011

Murakoshi, H., Shin, M. E., Parra-Bueno, P., Szatmari, E. M., Shibata, A. C. E., & Yasuda, R. (2017). Kinetics of Endogenous CaMKII Required for Synaptic Plasticity Revealed by Optogenetic Kinase Inhibitor. *Neuron*, *94*(1), 37-47.e5. https://doi.org/10.1016/j.neuron.2017.02.036

Murakoshi, H., Wang, H., & Yasuda, R. (2011). Local, persistent activation of Rho GTPases during plasticity of single dendritic spines. *Nature*, *472*(7341), 100–106. https://doi.org/10.1038/nature09823

Nagel, S., Sandy, J. D., Meyding-Lamade, U., Schwark, C., Bartsch, J. W., & Wagner, S. (2005). Focal cerebral ischemia induces changes in both MMP-13 and aggrecan around individual neurons. *Brain Research*, *1056*(1), 43–50. https://doi.org/10.1016/j.brainres.2005.07.036

Nagy, V., Bozdagi, O., Matynia, A., Balcerzyk, M., Okulski, P., Dzwonek, J., Costa, R. M., Silva, A. J., Kaczmarek, L., & Huntley, G. W. (2006). Matrix Metalloproteinase-9 Is Required for Hippocampal Late-Phase Long-Term Potentiation and Memory. *The Journal of Neuroscience*, *26*(7), 1923–1934. https://doi.org/10.1523/JNEUROSCI.4359-05.2006

Nakahata, Y., & Yasuda, R. (2018). Plasticity of spine structure: Local signaling, translation and cytoskeletal reorganization. *Frontiers in Synaptic Neuroscience*, *10*(AUG), 1–13. https://doi.org/10.3389/fnsyn.2018.00029

Nedivi, E., Hevroni, D., Naot, D., Israeli, D., & Citri, Y. (1993). Numerous candidate plasticity-related genes revealed by differential cDNA cloning. *Nature*, *363*(6431), 718–722. https://doi.org/10.1038/363718a0

Ng, M., Roorda, R. D., Lima, S. Q., Zemelman, B. V., Morcillo, P., & Miesenböck, G. (2002). Transmission of olfactory information between three populations of neurons in the antennal lobe of the fly. *Neuron*, *36*(3), 463–474. https://doi.org/10.1016/S0896-6273(02)00975-3

Nishijima, T., Piriz, J., Duflot, S., Fernandez, A. M., Gaitan, G., Gomez-Pinedo, U., Verdugo, J. M. G., Leroy, F., Soya, H., Nuñez, A., & Torres-Aleman, I. (2010). Neuronal Activity Drives Localized Blood-Brain-Barrier Transport of Serum Insulin-like Growth Factor-I into the CNS. *Neuron*, *67*(5), 834–846. https://doi.org/10.1016/j.neuron.2010.08.007

Noriega-Prieto, J. A., Maglio, L. E., Perez-Domper, P., Dávila, J. C., Gutiérrez, A., Torres-Alemán, I., & Fernández de Sevilla, D. (2024). Bidirectional modulation of synaptic transmission by insulin-like growth factor-I. *Frontiers in Cellular Neuroscience*, *18*(June). https://doi.org/10.3389/fncel.2024.1390663

Nuñez, A., Zegarra-Valdivia, J., Fernandez de Sevilla, D., Pignatelli, J., & Torres Aleman, I. (2023). The neurobiology of insulin-like growth factor I: From neuroprotection to modulation of brain states. *Molecular Psychiatry*, *28*(8), 3220–3230. https://doi.org/10.1038/s41380-023-02136-6

Ogundele, O. M., Pardo, J., Francis, J., Goya, R. G., & Lee, C. C. (2018). A putative mechanism of age-related synaptic dysfunction based on the impact of IGF-1 receptor signaling on synaptic CaMKIIα phosphorylation. *Frontiers in Neuroanatomy*, *12*(May), 1–14. https://doi.org/10.3389/fnana.2018.00035

Okada, Y., Gonoji, Y., Naka, K., Tomita, K., Nakanishi, I., Iwata, K., Yamashita, K., & Hayakawa, T. (1992). Matrix metalloproteinase 9 (92-kDa gelatinase/type IV collagenase) from HT 1080 human fibrosarcoma cells. Purification and activation of the precursor and enzymic properties. *Journal of Biological Chemistry*, *267*(30), 21712–21719. https://doi.org/10.1016/s0021-9258(19)36670-0

Pachitariu, M., Stringer, C., Dipoppa, M., Schröder, S., Rossi, L. F., Dalgleish, H., Carandini, M., & Harris, K. D. (2017). Suite2p: beyond 10,000 neurons with standard two-photon microscopy. bioRxiv. *Bioarxiv*, *20*, 2017.

Pang, P. T., & Lu, B. (2004). Regulation of late-phase LTP and long-term memory in normal and aging hippocampus: Role of secreted proteins tPA and BDNF. *Ageing Research Reviews*, *3*(4), 407–430. https://doi.org/10.1016/j.arr.2004.07.002

Pang, P. T., Nagappan, G., Guo, W., & Lu, B. (2016). Extracellular and intracellular cleavages of proBDNF required at two distinct stages of late-phase LTP. *Npj Science of Learning*, *1*(1), 16003. https://doi.org/10.1038/npjscilearn.2016.3

Park, H., & Poo, M. M. (2012). Neurotrophin regulation of neural circuit development and function. In *Nature Reviews Neuroscience* (Vol. 14, Issue 1, pp. 7–23). Nature Publishing Group. https://doi.org/10.1038/nrn3379

Park, M., Salgado, J. M., Ostroff, L., Helton, T. D., Robinson, C. G., Harris, K. M., & Ehlers, M. D. (2006). Plasticity-Induced Growth of Dendritic Spines by Exocytic Trafficking from Recycling Endosomes. *Neuron*, *52*(5), 817–830. https://doi.org/10.1016/j.neuron.2006.09.040

Patterson, M. A., Szatmari, E. M., & Yasuda, R. (2010). AMPA receptors are exocytosed in stimulated spines and adjacent dendrites in a Ras-ERK-dependent manner during long-term potentiation. *Proceedings of the National Academy of Sciences of the United States of America*, *107*(36), 15951–15956. https://doi.org/10.1073/pnas.0913875107

Peixoto, R. T., Kunz, P. A., Kwon, H., Mabb, A. M., Sabatini, B. L., Philpot, B. D., & Ehlers, M. D. (2012). Transsynaptic Signaling by Activity-Dependent Cleavage of Neuroligin-1. *Neuron*, *76*(2), 396–409. https://doi.org/10.1016/j.neuron.2012.07.006

Poo, M. ming. (2001). Neurotrophins as synaptic modulators. *Nature Reviews Neuroscience*, *2*(1), 24–32. https://doi.org/10.1038/35049004

Prudova, A., Auf Dem Keller, U., Butler, G. S., & Overall, C. M. (2010). Multiplex N-terminome analysis of MMP-2 and MMP-9 substrate degradomes by iTRAQ-TAILS quantitative proteomics. *Molecular and Cellular Proteomics*, *9*(5), 894–911. https://doi.org/10.1074/mcp.M000050-MCP201

Ramón y Cajal, S. (1894). The Croonian lecture.—La fine structure des centres nerveux. *Proceedings of the Royal Society of London*, *55*(331–335), 444–468. https://doi.org/10.1098/rspl.1894.0063

Rorive, S., Berton, A., D'haene, N., Takacs, C. N., Debeir, O., Decaestecker, C., & Salmon, I. (2008). Matrix metalloproteinase-9 interplays with the IGFBP2-IGFII complex to promote cell growth and motility in astrocytomas. *GLIA*, *56*(15), 1679–1690. https://doi.org/10.1002/glia.20719

Rosenblum, G., Van den Steen, P. E., Cohen, S. R., Grossmann, J. G., Frenkel, J., Sertchook, R., Slack, N., Strange, R. W., Opdenakker, G., & Sagi, I. (2007). Insights into the Structure and Domain Flexibility of Full-Length Pro-Matrix Metalloproteinase-9/Gelatinase B. *Structure*, *15*(10), 1227–1236. https://doi.org/10.1016/j.str.2007.07.019

Rowsell, S., Hawtin, P., Minshull, C. A., Jepson, H., Brockbank, S. M. V., Barratt, D. G., Slater, A. M., McPheat, W. L., Waterson, D., Henney, A. M., & Pauptit, R. A. (2002). Crystal structure of human MMP9 in complex with a reverse hydroxamate inhibitor. *Journal of Molecular Biology*, *319*(1), 173–181. https://doi.org/10.1016/S0022-2836(02)00262-0

Russo, V., Gluckman, P. D., Feldman, E. L., & Werther, G. A. (2005). The insulin-like growth factor system and its pleiotropic functions in brain. *Endocrine Reviews*, *26*(7), 916–943. https://doi.org/10.1210/er.2004-0024

Russo, V., Rekaris, G., Baker, N. L., Bach, L. A., & Werther, G. A. (1999). Basic fibroblast growth factor induces proteolysis of secreted and cell membrane-associated insulin-like growth factor binding protein-2 in human neuroblastoma cells. *Endocrinology*, *140*(7), 3082–3090. https://doi.org/10.1210/endo.140.7.6771

Sakuragi, S., Tominaga-Yoshino, K., & Ogura, A. (2013). Involvement of TrkB- and p75MNTR-signaling pathways in two contrasting forms of long-lasting synaptic plasticity. *Scientific Reports*, *3*, 1–7. https://doi.org/10.1038/srep03185

Santi, S., Cappello, S., Riccio, M., Bergami, M., Aicardi, G., Schenk, U., Matteoli, M., & Canossa, M. (2006). Hippocampal neurons recycle BDNF for activity-dependent secretion and LTP maintenance. *EMBO Journal*, *25*(18), 4372–4380. https://doi.org/10.1038/sj.emboj.7601303

Sasi, M., Vignoli, B., Canossa, M., & Blum, R. (2017). Neurobiology of local and intercellular BDNF signaling. *Pflugers Archiv European Journal of Physiology*, *469*(5–6), 593–610. https://doi.org/10.1007/S00424-017-1964-4

Schneider, M. R., Lahm, H., Wu, M., Hoeflich, A., & Wolf, E. (2000). Transgenic mouse models for studying the functions of insulin-like growth factor-binding proteins. *The FASEB Journal*, *14*(5), 629–640. https://doi.org/10.1096/fasebj.14.5.629

Schratt, G. M., Nigh, E. A., Chen, W. G., Hu, L., & Greenberg, M. E. (2004). BDNF regulates the translation of a select group of mRNAs by a mammalian target of rapamycin-phosphatidylinositol 3-kinase-dependent pathway during neuronal development. *Journal of Neuroscience*, *24*(33), 7366–7377. https://doi.org/10.1523/JNEUROSCI.1739-04.2004

Shinoda, H., Ma, Y., Nakashima, R., Sakurai, K., Matsuda, T., & Nagai, T. (2018). Acid-Tolerant Monomeric GFP from Olindias formosa. *Cell Chemical Biology*, *25*(3), 330-338.e7. https://doi.org/10.1016/j.chembiol.2017.12.005

Sonderegger, P., & Matsumoto-Miyai, K. (2014). Activity-controlled proteolytic cleavage at the synapse. *Trends in Neurosciences*, *37*(8), 413–423. https://doi.org/10.1016/j.tins.2014.05.007

Srinivasan, R., Lu, T. Y., Chai, H., Xu, J., Huang, B. S., Golshani, P., Coppola, G., & Khakh, B. S. (2016). New Transgenic Mouse Lines for Selectively Targeting Astrocytes and Studying Calcium Signals in Astrocyte Processes In Situ and In Vivo. *Neuron*, *92*(6), 1181–1195. https://doi.org/10.1016/j.neuron.2016.11.030

Stawarski, M., Rutkowska-Wlodarczyk, I., Zeug, A., Bijata, M., Madej, H., Kaczmarek, L., & Wlodarczyk, J. (2014). Genetically encoded FRET-based biosensor for imaging MMP-9

activity. *Biomaterials*, *35*(5), 1402–1410. https://doi.org/10.1016/j.biomaterials.2013.11.033

Stein, I. S., & Zito, K. (2019). Dendritic Spine Elimination: Molecular Mechanisms and Implications. *Neuroscientist*, *25*(1), 27–47. https://doi.org/10.1177/1073858418769644

Stern, S. A., Chen, D. Y., & Alberini, C. M. (2014). The effect of insulin and insulin-like growth factors on hippocampus- and amygdala-dependent long-term memory formation. *Learning and Memory*, *21*(10), 556–563. https://doi.org/10.1101/lm.029348.112

Sun, W., Liu, Z., Jiang, X., Chen, M. B., Dong, H., Liu, J., Südhof, T. C., & Quake, S. R. (2024). Spatial transcriptomics reveal neuron–astrocyte synergy in long-term memory. *Nature*, *627*(8003), 374–381. https://doi.org/10.1038/s41586-023-07011-6

Sun, Y., Smirnov, M., & Kamasawa, N. (2021). *Rapid Ultrastructural Changes in the PSD and Surrounding_Yasuda R_J Neurosci_2021.pdf*. *41*(33), 7003–7014.

Szepesi, Z., Hosy, E., Ruszczycki, B., Bijata, M., Pyskaty, M., Bikbaev, A., Heine, M., Choquet, D., Kaczmarek, L., & Wlodarczyk, J. (2014). Synaptically released matrix metalloproteinase activity in control of structural plasticity and the cell surface distribution of GluA1-AMPA receptors. *PLoS ONE*, *9*(5). https://doi.org/10.1371/journal.pone.0098274

Szklarczyk, A., Lapinska, J., Rylski, M., McKay, R. D. G., & Kaczmarek, L. (2002). Matrix metalloproteinase-9 undergoes expression and activation during dendritic remodeling in adult hippocampus. *Journal of Neuroscience*, *22*(3), 920–930. https://doi.org/10.1523/jneurosci.22-03-00920.2002

Tang, S., & Yasuda, R. (2017). Imaging ERK and PKA Activation in Single Dendritic Spines during Structural Plasticity. *Neuron*, *93*(6), 1315-1324.e3. https://doi.org/10.1016/j.neuron.2017.02.032

Tomimatsu, Y., Idemoto, S., Moriguchi, S., Watanabe, S., & Nakanishi, H. (2002). Proteases involved in long-term potentiation. *Life Sciences*, *72*(4–5), 355–361. https://doi.org/10.1016/S0024-3205(02)02285-3

Tongiorgi, E., Armellin, M., Giulianini, P. G., Bregola, G., Zucchini, S., Paradiso, B., Steward, O., Cattaneo, A., & Simonato, M. (2004). Brain-derived neurotrophic factor mRNA and protein are targeted to discrete dendritic laminas by events that trigger epileptogenesis. *Journal of Neuroscience*, *24*(30), 6842–6852. https://doi.org/10.1523/JNEUROSCI.5471-03.2004

Trachtenberg, J. T., Chen, B. E., Knott, G. W., Feng, G., Sanes, J. R., Welker, E., & Svoboda, K. (2002). Long-term in vivo imaging of experience-dependent synaptic plasticity in adult cortex. *Nature*, *420*(6917), 788–794. https://doi.org/10.1038/nature01273

Trejo, J. I., Piriz, J., Llorens-Martin, M. V., Fernandez, A. M., Bolós, M., LeRoith, D., Nuñez, A., & Torres-Aleman, I. (2007). Central actions of liver-derived insulin-like growth factor I underlying its pro-cognitive effects. *Molecular Psychiatry*, *12*(12), 1118–1128. https://doi.org/10.1038/sj.mp.4002076

Tsilibary, E., Tzinia, A., Radenovic, L., Stamenkovic, V., Lebitko, T., Mucha, M., Pawlak, R., Frischknecht, R., & Kaczmarek, L. (2014). Neural ECM proteases in learning and synaptic plasticity. In *Progress in Brain Research* (1st ed., Vol. 214). Elsevier B.V. https://doi.org/10.1016/B978-0-444-63486-3.00006-2

Tu, X., Jain, A., Bueno, P. P., Decker, H., Liu, X., & Yasuda, R. (2023). Local autocrine plasticity signaling in single dendritic spines by insulin-like growth factors. *Science Advances*, *9*(31), 1–15. https://doi.org/10.1126/sciadv.adg0666

Tullis, J. E., Larsen, M. E., Rumian, N. L., Freund, R. K., Boxer, E. E., Brown, C. N., Coultrap, S. J., Schulman, H., Aoto, J., Dell'Acqua, M. L., & Bayer, K. U. (2023). LTP induction by structural rather than enzymatic functions of CaMKII. *Nature*, *621*(7977), 146–153. https://doi.org/10.1038/s41586-023-06465-y

Van den Steen, P. E., Dubois, B., Nelissen, I., Rudd, P. M., Dwek, R. A., & Opdenakker, G. (2002). Biochemistry and Molecular Biology of Gelatinase B or Matrix Metalloproteinase-9 (MMP-9). *Critical Reviews in Biochemistry and Molecular Biology*, *37*(6), 375–536. https://doi.org/10.1080/10409230290771546

Van Den Steen, P. E., Van Aelst, I., Hvidberg, V., Piccard, H., Fiten, P., Jacobsen, C., Moestrup, S. K., Fry, S., Royle, L., Wormald, M. R., Wallis, R., Rudd, P. M., Dwek, R. A., &

Opdenakker, G. (2006). The hemopexin and O-glycosylated domains tune gelatinase B/MMP-9 bioavailability via inhibition and binding to cargo receptors. *Journal of Biological Chemistry*, *281*(27), 18626–18637. https://doi.org/10.1074/jbc.M512308200

Vignoli, B., & Canossa, M. (2017). Glioactive ATP controls BDNF recycling in cortical astrocytes. *Communicative and Integrative Biology*, *10*(1), 1–5. https://doi.org/10.1080/19420889.2016.1277296

Vignoli, B., Sansevero, G., Sasi, M., Rimondini, R., Blum, R., Bonaldo, V., Biasini, E., Santi, S., Berardi, N., Lu, B., & Canossa, M. (2021). Astrocytic microdomains from mouse cortex gain molecular control over long-term information storage and memory retention. *Communications Biology*, *4*(1), 1–17. https://doi.org/10.1038/s42003-021-02678-x

Wang, X., Bozdagi, O., Nikitczuk, J. S., Zhai, Z. W., Zhou, Q., & Huntley, G. W. (2008). Extracellular proteolysis by matrix metalloproteinase-9 drives dendritic spine enlargement and long-term potentiation coordinately. *Proceedings of the National Academy of Sciences*, *105*(49), 19520–19525. https://doi.org/10.1073/pnas.0807248105

Wieboldt, R., Gee, K. R., Niu, L., Ramesh, D., Carpenter, B. K., & Hess, G. P. (1994). Photolabile precursors of glutamate: Synthesis, photochemical properties, and activation of glutamate receptors on a microsecond time scale. *Proceedings of the National Academy of Sciences of the United States of America*, *91*(19), 8752–8756. https://doi.org/10.1073/pnas.91.19.8752

Wiera, G., Wozniak, G., Bajor, M., Kaczmarek, L., & Mozrzymas, J. W. (2013). Maintenance of long-term potentiation in hippocampal mossy fiber-CA3 pathway requires fine-tuned MMP-9 proteolytic activity. *Hippocampus*, *23*(6), 529–543. https://doi.org/10.1002/hipo.22112

Wilczynski, G. M., Konopacki, F. A., Wilczek, E., Lasiecka, Z., Gorlewicz, A., Michaluk, P., Wawrzyniak, M., Malinowska, M., Okulski, P., Kolodziej, L. R., Konopka, W., Duniec, K., Mioduszewska, B., Nikolaev, E., Walczak, A., Owczarek, D., Gorecki, D. C., Zuschratter, W., Ottersen, O. P., & Kaczmarek, L. (2008). Important role of matrix metalloproteinase 9 in epileptogenesis. *Journal of Cell Biology*, *180*(5), 1021–1035. https://doi.org/10.1083/jcb.200708213

Wong, S. T., Athos, J., Figueroa, X. A., Pineda, V. V., Schaefer, M. L., Chavkin, C. C., Muglia, L. J., & Storm, D. R. (1999). Calcium-Stimulated Adenylyl Cyclase Activity Is Critical for Hippocampus-Dependent Long-Term Memory and Late Phase LTP. *Neuron*, *23*(4), 787–798. https://doi.org/10.1016/S0896-6273(01)80036-2

Woo, N. H., Teng, H. K., Siao, C. J., Chiaruttini, C., Pang, P. T., Milner, T. A., Hempstead, B. L., & Lu, B. (2005). Activation of p75NTR by proBDNF facilitates hippocampal long-term depression. *Nature Neuroscience*, *8*(8), 1069–1077. https://doi.org/10.1038/nn1510

Woods, G., & Zito, K. (2008). Preparation of gene gun bullets and biolistic transfection of neurons in slice culture. *Journal of Visualized Experiments*, *12*, 3–6. https://doi.org/10.3791/675

Wu, Y. J., Krüttgen, A., Möller, J. C., Shine, D., Chan, J. R., Shooter, E. ., & Cosgaya, J. M. (2004). Nerve growth factor, brain-derived neurotrophic factor, and neurotrophin-3 are sorted to dense-core vesicles and released via the regulated pathway in primary rat cortical neurons. *Journal of Neuroscience Research*, *75*(6), 825–834. https://doi.org/10.1002/jnr.20048

Yang, J., Ma, R. N., Dong, J. M., Hu, S. Q., Liu, Y., & Yan, J. Z. (2024). Phosphorylation of 4.1N by CaMKII Regulates the Trafficking of GluA1-containing AMPA Receptors During Long-term Potentiation in Acute Rat Hippocampal Brain Slices. *Neuroscience*, *536*, 131–142. https://doi.org/10.1016/j.neuroscience.2023.11.016

Yang, Y., Chen, J., Chen, X., Li, D., He, J., Wang, S., Zhao, S., Yang, X., Deng, S., Tong, C., Wang, D., Guo, Z., Li, D., Ma, C., Liang, X., Shi, Y. S., & Liu, J. J. (2021). Endophilin a1 drives acute structural plasticity of dendritic spines in response to Ca2+/calmodulin. *Journal of Cell Biology*, *220*(6). https://doi.org/10.1083/jcb.202007172

Yasuda, R. (2012). Studying signal transduction in single dendritic spines. *Cold Spring Harbor Perspectives in Biology*, *4*(10), 1–16. https://doi.org/10.1101/cshperspect.a005611

Yeghiazaryan, M., Żybura-Broda, K., Cabaj, A., Włodarczyk, J., Sławińska, U., Rylski, M., & Wilczyński, G. M. (2012). Fine-structural distribution of MMP-2 and MMP-9 activities in the rat skeletal muscle upon training: A study by high-resolution in situ zymography. *Histochemistry and Cell Biology*, *138*(1), 75–87. https://doi.org/10.1007/s00418-012-0940-

5

Zagulska-Szymczak, S., Filipkowski, R. K., & Kaczmarek, L. (2001). Kainate-induced genes in the hippocampus: Lessons from expression patterns. *Neurochemistry International*, *38*(6), 485–501. https://doi.org/10.1016/S0197-0186(00)00101-7

Zakharenko, S. S., Patterson, S. L., Dragatsis, I., Zeitlin, S. O., Siegelbaum, S. A., Kandel, E. R., & Morozov, A. (2003). Presynaptic BDNF required for a presynaptic but not postsynaptic component of LTP at hippocampal CA1-CA3 synapses. *Neuron*, *39*(6), 975–990. https://doi.org/10.1016/S0896-6273(03)00543-9

Zuo, Y., Lin, A., Chang, P., & Gan, W. B. (2005). Development of long-term dendritic spine stability in diverse regions of cerebral cortex. *Neuron*, *46*(2), 181–189. https://doi.org/10.1016/j.neuron.2005.04.001

PUBLICATION RECORD OF THE PHD CANDIDATE

- **Legutko, D**., Kuźniewska, B., Kalita, K., Yasuda, R., Kaczmarek, L., Michaluk, P. BDNF signaling requires Matrix Metalloproteinase-9 during structural synaptic plasticity. Preprint, DOI: 10.1101/2023.12.08.569797

- Poliński, P., Cuesta, M., Zamora-Moratalla, A., Mantica, F., Cantero-Recasens,G., Normanno, D., Rabago, L., Morenilla-Palao, C., Ordoño, P., Bonnal, S., Gómez Riera, R., Martínez De Lagrán Cabredo, M., Fernández-Blanco, Á., Rodríguez-Marin, C., Permanyer, J., Fölsz, O., Sierra, C., **Legutko, D**., Wojnacki, J., Musoles Lleo, J., Herrera, E., Dierssen, M., Irimia, M. A novel regulatory mechanism of actin cytoskeleton dynamics through a neural microexon in DAAM1 is important for proper memory formation. Preprint, DOI: 10.1101/2023.01.12.523772

- Stefaniuk, M., Pawłowska, M., Barański, M., Nowicka, K., Zieliński, Z., Bijoch, Ł., **Legutko, D**.,Majka, P., Bednarek, S ., Jermakow, N., Wójcik, D., Kaczmarek, L. (2023). Global brain c-Fos profiling reveals major functional brain networks rearrangements after alcohol reexposure. Neurobiology of Disease, 178, 106006.

- Bijoch, Ł., Klos, J., Pawłowska, M., Wiśniewska, J., **Legutko, D.**, Szachowicz, U., Kaczmarek, L., Beroun, A. (2023). Whole-brain tracking of cocaine and sugar rewards processing. Translational Psychiatry, 13(1), 20.

- Salamian A., **Legutko D.**, Nowicka K., Badyra B., Kaźmierska-Grębowska P., Caban B., Kowalczyk T., Kaczmarek L., Beroun A. (2021) Inhibition of matrix metalloproteinase 9 activity promotes synaptogenesis in the hippocampus. Cerebral Cortex, 31: 3161-3163.

- Florkowska A, Meszka I, Zawada M, **Legutko D**, Proszynski TJ, Janczyk-Ilach K, Streminska W, Ciemerych MA, Grabowska I. (2020) Pax7 as molecular switch regulating early and advanced stages of myogenic mouse ESC differentiation in teratomas. Stem Cell Res Ther 11, 238.

- Pawłowska, M., Stefaniuk, M., **Legutko, D**., Kaczmarek, L. (2019). Light-Sheet Microscopy for Whole-Brain Imaging. In Advanced Optical Methods for Brain Imaging (pp. 69-81). Springer, Singapore.

- Pawłowska, M., **Legutko, D**., Stefaniuk, M. (2017). Getting an insight into the brain-new optical clearing techniques and imaging using light-sheet microscope. Postępy biochemii, 63(1), 8-15.

- Stefaniuk, M., Gualda, E. J., Pawlowska, M., **Legutko, D**., Matryba, P., Koza, P., Konopka, W., Owczarek, D., Wawrzyniak, M., Loza-Alvarez, P., Kaczmarek, L. (2016). Light-sheet microscopy imaging of a whole cleared rat brain with Thy1-GFP transgene. Scientific reports, 6, srep28209.

List of Figures